



This is to certify that the

dissertation entitled An Interlayer Shear Slip Theory for Composite Laminates with Nonrigid Bonding

presented by

Xianqiang Lu

has been accepted towards fulfillment of the requirements for

Ph.D. degree in Mechanics

Date Sept. 11, 1991

LIBRARY Michigan State University

PLACE IN RETURN BOX to remove this checkout from your record. TO AVOID FINES return on or before date due.

DATE DUE	DATE DUE	DATE DUE
5 5 1997		
MAY 2 8 200		

MSU is An Affirmative Action/Equal Opportunity Institution excircidatedus.pm3-p.1

AN INTERLAYER SHEAR SLIP THEORY FOR COMPOSITE LAMINATES WITH NONRIGID BONDING

Ву

Xianqiang Lu

A DISSERTATION

Submitted to

Michigan State University

in partial fulfillment of the requirements

for the degree of

DOCTOR OF PHILOSOPHY

in

Engineering Mechanics

Department of Metallurgy, Mechanics, and Materials Science

1991

ABSTRACT

An Interlayer Shear Slip Theory for Composite Laminates with Nonrigid Bonding

By

Xianqiang Lu

An interlayer shear slip theory (ISST) is presented to study composite laminates with different kinds of interfacial bonding conditions. It is a displacement-based multiple-layer technique which satisfies the continuity requirements for the interlaminar shear stresses across the composite interfaces. By allowing the discontinuity of the displacements on the composite interfaces, the mechanical behavior of nonrigid interface is simulated by a linear shear slip law. The governing equations and associated boundary conditions for composite laminates with nonrigid bonding are derived from the principle of virtual displacement.

In assessing the ISST, some numerical results from ISST are compared with those from elasticity analysis and embedded-layer technique. Excellent agreements are concluded. In addition, the comparison between the results from experiments and ISST analysis are performed. A reasonable agreement is achieved.

A comprehensive application of ISST in the analysis of composite laminates with delaminations of different kinds of size, location and position is performed. It is concluded that the transverse shear effect should be considered in the delamination analysis. In addition, with the use of finite element technique, some cases of static and vibration analysis are examined. The effect of delamination on the transverse deflection, natural frequencies, and vibration mode shapes are investigated. The results from these studies further verify the feasibility of using ISST in studying the composite laminates with nonrigid bonding.

ACKNOWLEDGMENTS

Special tribute goes to my advisor, Dr. Dahsin Liu, for his invaluable guidance, support and unlimited patience through the course of this research. His enthusiasm and dedication constitute a very important factor for the conclusion and achievements of this work.

I am greatly indebted to the members of my thesis committee, Professors N. Altiero, Y. Jasiuk, T. Pence, and D. Yen for the academic support and encouragement provided through years.

I would also like to express my deep appreciation for the help received from faculties and students in the Department of Metallurgy, Mechanics, and Material Science. In particular, I like to thank my friends Dr. C. Y. Lee and Dr. C. C. Chiu for many conversations which helped me a lot in my research.

I am very grateful to my father, mother, and my aunts, Tingsun Lu and Rosa Yu for their love and support. They showed me how to recognize values of life.

Finally, special thanks are given to my wife, Qingmei Liu. Without her love, encouragement and help, this dissertation would never be completed. To her this thesis is dedicated.

Table of Contents

List of Tables	vii
List of Figures	viii
Chapter 1 - Introduction	1
1.1 Motivation	1
1.2 Literature Review	3
1.2.1 Perfectly Bonded Laminates	3
1.2.2 Imperfectly Bonded Laminates	6
1.3 Present Research	8
Chapter 2 - Interlayer Shear Slip Theory	10
2.1 Introduction	10
2.2 Displacement Field	11
2.2.1 Rigid Interface	14
2.2.2 Nonrigid Interface	18
2.3 Equilibrium Equations	19
2.3.1 Nonrigid Interface	19
2.3.2 Rigid Interface	22

Chapter 3 - Assessments of the Interlayer Shear Slip Theory	24
3.1 Closed-form Solution	24
3.2 Embedded-layer Approach	28
3.3 Results and Discussions	31
3.3.1 Rigidly Bonded Laminates	31
3.3.2 Nonrigidly Bonded Laminates	41
Chapter 4 - Experimental Verifications	57
4.1 Test Setup and Specimen Preparation	57
4.1.1 Three-point Bend Test	57
4.1.2 Free-free Vibration	61
4.2 Analytical Solutions	61
4.2.1 Static Analysis	61
4.2.2 Vibration Analysis	70
4.3 Comparisons and Discussions	70
4.3.1 Static Test	70
4.3.2 Vibration Test	71
Chapter 5 - Applications of the Interlayer Shear Slip Theory	73
5.1 Introduction	
5.2 Static Analysis	73

5.3 Vibration Analysis	75
5.3.1 Delamination Length	80
5.3.2 Delamination location	80
5.3.3 Delamination Position	80
5.4 Conclusions	92
Chapter 6 - Conclusions and Suggestions	93
6.1 Conclusions.	
6.2 Suggestions	95
Appendix - Analysis of Singular Points Based on Classical Beam Theory	96
1. Two-layer Laminates	96
2. Three-layer Laminates	99
List of References	104

List of Tables

Table 3.1 - Comparison of numerical results between elasticity analysis and prese	ent
theory	33
Table 4.1 - Central deflections of glass/epoxy beams from three-point bending	
test	59
Table 4.2 - Natural frequencies of glass/epoxy beams from free-free vibration	
test	64
Table 4.3 - Natural frequencies of glass beams from free-free vibration	
test	65
Table 5.1 - Comparisons of natural frequencies calculated from ISST, CLT, and e	lasticity
analysis	79
Table A1 - Singular points in a [0/0] beam	102
Table A2 - Singular points in a [90/0] beam	103
Table A3 - Singular points in a [0/90//0] beam	103

List of Figures

Figure 2.1 - Nodal variables and the coordinate system
Figure 2.2 - Reduced displacement variables and the coordinate system17
Figure 3.1- Cylindrical bending of a laminated orthotropic beam25
Figure 3.2 - Pure shear deformation in embedded layer30
Figure 3.3 - Normalized maximum deflection as a function of aspect ratio S in a logarith-
mic scale32
Figure 3.4 - Comparison of \overline{u} between elasticity analysis and present theory for a $[0/90/0]$
laminate35
Figure 3.5 - Comparison of $\overline{\sigma}_x$ between elasticity analysis and present theory for a [0/90/0]
laminate36
Figure 3.6 - Comparison of $\bar{\tau}_{xz}$ between elasticity analysis and present theory for a [0/90/0]
laminate37
Figure 3.7 - Comparison of \overline{u} between elasticity analysis and present theory for a [90/0]
laminate38
Figure 3.8 - Comparison of $\overline{\sigma}_x$ between elasticity analysis and present theory for a [90/0]
laminate39
Figure 3.9 - Comparison of $\overline{\tau}_{xz}$ between elasticity analysis and present theory for a [90/0]
laminate40
Figure 3.10 - Maximum deflections of [0/0] laminates as functions of bonding coeffi-
cients42

Figure 3.11 - In-plane normal stresses through the thickness in [0/0] laminates44
Figure 3.12 - Transverse shear stresses through the thickness in [0/0] laminates45
Figure 3.13 - In-plane displacements through the thickness in [0/0] laminates46
Figure 3.14 - Maximum deflections of [90/0] laminates as functions of bonding coeffi-
cients48
Figure 3.15 - In-plane normal stresses through the thickness in [90/0] laminates49
Figure 3.16 - Transverse shear stresses through the thickness in [90/0] laminates50
Figure 3.17 - In-plane displacements through the thickness in [90/0] laminates51
Figure 3.18 - Maximum deflections of [0/90/0] laminates as functions of bonding coeffi-
Figure 3.19 - In-plane normal stresses through the thickness in [0/90/0] laminates54
Figure 3.20 - Transverse shear stresses through the thickness in [0/90/0] laminates55
Figure 3.21 - In-plane displacements through the thickness in [0/90/0] laminates56
Figure 4.1 - Three-point bending test
Figure 4.2 - Normalized central deflection of a glass/epoxy beam with a central midplane
delamination of various lengths60
Figure 4.3 - The dimensions of specimens for free-free vibration test
Figure 4.4 - Block diagram of the apparatus for resonance frequency measurement63
Figure 4.5 - Normalized natural frequencies of a glass/epoxy beam with central midplane
delamination of various lengths66
Figure 4.6 - Normalized natural frequencies of a glass beam with a central midplane
delamination of various lengths67
Figure 5.1 - Normalized central deflection of a glass/epoxy beam with 25.4 mm midplane

x	
delamination at various locations	74
Figure 5.2 - Normalized central deflection of a glass/epoxy beam with an end r	nidplane
delamination of different lengths	76
Figure 5.3 - Normalized central deflection of glass/epoxy beams with a central n	nidplane
delamination of various lengths	77
Figure 5.4 - Normalized central deflections of glass/epoxy beams with 25.4 mm	and 50.8
mm central delaminations at various positions	78
Figure 5.5 - Normalized natural frequencies of graphite/epoxy beams with cent	ral mid-
plane delamination as a function of delamination length	81
Figure 5.6 - Normalized natural frequencies of graphite/epoxy beam with 20% n	nidplane
delamination at different locations	82
Figure 5.7 - Normalized first mode shape of a graphite/epoxy beam with 20% de	elamina-
tion which has center at x=0.5	83
Figure 5.8 - Normalized second mode shape of a graphite/epoxy beam with 20%	delami-
nation which has center at x=0.5	84
Figure 5.9 - Normalized third mode shape of a graphite/epoxy beam with 20% de	elamina-
tion which has center at x=0.5	85
Figure 5.10 - Normalized fourth mode shape of a graphite/epoxy beam with 20%	delami-
nation which has center at x=0.5	86
Figure 5.11 - Normalized first mode shape of a graphite/epoxy beam with 20% de	elamina-
tion which has center at x=0.2	
Figure 5.12 - Normalized second mode shape of a graphite/epoxy beam with 20%	delami-
nation which has center at x=0.2	
Figure 5.13 - Normalized third mode shape of a graphite/epoxy beam with 20% de	elamina-
tion which has center at x=0.2	

Figure 5.14 - Normalized fourth mode shape of a graphite/epoxy beam with 209	6 delami
nation which has center at x=0.2	90
Figure 5.15 - Normalized natural frequencies of graphite/epoxy beams with 20	% central
delamination at different positions	92
Figure A1 - The geometry and coordinate system of a two-layer beam	97
Figure A2 - The resultant forces and moments at the cross-section C1-C2	98
Figure A3 - The geometry and coordinate system of a three-layer beam	101
Figure A4 - The resultant forces and moments at the cross-section C3-C4	101

Chapter 1

INTRODUCTION

1.1 Motivation

Fiber-reinforced polymer matrix composite laminates have high in-plane strength but low density. They are excellent materials for high performance structures such as space vehicles and aircraft. The purpose of stacking layers of dissimilar properties together to form a composite laminate is to produce a structural component which is capable of resisting load in some particular directions. In studying composite laminates, the knowledge of stress and deformation is essentially important to understand the composite behavior. However, because of the heterogeneity of the composite laminates in the thickness direction and the anisotropy in the individual layers, the design techniques, testing methods, and analytical approaches developed for conventional isotropic materials cannot be applied to their composite counterparts directly. Because of the important role of composite materials in modern engineering design, the investigation of new techniques for studying composite stress and deformation has become an important issue.

The first attempt to study composite laminate is by classical laminate theory (CLT). Although the stress state in a composite laminate is three-dimensional in nature, the Kirchhoff assumption used in isotropic plate analysis is borrowed for studying composite laminates. However, it should be noted that CLT is only accurate for thin composite laminates [1,2]. For thick composite laminates, the transverse shear deformation, which is neglected in CLT, should be considered.

In order to consider the transverse shear effect, a possible technique is to introduce a high-order displacement field. The methods which belong to this category are usually called high-order shear deformation theories (HSDT) [3-7]. Although the fiber orientation and the material properties of the individual layers are considered, HSDT indeed treats the composite laminate as a single-layer material. The individual properties are actually counted in an average sense. In general, HSDT can provide accurate results for displacements and in-plane stresses of moderate thick laminates. However, they are not suitable for interlaminar stress analysis.

Polymer matrix composite laminates are simply bonded by polymer matrix in the thickness direction. Sometimes, because of the poor mechanical properties of polymer matrix and sometimes the weak bonding with fiber materials, delamination can easily happen on the composite interface. From mechanics viewpoint, delamination is the result of interlaminar stress concentration, which is caused by the mismatch of material properties between different layers. Since delamination can significantly affect the integrity of a composite laminate, the study of interlaminar stress has become an important issue in the laminate research. In order to study the interlaminar stress, it is noted that the composite laminates have to be formulated layer by layer. Such a technique which is usually called a multiple-layer approach can satisfy the continuity requirements for both displacement and interlaminar stress across the composite interface. In addition, it can give accurately stress distribution on the composite interface directly. Several multiple-layer techniques have been developed by different investigators. A brief review of these techniques will be given in a latter section.

In addition to poor matrix property and weak bonding between fiber and matrix, the composite interface may have defects resulting from fabrication and damages due to service. For a composite laminate with delamination or imperfect bonding on its interface, displacement discontinuity can take place on the interface. However, the conventional laminate theories, including CLT, HSDT, and most multiple-layer theories, are based on

the assumption of perfect bonding on the composite interface. In this study, it is desired to develop a laminate theory considering the transverse shear effect, the continuity requirements for interlaminar stresses on the composite interfaces, and the displacement discontinuity on the damaged and imperfect interfaces.

1.2 Literature Review

Many techniques have been developed for composite laminate analysis. Some comprehensive reviews for these techniques can be found in several articles [8-11]. This section presents a brief review of the literatures related to develop a theory for composite laminates with damaged and imperfect interfaces.

1.2.1 Perfectly Bonded Laminates

In conventional composite analysis, the displacements are usually assumed to be continuous across the bonding surfaces and no slip between layers can take place. Although the stress state in a composite laminate is three-dimensional in nature. As mentioned in a previous section, the assumptions used in classical plate theories are first employed in classical laminate theory (CLT). However, CLT is only accurate for composite laminates with large dimension-to-thickness ratios, i.e., thin laminates, [1,2]. For thick composite laminates, the transverse shear deformation should be considered. In addition to thickness, the low shear modulus of polymer matrices also has a significant effect on the transverse shear deformation [12,13]. Consequently, the transverse shear deformation is an important consideration in the composite analysis.

In order to overcome the shortcoming of CLT, many techniques have been developed. Among them, the one which receives the most attention in recent years is the socalled high-order shear deformation theory (HSDF). By introducing different kinds of high-order displacement fields, many HSDT [3-7] have been presented for both displacement and in-plane stress analysis. Recently, Reddy has indicated that the high-order theories can be unified by a so-called generalized laminated plate theory (GLPT) [14] which is developed from a layer-wise displacement field. GLPT can give accurate results for displacements and in-plane stresses for laminate analysis [15]. However, it is not suitable for interlaminar stresses.

In composite analysis, due to the high interlaminar stresses and weak bonding between the composite layers, delamination can easily occur on the composite interface. Two types of delamination, namely edge delamination [16] and central delamination [17], have been widely investigated. Both of them can be viewed as a result of interlaminar stress concentration caused by material property mismatch in the thickness direction. Because delamination can significantly affect the total performance of composite structures, the study of interlaminar stresses has become an important issue in composite analysis. Since HSDT and GLPT do not take the interlaminar stress continuity conditions into consideration, the interlaminar stresses cannot be obtained from the constitutive equations directly. Although it is possible to recover the interlaminar stresses through the equilibrium equations [18], it is tedious and not suitable for structures with complex configurations.

In order to include the continuity of interlaminar stresses on the composite interface, it is necessary to formulate the composite laminate layer by layer. Ambartsumyan [19] was among the earliest to present a multiple-layer technique in the composite laminate analysis. Based on a parabolic distribution for the transverse shear stresses in the composite layers, he presented a shear deformation theory which satisfied the continuity conditions. Similar to this work, refined theories for multi-layered symmetric plates were presented by Whitney [20] and Librescu and Reddy [21]. Another stress-based technique which included the interlaminar stress continuity was presented by Mau, Tong, and Pian [22]. This technique was named hybrid-stress finite element method. Spilker [23] and many other investigators extended this technique for studies with high-order stress assumptions. In addition

to the finite element analysis, Pagano [24] assumed a stress distribution in each layer. He derived the governing equations for laminate analysis with the use of a variational approach. The continuity of interlaminar stresses was also satisfied in his formulation.

Instead of assuming stresses, DiSciuva [25] presented a displacement-based approach which had piecewise linear in-plane displacements through the thickness while the out-of-plane displacement was constant. A variational method was used to formulate the governing equations. However, due to the low order of assumed displacement field, the transverse shear stresses were constant through the thickness. Toledano and Murakami [26] used similar displacement field in their analysis. However, they also assumed quadratic transverse shear stress distribution for each composite layer independently. Reissner's mixed variational principle [27] was used together with the interlaminar shear stress continuity condition in their formulation. This technique was valid for improving in-plane deformation. However, the interlaminar shear stresses were suggested to be recovered by equilibrium equations because of accuracy reason [26]. In addition, by imposing cubic-spline function to model the through-the-thickness deformation, Hinrichsen and Palazotto [28] presented a quasi-three-dimensional nonlinear finite element analysis for thick composite plates. This theory was successfully used to study the transverse deflection and in-plane stresses and deformation of composite laminates with various thicknesses.

In view of the advantages and disadvantages of the techniques reported, it was concluded that an accurate theory for interlaminar stress analysis should consider the transverse shear effect and the continuity requirements for both displacements and interlaminar stresses on the composite interface. The interlaminar stresses can then be obtained directly from the constitutive equations instead of from the equilibrium equations. Besides, it is important that the formulation should be variational consistent [7] and can be extended to finite element analysis for structures with complex configurations. Based on these understandings, an interlaminar shear stress continuity theory (ISSCT) was developed by Lu and Liu [29] with a displacement field refined from the GLPT [14]. Because

of its quasi-three-dimension in nature, this technique was suitable for both thick and thin composite laminates. However, ISSCT neglected the effect of transverse normal deformation which was important under some circumstances [30]. A refined theory accounted for the transverse normal stress was presented by Lee and Liu [31].

1.2.2 Imperfectly Bonded Laminates

All the theories reviewed in the previous sections are based on the assumption of rigid bonding, i.e., the displacement components on the composite interface remain to be single-valued. However, in contrast to the strength in the fiber direction, the transversely tensile and interlaminar shear strengths of composite laminates are relatively low. As a consequence, the composite laminates are susceptible to delamination from a wide variety of sources such as fabrication stress, hydrothermal cycling, handling damage, and foreign object impact. Under these circumstances, the interlayer connection may become nonrigid. It has been recognized that the interfacial bonding condition can strongly affect the performance of a composite structure. Hence, in order to accurately predict the behavior of a composite structure with imperfect bonding on its interface, it is necessary to account for the bonding effect in the composite analysis.

Pioneering work in the study of nonrigidly bonded interface for composite structures was performed by Newmark, Siess, and Viest [32]. Based on Bernoulli-Euler beam theory, a laminated beam theory with a shear slip on the layer interface was developed. A linear slip law was employed to model the nonrigid connection between the layers. One of the applications of their theory was used for studying beams connected by nails. Their theory was later extended for plate analysis by subsequent investigators. In addition, different slip laws were also introduced for nonrigid interface analysis [33-36]. However, due to the fundamental assumptions of Kirchhoff hypothesis for both beam theory and plate theory, the transverse shear effect was not considered in these studies. Barbero and Reddy extended Reddy's generalized laminated plate theory (GLPT) to include the discontinuity of dis-

placement for damaged interfaces [37]. Their analysis considered the transverse shear effect. However, the continuity requirements for interlaminar stresses across the composite interface were not satisfied.

Toledano and Murakami [38], to the author's best knowledge, was the first to use a laminate theory which accounted for both transverse shear effect and interlaminar shear stress continuity in study nonrigid bonding interface. They presented a technique which incorporated a slip law in their laminate theory [26]. However, the interlaminar shear stresses that governed the shear slip at the interface were not accurate because of the low order of the assumed displacements and stresses. In addition to laminate analysis, elasticity studies on sandwich beams with nonrigid bonding interface were presented by Rao and Ghosh [39], and Fazio, Hussein, and Ha [40]. Because of the complexity of analysis, only limited cases were examined. An alternative way was to use the elasticity-based finite element approach. However, this technique might not be efficient because it required a huge number of elements [41,42].

In order to study the delamination initiation and propagation, it is necessary to study the interlaminar tensile fracture toughness and interlaminar shear fracture toughness, i.e., G_{IC} and G_{IIC} , respectively. Many testing procedures have been developed for measuring the static interlaminar fracture toughness. For example, the technique of double cantilever beam (DCB) is for Mode I fracture [43] while end notch flexure (ENF) and central notch flexure (CNF) are for Mode II [44,45]. For data reductions, CLT [44,45], HSDT [46], and two-dimensional elasticity-based finite element approach [45,47] are usually employed for numerical analysis.

Since delamination can significantly degrade a composite structure, the investigation of delamination has become an important issue in composite analysis. However, delamination is usually barely visible. Hence, quite a few destructive and nondestructive techniques have been developed for delamination detection [48,49,50,51]. One efficient technique is modal analysis. By studying the degradation of dynamic response of a com-

posite laminate, it is possible to detect the size and location of the delamination [51,52].

1.3 Present Research

Upon the demanding of an advanced theory for composite analysis, it is the objective of this study to develop a technique which can be employed to analyze both thin and thick composite laminates with various types of interfacial bonding condition. It is also desired that the theory satisfies the interlaminar shear stress continuity requirements on the composite interface. The interlaminar shear stresses can then be directly calculated from the constitutive equations instead of being recovered from the equilibrium equations. In addition, if the theory is of variational consistence, it can be easily extended to finite element formulation and be used to study composite laminates with complex configurations and boundary conditions.

In Chapter 2, a so-called interlayer shear slip theory (ISST) is developed to meet the above demands. It is a displacement-based multiple-layer technique and is extended from a previous study on perfectly bonded laminates [29]. The nonrigid interface is simulated by allowing the displacement slips, which are complemented by using a linear shear slip law, on the composite interface. The principle of virtual displacement is used to derive the governing equations and associated boundary conditions. By adjusting the parameters for interfacial bonding, the governing equations for cross-ply laminates with different kinds of interfacial bonding conditions can be presented.

In order to verify the feasibility and accuracy of ISST, the cylindrical bending of an infinitely long strip examined by Pagano [1] is studied in Chapter 3. The closed-form solutions of [0/0], [0/90] and [0/90/0] laminates with different kinds of interfacial bonding conditions are presented. The numerical results from the closed-form solutions for perfectly boned laminates are compared with those from Pagano's elasticity analysis [1]. In addi-

tion to ISST, an embedded layer approach is also presented for laminates with imperfect bondings. The numerical results from ISST for imperfectly bonded laminate are compared with those from embedded layer approach and classical beam theory. The effects of non-rigid interface on the transverse deflection and stress distribution of the composite laminate are investigated in this chapter.

Chapter 4 can be regarded as an experimental verification for ISST. Two kinds of tests are performed. One is three-point bend test and the other is free-free vibration measurement for central notched specimens. A finite element scheme based on ISST is derived for both static and vibration analysis for composite beams with delamination. Discussion of the experimental results and finite element analysis are given in this chapter. Comments on the preparation of specimen are also made.

In Chapter 5, ISST is used to study central notched and end notched specimens under both static loading and free vibration. The effects on the transverse deflection, natural frequencies, and vibration modes in terms of delamination size and location along the beam length as well as delamination position in the thickness direction are examined.

Chapter 6 is the summary of this thesis. Some important conclusions are drawn and several suggestions for future studies are given.

Chapter 2

INTERLAYER SHEAR SLIP THEORY

2.1 Introduction

In conventional analysis for laminated composite materials, the bonding between composite layers is assumed to be perfect, namely rigid bonding. In other words, the displacements in the composite laminates are assumed to be continuous across the laminate interfaces. However, due to the low shear modulus of polymer matrix and imperfect bonding from manufacturing and service, the composite interfaces can be nonrigid. It has been recognized that the interfacial condition can strongly affect the composite performance. Hence, it is necessary to account for the bonding condition in the composite analysis.

The objective of this chapter is to present a technique which can be applied to study composite laminates with different grades of bonding on the interfaces. From the previous chapter, it has been recognized that a useful theory in the study of composite laminates, especially those with imperfect bonding interfaces, should consider the transverse shear effect and the continuity requirements for interlaminar stresses on the composite interface. In addition, in formulating the governing equations, a variationally consistent approach can be extended to finite element formulation and subsequently used for laminated structures with complex configurations. Based on this understanding, a so-called interlayer shear slip theory (ISST) is developed to study the effect of interfacial bonding conditions on the composite behavior. By using the principle of virtual displacement, the governing equations and associated boundary conditions for cross-ply laminates with both

rigid and nonrigid interfaces are derived in this chapter.

2.2 Displacement Field

A composite laminate composed of n layers, as shown in Figure 2.1, is considered. A Cartesian coordinate system is chosen such that the midplane of the laminate occupies a domain Ω in the x-y plane while the z-axis is normal to this plane. The displacements u, v, and w at a generic point (x, y, z) in the laminate are assumed as follows.

$$u(x, y, z) = \sum_{i=1}^{n} \left\{ U_{i-1}^{(T)}(x, y) \phi_{1}^{(i)}(z) + U_{i}^{(B)}(x, y) \phi_{2}^{(i)}(z) + S_{2i-2}(x, y) \phi_{3}^{(i)}(z) + S_{2i-1}(x, y) \phi_{4}^{(i)}(z) \right\}$$

$$v(x, y, z) = \sum_{i=1}^{n} \left\{ V_{i-1}^{(T)}(x, y) \phi_{1}^{(i)}(z) + V_{i}^{(B)}(x, y) \phi_{2}^{(i)}(z) + T_{2i-2}(x, y) \phi_{3}^{(i)}(z) + T_{2i-1}(x, y) \phi_{4}^{(i)}(z) \right\}$$

$$(2.1)$$

$$w(x, y, z) = w(x, y)$$

where $\varphi_j^{\,(i)}$ are Hermite cubic shape functions and are defined below

$$\phi_{1}^{(i)} = 1 - 3 [(z - z_{i-1})/h_{i}]^{2} + 2 [(z - z_{i-1})/h_{i}]^{3}$$

$$\phi_{2}^{(i)} = 3 [(z - z_{i-1})/h_{i}]^{2} - 2 [(z - z_{i-1})/h_{i}]^{3}$$

$$\phi_{3}^{(i)} = (z - z_{i-1}) [1 - (z - z_{i-1})/h_{i}]^{2}$$

$$\phi_{4}^{(i)} = (z - z_{i-1})^{2} ([(z - z_{i-1})/h_{i} - 1]/h_{i})$$

$$\phi_{1}^{(i)} = \phi_{2}^{(i)} = \phi_{3}^{(i)} = \phi_{4}^{(i)} = 0$$

$$z < z_{i-1} \quad \text{or} \quad z > z_{i}$$

In the above equations, the superscript (i) represents for the layer number, i.e., the i-th layer of the composite laminate, and h_i the thickness of layer (i). As shown in Figure 2.1,

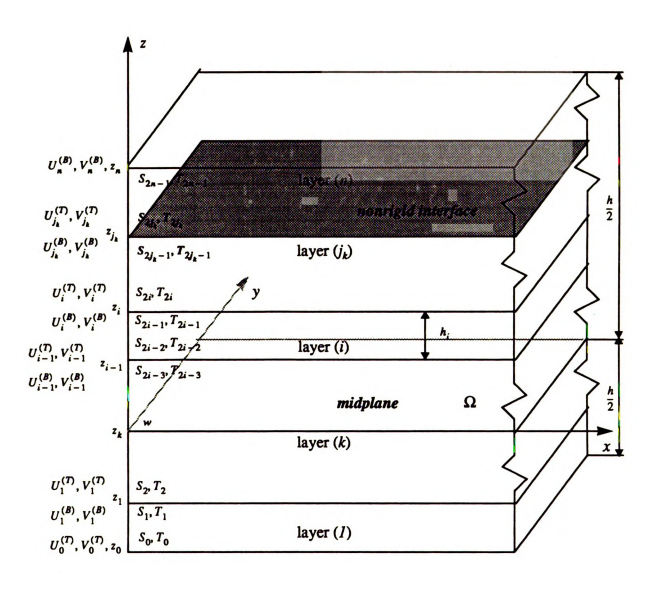


Figure 2.1 - Nodal variables and the coordinate system.

 $U_i^{(B)}$ and $V_i^{(B)}$ are the displacements at a point (x,y,z_i) in layer (i) while $U_i^{(T)}$ and $V_i^{(T)}$ at the same point but in layer (i+1). Meanwhile, S and T are the first derivatives of u and v with respect to z-axis, respectively. More specifically, S_{2i} and T_{2i} represent for the nodal values of $\frac{\partial u}{\partial z}$ and $\frac{\partial v}{\partial z}$ at the point (x, y, z_i) in layer (i+1) while S_{2i-1} and T_{2i-1} at the same point but in layer (i). Figure 2.1 depicts the displacement variables. Since the composite interfaces are not necessary to be rigidly bonded, displacement slips can exist on the interfaces. Hence, $U_i^{(B)}$ and $V_i^{(B)}$ can be different from $U_i^{(T)}$ and $V_i^{(T)}$, respectively. It is also noted that the continuity conditions for the interlaminar shear stresses must be satisfied for both rigid and nonrigid bonding interfaces although the continuity conditions are not required for the interlaminar shear strains. Consequently, S_{2i} and S_{2i-1} are not necessary to be of the same, neither are T_{2i} and T_{2i-1} .

The displacement w in the thickness direction is assumed to be constant due to the relatively small value of transverse normal stress, σ_z , compared to other stress components [19,53]. Accordingly, the total number of assumed variables is 8n+1. However, it should be noted that σ_z is important under some circumstances [30].

If the composite laminate of interest is of cross-ply sequence, the constitutive equations for orthotropic materials can be employed. For layer (i), they are [53]

$$\begin{bmatrix} \sigma_{x} \\ \sigma_{y} \\ \sigma_{z} \\ \tau_{xy} \end{bmatrix}^{(i)} = \begin{bmatrix} Q_{11} & Q_{12} & Q_{13} & 0 \\ Q_{12} & Q_{22} & Q_{23} & 0 \\ Q_{13} & Q_{23} & Q_{33} & 0 \\ 0 & 0 & 0 & 2Q_{66} \end{bmatrix}^{(i)} \begin{bmatrix} \varepsilon_{x} \\ \varepsilon_{y} \\ \varepsilon_{z} \\ \varepsilon_{xy} \end{bmatrix}^{(i)}, \qquad (2.3)$$

$$\begin{bmatrix} \tau_{yz} \\ \tau_{xz} \end{bmatrix}^{(i)} = \begin{bmatrix} 2Q_{44} & 0 \\ 0 & 2Q_{55} \end{bmatrix}^{(i)} \begin{bmatrix} \varepsilon_{yz} \\ \varepsilon_{xz} \end{bmatrix}^{(i)}$$

It is assumed in this study that the deformation of composite laminates is within a linear

elastic range. Therefore, the following strain-displacement relations are employed.

$$\varepsilon_{x} = \frac{\partial u}{\partial x} \quad ; \qquad \varepsilon_{y} = \frac{\partial v}{\partial y} \quad ; \qquad \varepsilon_{z} = \frac{\partial w}{\partial z} = 0 \quad ; \qquad \varepsilon_{xy} = \frac{1}{2} \left(\frac{\partial u}{\partial y} + \frac{\partial v}{\partial x} \right)$$

$$\varepsilon_{xz} = \frac{1}{2} \left(\frac{\partial u}{\partial z} + \frac{\partial w}{\partial x} \right) \quad ; \qquad \varepsilon_{yz} = \frac{1}{2} \left(\frac{\partial v}{\partial z} + \frac{\partial w}{\partial y} \right)$$

$$(2.4)$$

In addition, on the composite interfaces, both displacements and interlaminar shear stresses have the following relations, i.e.,

$$\Delta U_i = U_i^{(T)} - U_i^{(B)} \tag{2.5a}$$

$$\Delta V_i = V_i^{(T)} - V_i^{(B)} \tag{2.5b}$$

$$i = 1, 2, ..., n-1$$
.

$$\lim_{\varepsilon \to \varepsilon_i} \tau_{zz}^{(i+1)} = \lim_{\varepsilon \to \varepsilon_i} \tau_{xz}^{(i)} \tag{2.5c}$$

$$\lim_{z \to z_i} \tau_y^{(i+1)} = \lim_{z \to z_i} \tau_y^{(i)}$$
 (2.5d)

where ΔU_i and ΔV_i are called interlayer shear slips. In this study, the interlayer slip in z-direction is not considered.

2.2.1 Rigid Interface

If shear slips vanish, i.e., $\Delta U_i = \Delta V_i = 0$, the interface between layer (i) and layer (i+1) becomes a rigidly bonded one, namely rigid interface. And the bonding condition on the interface is called rigid bonding. Otherwise, it is a nonrigid interface associated with a nonrigid bonding condition.

For a rigid interface, Equations (2.5a) and (2.5b) result in

$$U_i^{(T)} = U_i^{(B)} = U_i$$
 and $V_i^{(T)} = V_i^{(B)} = V_i$ (2.6)

By substituting Equation (2.1) along with Equation (2.4) into Equation (2.3), the stresses

can be expressed in terms of displacements. More specifically, the interlaminar shear stresses have the following expressions.

$$\tau_{yz}^{(i)} = Q_{44}^{(i)} \left[\frac{\partial w}{\partial y} + V_{i-1}^{(T)}(x, y) \phi_{1, z}^{(i)} + V_{i}^{(B)}(x, y) \phi_{2, z}^{(i)} + T_{2i-2}(x, y) \phi_{3, z}^{(i)} + T_{2i-1}(x, y) \phi_{4, z}^{(i)} \right]$$

$$(2.7)$$

$$\tau_{xz}^{(i)} = Q_{55}^{(i)} \left[\frac{\partial w}{\partial x} + U_{i-1}^{(T)}(x, y) \phi_{1, z}^{(i)} + U_{i}^{(B)}(x, y) \phi_{2, z}^{(i)} + S_{2i-2}(x, y) \phi_{3, z}^{(i)} + S_{2i-1}(x, y) \phi_{4, z}^{(i)} \right]$$

With the use of continuity conditions for the interlaminar stresses in Equations (2.5c) and (2.5d), S_{2i-1} and T_{2i-1} can be expressed as functions of S_{2i} and T_{2i} respectively.

$$S_{2i-1} = \frac{Q_{55}^{(i+1)}}{Q_{55}^{(i)}} S_{2i} + \left[\frac{Q_{55}^{(i+1)}}{Q_{55}^{(i)}} - 1 \right] \frac{\partial w}{\partial x}$$

$$T_{2i-1} = \frac{Q_{44}^{(i+1)}}{Q_{52}^{(i)}} T_{2i} + \left[\frac{Q_{44}^{(i+1)}}{Q_{52}^{(i)}} - 1 \right] \frac{\partial w}{\partial y}$$
(2.8)

If both the top and bottom surfaces of the composite laminate are shear-traction free, the following two equations are valid,

$$\tau_{xz}\Big|_{z=\pm\frac{h}{2}} = 0$$
 ; $\tau_{yz}\Big|_{z=\pm\frac{h}{2}} = 0$ (2.9)

where h is the total thickness of the laminate. With the same fashion as used in obtaining Equation (2.8), four more variables can be eliminated, i.e.,

$$S_0 = S_{2n-1} = -\frac{\partial w}{\partial x}$$

$$T_0 = T_{2n-1} = -\frac{\partial w}{\partial y}$$
(2.10)

It then is concluded that it needs only four variables, U_{i} , V_{i} , S_{2i} , and T_{2i} , to express

each nodal point located between the top and bottom surfaces. However, there are only two independent variables on the top or bottom surface. Hence, including w, the total number of independent displacement variables is reduced to be 4n+1. The reduced variables are assigned with new notations and shown in Figure 2.2. The displacement field can then be rewritten as follows.

$$u(x, y, z) = \sum_{j=0}^{n} U_{j} \Phi^{j} + \sum_{j=1}^{n-1} \tilde{S}_{j} \Psi_{1}^{j} + \left[\sum_{j=1}^{n-1} \left(\frac{Q_{55}^{(j+1)}}{Q_{55}^{(j)}} - 1 \right) \Theta_{j}^{(1)} - \phi_{3}^{(1)} - \phi_{4}^{(n)} \right] \frac{\partial w}{\partial x}$$

$$v(x, y, z) = \sum_{j=0}^{n} V_{j} \Phi^{j} + \sum_{j=1}^{n-1} \tilde{T}_{j} \Psi_{2}^{j} + \left[\sum_{j=1}^{n-1} \left(\frac{Q_{44}^{(j+1)}}{Q_{44}^{(j)}} - 1 \right) \Theta_{j}^{(1)} - \phi_{3}^{(1)} - \phi_{4}^{(n)} \right] \frac{\partial w}{\partial y}$$

$$w(x, y, z) = w(x, y)$$

$$(2.11)$$

In the above equations, the shape functions are redefined by the following equations.

j≠i

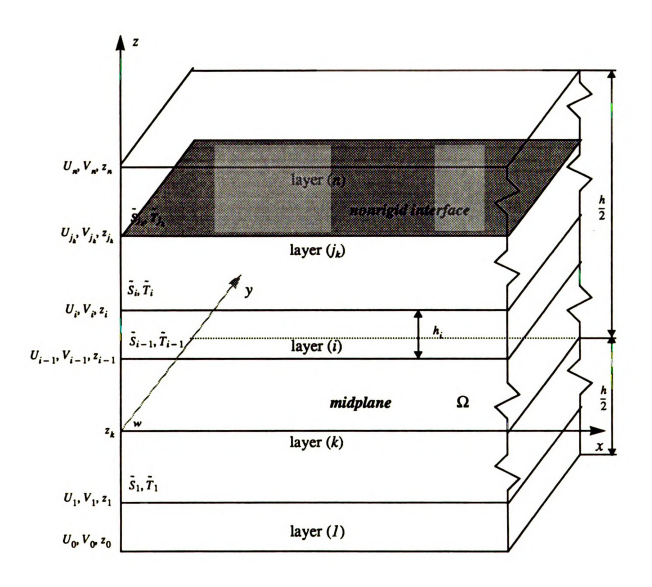


Figure 2.2 - Reduced displacement variables and the coordinate system.

2.2.2 Nonrigid Interface

Assume that the composite laminate of interest has n_l $(n_1 \le n-1)$ nonrigid bonding interfaces which are located between layer (j_k) and layer (j_k+1) as shown in Figure 2.1. A set Π which contains all nonrigid interfaces j_k , $k=1, 2, ..., n_l$, is defined. In order to model a nonrigidly bonded interface, a linear shear slip law presented by Newmark et al [32] is employed, i.e.,

$$\Delta U_{j_k} = \mu_{j_k} \tau_{xx}^{(j_k)} \qquad \qquad \mu_{j_k} \ge 0$$

$$\Delta V_{j_k} = \nu_{j_k} \tau_{yx}^{(j_k)} \qquad , \qquad \nu_{j_k} \ge 0$$

$$j_k \in \Pi \qquad (2.13)$$

The coefficients μ and ν are used to represent for interfacial shear bonding conditions. For rigid bonding, μ and ν vanish. On the contrary, μ and ν go to $+\infty$ if there is no bonding on the interface, e.g., the interface is delaminated. Since the shear slips ΔU and ΔV should be finite values, τ_{xz} and τ_{yz} must vanish on the delaminated interface. Hence, the delaminated interface in this study is defined as an interface which has no ability to transfer shear force. The values of μ and ν between 0 and ν are corresponding to imperfect (nonrigid) interfaces which have lower ability of transferring shear stresses between layers.

Substituting Equation (2.13) into Equations (2.5a) and (2.5b), the displacements above and below the nonrigid interface have the following relations.

$$U_{j_{k}}^{(B)} = U_{j_{k}} - \mu_{j_{k}} \tau_{xx}^{(j_{k})} , \qquad U_{j_{k}} = U_{j_{k}}^{(T)}$$

$$j_{k} \in \Pi$$

$$V_{j_{k}}^{(B)} = V_{j_{k}} - \nu_{j_{k}} \tau_{yx}^{(j_{k})} , \qquad V_{j_{k}} = V_{j_{k}}^{(T)}$$

$$(2.14)$$

It can be found that Equation (2.14) is also valid for rigid bonding condition as stated by Equation (2.6) when μ and ν vanish. Besides, the continuity conditions of interlaminar shear stresses, Equation (2.8), should remain valid for nonrigid interfaces. Therefore, it still requires four variables, U_i , V_i , S_{2i} , and T_{2i} , to express every nodal point located between the top and bottom surfaces. Based on the same argument as used in the rigid bond-

ing case, it can be concluded that the total number of independent variables remains to be 4n+1. The displacement field for a composite laminate which includes n_1 nonrigid bonding interfaces then becomes

$$u(x, y, z) = \sum_{j=0}^{n} U_{j} \Phi^{j} + \sum_{j=1}^{n-1} \tilde{S}_{j} (\Psi_{1}^{j} - \mu_{j} Q_{55}^{(j+1)} \Theta_{j}^{(2)})$$

$$+ \left\{ \sum_{j=1}^{n-1} \left[\left(\frac{Q_{55}^{(j+1)}}{Q_{55}^{(j)}} - 1 \right) \Theta_{j}^{(1)} - \mu_{j} Q_{55}^{(j+1)} \Theta_{j}^{(2)} \right] - \phi_{3}^{(1)} - \phi_{4}^{(n)} \right\} \frac{\partial w}{\partial x}$$

$$v(x, y, z) = \sum_{j=0}^{n} V_{j} \Phi^{j} + \sum_{j=1}^{n-1} \tilde{T}_{j} (\Psi_{2}^{j} - v_{j} Q_{44}^{(j+1)} \Theta_{j}^{(2)})$$

$$+ \left\{ \sum_{j=1}^{n-1} \left[\left(\frac{Q_{44}^{(j+1)}}{Q_{44}^{(j)}} - 1 \right) \Theta_{j}^{(1)} - v_{j} Q_{44}^{(j+1)} \Theta_{j}^{(2)} \right] - \phi_{3}^{(1)} - \phi_{4}^{(n)} \right\} \frac{\partial w}{\partial y}$$

$$w(x, y, z) = w(x, y)$$

where

$$\mu_{j} = v_{j} = 0 \qquad \text{if } j \notin \Pi$$

$$\Theta_{j}^{(2)} = \begin{cases} \Phi_{2}^{(i)} & j = i \\ 0 & j \neq i \end{cases}$$

$$(2.16)$$

2.3 Equilibrium Equations

2.3.1 Nonrigid Interface

The principle of virtual displacement is employed to derive the equilibrium equations and associated boundary conditions. It can be expressed by the following equation.

$$\int_{-\frac{1}{2}}^{\frac{1}{2}} \int_{\Omega} (\sigma_{x} \delta \varepsilon_{x} + \sigma_{y} \delta \varepsilon_{y} + \sigma_{z} \delta \varepsilon_{z} + 2\tau_{xy} \delta \varepsilon_{xy} + 2\tau_{xz} \delta \varepsilon_{xz} + 2\tau_{yz} \delta \varepsilon_{yz}) dA dz$$

$$+ \sum_{i=1}^{n} \int_{\Omega} (\tau_{xz}^{(j)} \delta \Delta U_{j} + \tau_{yz}^{(j)} \delta \Delta V_{j}) dA - \int_{\Omega} P_{z} \delta w dA = 0$$
(2.17)

In the above equation, μ and ν are assumed to be independent of x and y. In other words, the bonding condition on each interface is uniform. By substituting Equation (2.15) into Equation (2.4), the strains can be expressed in terms of displacement variables.

$$\epsilon_{x} = \sum_{j=0}^{n} U_{j,x} \Phi^{j} + \sum_{j=1}^{n-1} \tilde{S}_{j,x} \tilde{\Psi}_{1}^{j} + \lambda_{1} \frac{\partial^{2} w}{\partial x^{2}}; \qquad \epsilon_{y} = \sum_{j=0}^{n} V_{j,y} \Phi^{j} + \sum_{j=1}^{n-1} \tilde{T}_{j,y} \tilde{\Psi}_{2}^{j} + \lambda_{2} \frac{\partial^{2} w}{\partial y^{2}}$$

$$\epsilon_{xx} = \frac{1}{2} \left\{ \sum_{j=0}^{n} U_{j} \Phi^{j}_{,x} + \sum_{j=1}^{n-1} \tilde{S}_{j} \tilde{\Psi}_{1,x}^{j} + (\frac{d\lambda_{1}}{dz} + 1) \frac{\partial w}{\partial x} \right\}$$

$$\epsilon_{yz} = \frac{1}{2} \left\{ \sum_{j=0}^{n} V_{j} \Phi^{j}_{,x} + \sum_{j=1}^{n-1} \tilde{T}_{j} \tilde{\Psi}_{2,z}^{j} + (\frac{d\lambda_{2}}{dz} + 1) \frac{\partial w}{\partial y} \right\}$$

$$\epsilon_{xy} = \frac{1}{2} \left\{ \sum_{j=0}^{n} (U_{j,y} + V_{j,x}) \Phi^{j} + \sum_{j=1}^{n-1} (\tilde{S}_{j,y} \tilde{\Psi}_{1}^{j} + \tilde{T}_{j,x} \tilde{\Psi}_{2}^{j}) + (\lambda_{1} + \lambda_{2}) \frac{\partial^{2} w}{\partial x \partial y} \right\}$$

$$\psi \text{here} \qquad \lambda_{1} = \sum_{j=1}^{n-1} \left[\left(\frac{Q_{55}^{(j+1)}}{Q_{55}^{(j)}} - 1 \right) \Theta_{j}^{(1)} - \mu_{j} Q_{55}^{(j+1)} \Theta_{j}^{(2)} \right] - \phi_{3}^{(1)} - \phi_{4}^{(n)} ,$$

$$\lambda_{2} = \sum_{j=1}^{n-1} \left[\left(\frac{Q_{44}^{(j+1)}}{Q_{44}^{(i)}} - 1 \right) \Theta_{j}^{(1)} - v_{j} Q_{44}^{(j+1)} \Theta_{j}^{(2)} \right] - \phi_{3}^{(1)} - \phi_{4}^{(n)} , \qquad (2.19)$$

$$\bar{\Psi}_1^j = (\Psi_1^j - \mu_j Q_{55}^{(j+1)} \Theta_j^{(2)}); \qquad \quad \bar{\Psi}_2^j = (\Psi_2^j - \nu_j Q_{44}^{(j+1)} \Theta_j^{(2)}).$$

By substituting Equation (2.18) along with Equation (2.3) into Equation (2.17), after integrating by parts and collecting similar terms, the governing equations become as follows.

$$\begin{split} \delta w \colon & Q_{x,x} + Q_{y,y} - \bar{\lambda}_{x,xx} - \bar{\lambda}_{xy,xy} - \bar{\lambda}_{y,yy} + \bar{\eta}_{x,x} + \bar{\eta}_{y,y} + P_{x} \\ & + \sum_{k=1}^{n_{1}} \left[\mu_{j_{k}} (Q_{55}^{j_{k}+1})^{2} \left(\bar{S}_{j_{k},x} + \frac{\partial^{2} w}{\partial x^{2}} \right) + v_{j_{k}} (Q_{44}^{j_{k}+1})^{2} \left(\bar{T}_{j_{k},y} + \frac{\partial^{2} w}{\partial y^{2}} \right) \right] = 0 \\ \delta U_{j} \colon & N_{x,x}^{j} + N_{xy,y}^{j} - Q_{x}^{j} = 0 \qquad j = 0, 1, ..., n \\ \delta V_{j} \colon & N_{xy,x}^{j} + N_{y,y}^{j} - Q_{y}^{j} = 0 \qquad j = 0, 1, ..., n \\ \delta \bar{S}_{j} \colon & M_{x,x}^{j} + M_{1xy,y}^{j} - R_{x}^{j} - \mu_{j} (Q_{55}^{j+1})^{2} (\bar{S}_{j} + \frac{\partial w}{\partial x}) \delta_{jj_{k}} = 0 \qquad j = 1, 2, ..., n-1 \qquad j_{k} \in \Pi \\ \delta \bar{T}_{j} \colon & M_{x,x}^{j} + M_{y,y}^{j} - R_{y}^{j} - v_{j} (Q_{44}^{j+1})^{2} (\bar{T}_{j} + \frac{\partial w}{\partial y}) \delta_{jj_{k}} = 0 \qquad j = 1, 2, ..., n-1 \qquad j_{k} \in \Pi \end{split}$$

 δ_{jj_k} in the above equations is Kronecker delta. The essential and natural boundary conditions can also be obtained from the above analysis. They are listed in the following two columns. It should be noted that one and only one boundary condition, either essential or natural, in each group needs to be specified.

Essential Boundary Conditions Natural Boundary Conditions

The resultant forces and moments shown in Equations (2.20) and (2.21) are defined by the

following equations.

$$(Q_{x}, Q_{y}) = \int_{-\frac{h}{2}}^{\frac{h}{2}} (\tau_{xx}, \tau_{yx}) dz \qquad ; \qquad (N_{x}^{j}, N_{y}^{j}, N_{xy}^{j}) = \int_{-\frac{h}{2}}^{\frac{h}{2}} (\sigma_{x}, \sigma_{y}, \tau_{xy}) \Phi^{j} dz$$

$$(M_{x}^{j}, M_{y}^{j}, M_{1xy}^{j}, M_{2xy}^{j}) = \int_{-\frac{h}{2}}^{\frac{h}{2}} (\sigma_{x} \tilde{\Psi}_{1}^{j}, \sigma_{y} \tilde{\Psi}_{2}^{j}, \tau_{xy} \tilde{\Psi}_{1}^{j}, \tau_{xy} \tilde{\Psi}_{2}^{j}) dz$$

$$(\tilde{\lambda}_{x}, \tilde{\lambda}_{y}, \tilde{\lambda}_{xy}) = \int_{-\frac{h}{2}}^{\frac{h}{2}} (\sigma_{x} \lambda_{1}, \sigma_{y} \lambda_{2}, \tau_{xy} \lambda_{1} + \tau_{xy} \lambda_{2}) dz$$

$$(\tilde{\eta}_{x}, \tilde{\eta}_{y}) = \int_{-\frac{h}{2}}^{\frac{h}{2}} (\tau_{xx} \frac{d\lambda_{1}}{dx}, \tau_{yx} \frac{d\lambda_{2}}{dx}) dz \qquad ; \qquad (Q_{x}^{j}, Q_{y}^{j}) = \int_{-\frac{h}{2}}^{\frac{h}{2}} (\tau_{xx} \frac{d\Phi^{j}}{dx}, \tau_{yx} \frac{d\Phi^{j}}{dx}) dz$$

$$(R_{x}^{j}, R_{y}^{j}) = \int_{-\frac{h}{2}}^{\frac{h}{2}} (\tau_{xx} \frac{d\tilde{\Psi}_{1}^{j}}{dx}, \tau_{yx} \frac{d\tilde{\Psi}_{2}^{j}}{dx}) dz$$

2.3.2. Rigid Interface

If all the interfaces are rigidly bonded, i.e., $\mu=\nu=0$, the governing equations can be simplified from Equation (2.20).

$$\delta w: \qquad Q_{x,x} + Q_{y,y} - \bar{\lambda}_{x,xx} - \bar{\lambda}_{xy,xy} - \bar{\lambda}_{y,yy} + \bar{\eta}_{x,x} + \bar{\eta}_{y,y} + P_{x} = 0$$

$$\delta U_{j}: \qquad N_{x,x}^{j} + N_{xy,y}^{j} - Q_{x}^{j} = 0 \qquad \qquad j = 0, 1, ..., n$$

$$\delta V_{j}: \qquad N_{xy,x}^{j} + N_{y,y}^{j} - Q_{y}^{j} = 0 \qquad \qquad j = 0, 1, ..., n$$

$$\delta \bar{S}_{j}: \qquad M_{x,x}^{j} + M_{1xy,y}^{j} - R_{x}^{j} = 0 \qquad \qquad j = 1, 2, ..., n - 1$$

$$\delta \bar{T}_{i}: \qquad M_{2xy,x}^{j} + M_{y,y}^{j} - R_{y}^{j} = 0 \qquad \qquad j = 1, 2, ..., n - 1$$

With the same fashion, the associated boundary conditions can be obtained from Equation

(2.21).

Natural Boundary Conditions Essential Boundary Conditions $(Q_x + \overline{\eta}_x - \overline{\lambda}_{x,x} - \frac{1}{2}\overline{\lambda}_{xy,y}) n_x + (Q_y + \overline{\eta}_y - \overline{\lambda}_{y,y} - \frac{1}{2}\overline{\lambda}_{xy,x}) n_y$ <u>9m</u> $\bar{\lambda}_x n_x + \frac{1}{2} \bar{\lambda}_{xy} n_y$ $\frac{1}{2}\bar{\lambda}_{xy}n_x + \bar{\lambda}_y n_y$ <u>9^</u> $N_x^j n_x + N_{xy}^j n_y$ j = 0, 1, ..., n U_{j} (2.24) $N_{xy}^{j}n_{x}+N_{y}^{j}n_{y}$ j=0,1,...,n V_{i} $M_x^j n_x + M_{1xy}^j n_y$ j = 1, 2, ..., n-1 \tilde{S}_{j} $M_{2xy}^j n_x + M_y^j n_y$ j = 1, 2, ..., n-1 \tilde{T}_{j}

Similarly, one and only one of the boundary conditions in each group needs to be specified in the composite analysis. In Equations (2.23) and (2.24), all the resultant forces and resultant moments can also be derived from Equations (2.19) and (2.22) by imposing μ =0 and ν =0.

Chapter 3

ASSESSMENTS OF THE INTERLAYER SHEAR SLIP THEORY

3.1 Closed-form Solution

In order to assess the interlayer shear slip theory for analyzing composite laminates with rigid and nonrigid interfaces, the cylindrical bending of an infinitely long strip presented by Pagano [1] is investigated. The configuration of the laminate is given in Figure 3.1. For the beam problem, the displacement components of Equation (2.15) are reduced to be functions of x and z only. And all the derivatives with respect to y in Equations (2.20) and (2.21) vanish. By combining Equation (2.22) with Equation (2.20) and using the definitions of stresses and strains in Equations (2.3) and (2.18), the governing equations can be expressed in terms of independent displacement variables.

$$(A_{55} + \overline{A}_{55} + \gamma_{2} + \overline{\gamma}_{2}) w_{,xx} + \sum_{j=0}^{n} [(B_{55}^{j} + \overline{B}_{55}^{j}) U_{j,x} - \overline{B}_{11}^{j} U_{j,xxx}]$$

$$+ \sum_{m=1}^{n-1} [(C_{55}^{m} + \overline{C}_{55}^{m}) \tilde{S}_{m,x} - \overline{C}_{11}^{m} \tilde{S}_{m,xxx}] + \sum_{k=1}^{n_{1}} \mu_{j_{k}} (Q_{55}^{j_{k}+1})^{2} (\overline{S}_{j_{k},x} + \frac{\partial^{2}w}{\partial x^{2}}) - \overline{\gamma}_{1} w_{,xxxx} + P_{z} = 0$$

$$\sum_{j=0}^{n} (D_{11}^{ij} U_{j,xx} - D_{55}^{ij} U_{j}) + \sum_{m=1}^{n-1} (E_{11}^{im} \tilde{S}_{m,xx} - E_{55}^{im} \tilde{S}_{m}) + \overline{B}_{11}^{l} w_{,xxx}$$

$$l = 0, 1, ..., n$$

$$- (B_{55}^{l} + \overline{B}_{55}^{l}) w_{,x} = 0$$

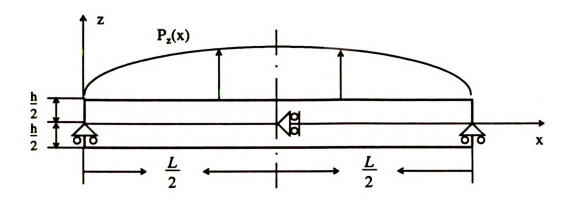
$$\sum_{j=0}^{n} (E_{11}^{jt} U_{j,xx} - E_{55}^{it} U_{j}) + \sum_{m=1}^{n-1} (F_{11}^{tm} \tilde{S}_{m,xx} - F_{55}^{tm} \tilde{S}_{m}) + \overline{C}_{11}^{l} w_{,xxx}$$

$$t = 1, 2, ..., n-1$$

$$- (C_{55}^{t} + \overline{C}_{55}^{t}) w_{,x} - \mu_{j_{k}} (Q_{55}^{j_{k}+1})^{2} (\tilde{S}_{j_{k}} + \frac{\partial w}{\partial x}) \delta_{j_{k}^{l}} = 0$$

$$j_{k} \in \Pi$$

In the above equations, \bar{B}_{11}^{j} , B_{55}^{j} , \bar{B}_{55}^{j} , \bar{C}_{11}^{m} , C_{55}^{m} , \bar{C}_{55}^{m} , D_{11}^{lj} , D_{55}^{lj} , E_{11}^{lm} , E_{55}^{lm} , F_{55}^{lm} , A_{55} ,



$$E_1 = 172 \text{ Gpa}, \qquad E_2 = E_3 = 6.89 \text{ Gpa}, \qquad G_{12} = G_{13} = 3.45 \text{ Gpa},$$

$$G_{23} = 1.38 \text{ Gpa}, \quad \text{and} \quad \upsilon_{12} = \upsilon_{13} = \upsilon_{23} = 0.25.$$

Figure 3.1 - Cylindrical bending of a laminated orthotropic beam.

 \overline{A}_{55} , γ_2 , $\overline{\gamma}_1$ and $\overline{\gamma}_2$ are the coefficients of laminate properties. They can be expressed as follows.

$$A_{55} = \sum_{j=1}^{n} \int_{z_{i-1}}^{z_{i}} Q_{55}^{(i)} dz; \qquad B_{55}^{j} = \sum_{j=1}^{n} \int_{z_{i-1}}^{z_{i}} Q_{55}^{(j)} \Phi^{j}_{,z} dz; \qquad C_{55}^{m} = \sum_{j=1}^{n} \int_{z_{i-1}}^{z_{i}} Q_{55}^{(j)} \tilde{\Psi}_{1,z}^{m} dz$$

$$\gamma_{2} = \sum_{j=1}^{n} \int_{z_{i-1}}^{z_{i}} Q_{55}^{(i)} \lambda_{1,z} dz; \qquad \tilde{\gamma}_{1} = \sum_{j=1}^{n} \int_{z_{i-1}}^{z_{i}} Q_{11}^{(i)} \lambda_{1,z}^{2} dz; \qquad \tilde{\gamma}_{2} = \sum_{j=1}^{n} \int_{z_{i-1}}^{z_{i}} Q_{55}^{(i)} \lambda_{1,z}^{2} dz$$

$$\bar{B}_{11}^{j} = \sum_{j=1}^{n} \int_{z_{i-1}}^{z_{i}} Q_{11}^{(i)} \Phi^{j} \lambda_{1} dz; \qquad \bar{C}_{55}^{m} = \sum_{j=1}^{n} \int_{z_{i-1}}^{z_{i}} Q_{11}^{(i)} \tilde{\Psi}_{1}^{m} \lambda_{1} dz; \qquad \bar{A}_{55} = \gamma_{2}$$

$$\bar{B}_{11}^{j} = \sum_{j=1}^{n} \int_{z_{i-1}}^{z_{i}} Q_{55}^{(i)} \Phi^{j}_{,z} \lambda_{1,z} dz; \qquad \bar{C}_{55}^{m} = \sum_{j=1}^{n} \int_{z_{i-1}}^{z_{i}} Q_{55}^{(i)} \tilde{\Psi}_{1,z}^{m} \lambda_{1,z} dz$$

$$D_{11}^{ij} = \sum_{j=1}^{n} \int_{z_{i-1}}^{z_{i}} Q_{11}^{(i)} \Phi^{i} \Phi^{j} dz; \qquad E_{15}^{im} = \sum_{j=1}^{n} \int_{z_{i-1}}^{z_{i}} Q_{11}^{(i)} \Phi^{i} \tilde{\Psi}_{1}^{m} dz$$

$$Q_{55}^{ij} = \sum_{j=1}^{n} \int_{z_{i-1}}^{z_{i}} Q_{55}^{(i)} \Phi^{j}_{,z} \Phi^{j}_{,z} dz; \qquad E_{55}^{im} = \sum_{j=1}^{n} \int_{z_{i-1}}^{z_{i}} Q_{55}^{(i)} \Phi^{j}_{,z} \tilde{\Psi}_{1,z}^{m} dz$$

$$F_{11}^{im} = \sum_{j=1}^{n} \int_{z_{i-1}}^{z_{i}} Q_{11}^{(i)} \tilde{\Psi}_{1}^{j} \tilde{\Psi}_{1}^{m} dz; \qquad F_{55}^{im} = \sum_{j=1}^{n} \int_{z_{i-1}}^{z_{i}} Q_{55}^{(i)} \tilde{\Psi}_{1,z}^{j} \tilde{\Psi}_{1,z}^{m} dz$$

Since the laminate of interest is simply supported at x = 0 and x = L, the boundary conditions can be expressed by the following equations.

$$w(0) = w(L) = 0; \overline{\lambda}_{x}(0) = \overline{\lambda}_{x}(L) = 0$$

$$N_{x}^{m}(0) = N_{x}^{m}(L) = 0 m = 0, 1, 2, ..., n$$

$$M_{x}^{m}(0) = M_{x}^{m}(L) = 0 m = 1, 2, ..., n - 1$$
(3.3)

For cylindrical bending, the loading is assumed to be of sinusoidal distribution, i.e.

$$P_x = P_0 \sin{(\beta x)} \tag{3.4}$$

where $\beta = \frac{\pi}{L}$. In order to satisfy the boundary conditions listed in Equation (3.3), the following displacement functions are assumed,

$$w = \underline{w} \sin (\beta x)$$

$$U_{j} = \underline{U}_{j} \cos (\beta x) \qquad j = 0, 1, 2, ..., n$$

$$\tilde{S}_{j} = S_{j} \cos (\beta x) \qquad j = 1, 2, ..., n - 1$$

$$(3.5)$$

where \underline{w} , \underline{U}_j and \underline{S}_j are coefficients to be determined. It is obvious that w satisfies the boundary conditions, i.e., w(0)=w(L)=0. The satisfaction of the remaining boundary conditions are also apparent. By expressing Equation (2.22) in terms of displacements, the following equations for force and moment resultants can be achieved.

$$\bar{\lambda}_{x} = \sum_{j=0}^{n} \bar{B}_{11}^{j} U_{1,x} + \sum_{j=1}^{n-1} \bar{C}_{11}^{j} \tilde{S}_{j,x} + \tilde{\gamma}_{1} w_{,xx}$$

$$N_{x}^{m} = \sum_{j=0}^{n} D_{11}^{mj} U_{1,x} + \sum_{j=1}^{n-1} E_{11}^{mj} \tilde{S}_{m,x} + \bar{B}_{11}^{m} w_{,xx}$$

$$M_{x}^{m} = \sum_{j=0}^{n} E_{11}^{mj} U_{1,x} + \sum_{j=1}^{n-1} F_{11}^{mj} \tilde{S}_{m,x} + \bar{C}_{11}^{m} w_{,xx}$$

$$(3.6)$$

It is clear that Equations (3.6) are of sine functions and satisfy the boundary conditions listed in Equation (3.3). Therefore, Equation (3.5) can be a set of solution to the governing equations, Equation (3.1). By substituting Equation (3.5) into Equation (3.1), it then results in

$$\begin{bmatrix} \underline{U}_{j} \\ \vdots \\ S_{m} \\ \vdots \\ \underline{Y} \end{bmatrix} = \begin{bmatrix} P_{0} \\ \overline{\beta} \\ 0 \\ \vdots \\ 0 \\ \vdots \\ \vdots \end{bmatrix}$$

$$l = 0, 1, ..., n$$

$$t = 1, 2, ..., n - 1$$

where

$$\kappa_1 = \sum_{k=1}^{n_1} \mu_{j_k} (Q_{55}^{j_k+1})^2; \qquad \kappa_2 = \mu_{j_k} (Q_{55}^{j_k+1})^2 \delta_{j_k t} \qquad j_k \in \Pi$$

The solution of Equation (3.7) gives the coefficients of the displacement function defined in Equation (3.5). The closed-form solution for the cylindrical bending of a cross-ply laminate with various interfacial bonding conditions can be achieved.

3.2 Embedded-layer Approach

Another method to study composite laminates with nonrigidly bonded interfaces is to introduce embedded layers on the composite interfaces. The controversy of this method is the determination of the thickness and the material properties of the embedded layer. In this study, the thickness of the embedded layer \bar{h} is assumed to be 0.0764 mm [53]. Since only the shear slip is considered, it is possible to simulate the nonrigid bonding by adjusting the transverse shear modulus G_{13} . The finite element method presented in [54] is used to study the deformation of the composite laminates with embedded layers. The numerical results are shown in a following section.

Although the interlayer shear slip theory and the embedded-layer technique are derived from different bases, a relation between them can be found by assuming that an embedded thin layer undergoes a pure shear deformation. As shown in Figure 3.2, 'ABCD' becomes 'abcd' due to a shear stress τ acting on the layer. The displacement field of the layer can be written as follows

$$x = X + \tan(\alpha_i) Z$$

 $z = Z$ $i = 1, if Z > 0; i = 2, if Z < 0$ (3.8)

where x and z represent for the coordinates in the deformed configuration while X and Z the undeformed configuration. Thus, τ can be expressed as

$$\tau = G_{13}^{(1)} \tan (\alpha_1) = G_{13}^{(2)} \tan (\alpha_2). \tag{3.9}$$

In addition, the difference between the displacements at $z=\overline{h}/2$ and $z=-\overline{h}/2$ can also be identified as

$$u(x, \frac{\bar{h}}{2}) - u(x, -\frac{\bar{h}}{2}) = [\tan(\alpha_1) - \tan(\alpha_2)] (\bar{h}/2). \tag{3.10}$$

If the embedded layer is thin enough to simulate the real interface, the difference described in Equation (3.10) can be regarded the same as the interlayer shear slip defined in Equation (2.5a). Accordingly, the relation between the embedded-layer approach and the interlayer shear slip theory is

$$\mu = \frac{\bar{h}}{2} \left(\frac{G_{13}^{(1)} + G_{13}^{(2)}}{G_{12}^{(1)} G_{22}^{(2)}} \right). \tag{3.11}$$

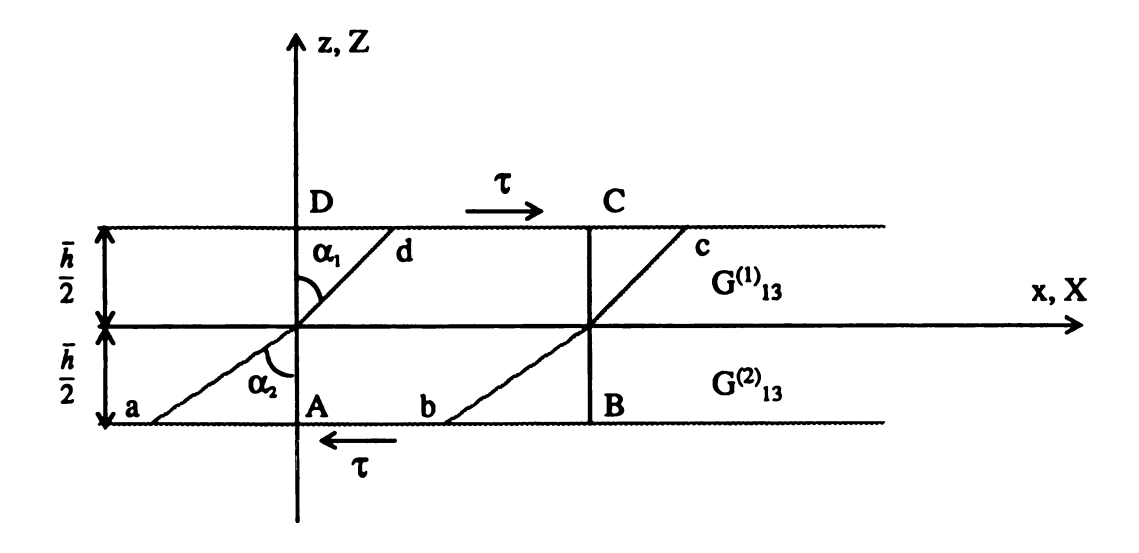


Figure 3.2 - Pure shear deformation in embedded layer.

This equation can help to compare the resultants from the two approaches and provide the fundamental information for assessing the interlayer shear slip theory.

3.3 Results and Discussions

In order to assess the accuracy of the interlayer shear slip theory in composite analysis, the cylindrical bending of [0/0], [0/90], and [0/90/0] laminates with various interfacial bonding conditions is investigated. The numerical results are summarized in the following sections with the nondimensional terms as introduced by Pagano [1].

$$\bar{\sigma}_{x} = \frac{\sigma_{x}(\frac{L}{2}, z)}{P_{0}} \qquad \bar{\tau}_{xy} = \frac{\tau_{xy}(0, z)}{P_{0}} \qquad \bar{u} = \frac{E_{2}u(0, z)}{hP_{0}}$$

$$\bar{w} = \frac{100h^{3}E_{2}w(\frac{L}{2})}{L^{4}P_{0}} \qquad \bar{z} = \frac{z}{h}$$
(3.12)

3.3.1 Rigidly Bonded Laminates

A. Transverse Deflection

By setting v = 0 for Equation (3.7), the closed-form solutions for perfectly bonded laminates under cylindrical bending can be obtained. The transverse deflection, \overline{w} , at the midspan of the laminates is shown in Figure 3.3 as a function of aspect ratio (S=L/h). Apparently, the results from the present theory agree quite well with those from the exact solutions [1] in both large and small aspect ratios. In order to further compare the results from both techniques, the numerical solutions for all three types of cross-ply laminate are listed in Table 3.1. In this study, three values of S, i.e., 4, 20, and 100, which represent for thick, intermediate, and thin laminates, are presented. Besides, three layer numbers are

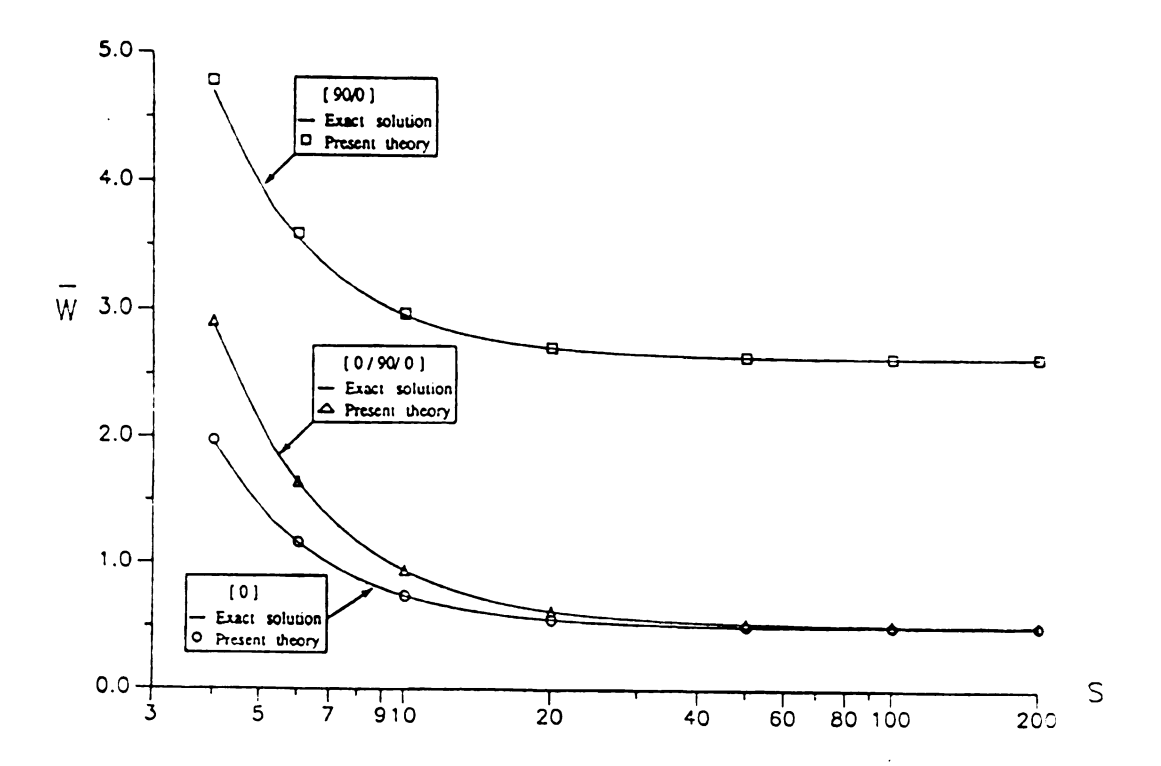


Figure 3.3 - Normalized maximum deflection as a function of aspect ratio S.

Table 3.1 - Comparison of numerical results between elasticity analysis and present theory.

	S	Pagano's	present theory		
		solutions	2-layer	4-layer	6-layer
[0/0]	4	1.9490	1.9672	1.9659	1.9659
	20	.5519	.5523	.5523	.5523
	100	.4940	.4940	.4940	.4940
[0/90]	4	4.6953	4.7773	4.7812	4.7812
	20	2.7027	2.7069	2.7069	2.7069
	100	2.6222	2.6230	2.6220	2.6220
[0/90/0]	4	2.8868			2.9098
	20	.6172			.6176
	100	.5140			.5140

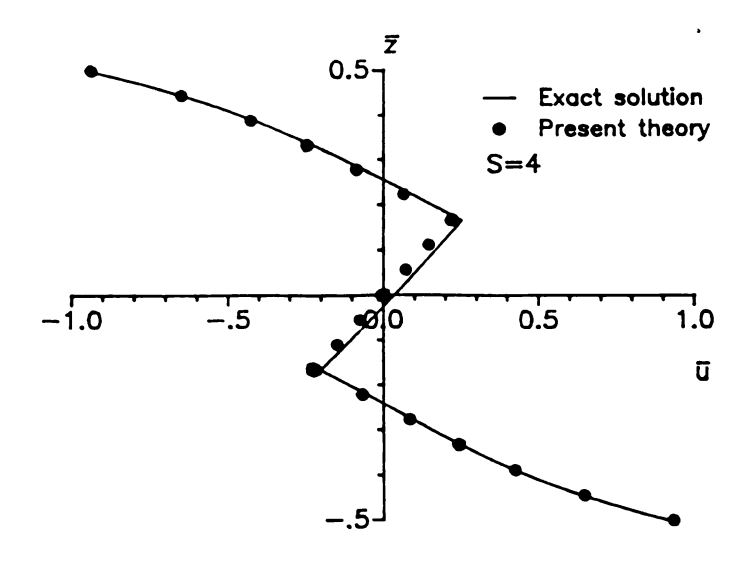
investigated to study the effect of layer number on the numerical accuracy. From the results in Table 3.1, it is concluded that the present theory gives excellent results of transverse deflection in all three types of lamination although the results in the laminates with lager aspect ratio seem to be more accurate. However, the increase in the layer number does not cause any significant effect on the results.

B. Symmetric Laminate [0/90/0]

Other than [0/0] laminates, [0/90/0] symmetric laminates with S=4 and S=10 are also investigated. The results of in-plane displacement, in-plane stress, and transverse shear stress based on a 6-layer model are shown in Figures 3.4, 3.5, and 3.6, respectively. Excellent agreements between the present theory and the elasticity analysis are concluded although a noticeable difference between the two techniques exists around the middle surface of the in-plane displacement in the case of S=4. It is believed that this is due to the assumption of constant transverse deflection in the present theory. In fact, just because of the constant displacement assumption, the distributions of both in-plane displacement and stress from the present theory are anti-symmetric to the middle surface while the interlaminar shear stress is symmetric.

C. Asymmetric Laminate [90/0]

Both S=4 and S=10 for a [90/0] asymmetric laminate are studied. Excellent results are again concluded. The results are shown in Figures 3.7, 3.8, and 3.9, for in-plane displacement, in-plane stress, and transverse shear stress, respectively.



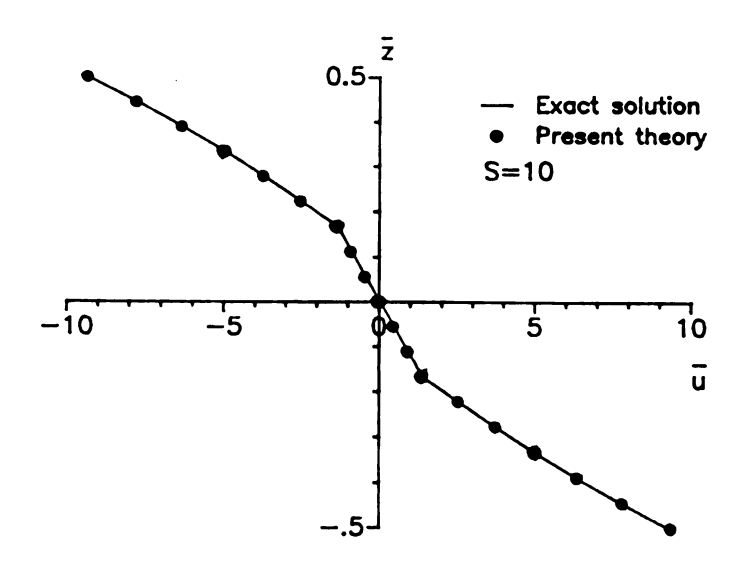
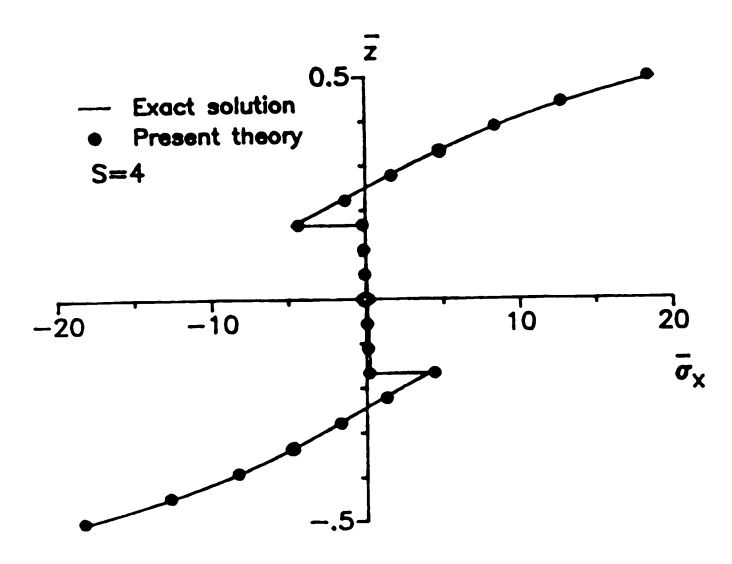


Figure 3.4 - Comparison of \overline{u} between elasticity analysis and present theory for a [0/90/0] laminate.



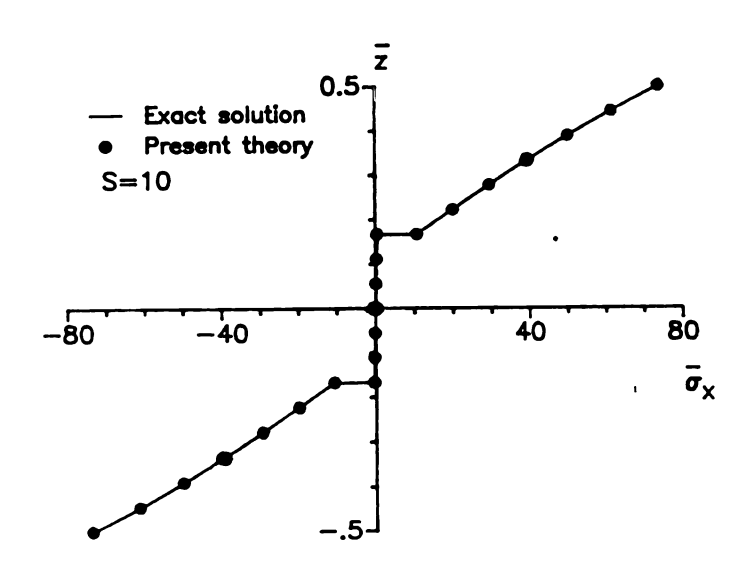
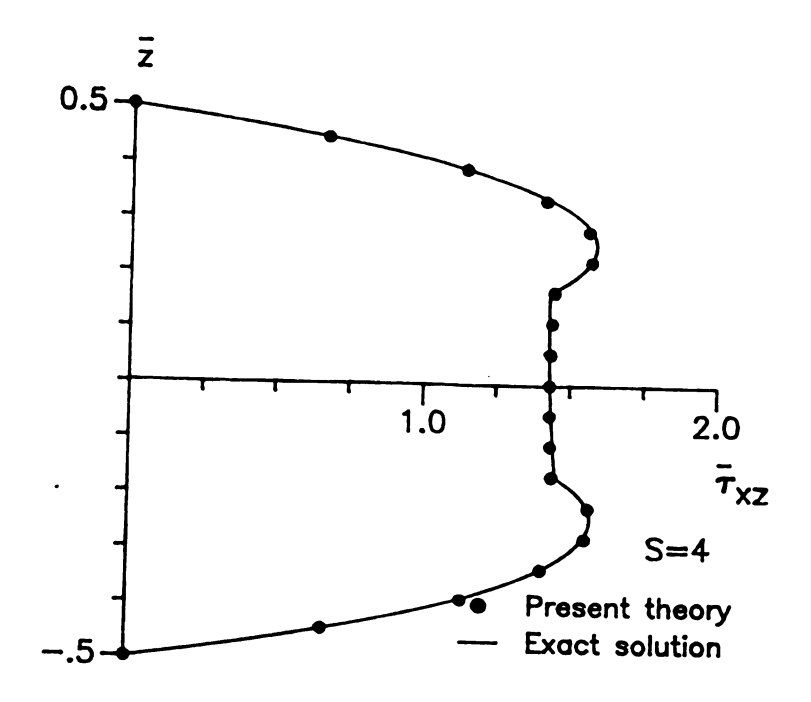


Figure 3.5 - Comparison of $\overline{\sigma}_x$ between elasticity analysis and present theory for a [0/90/0] laminate.



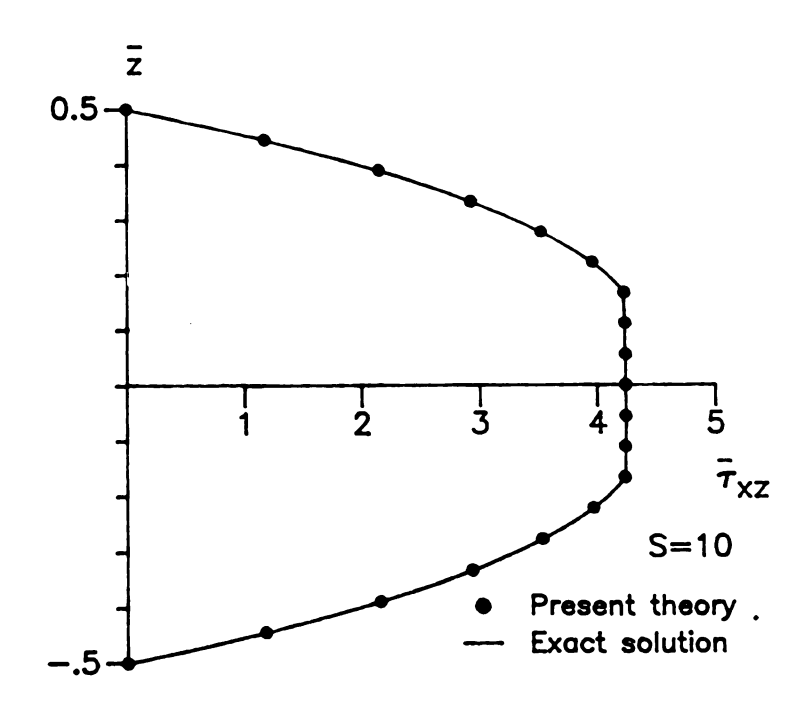
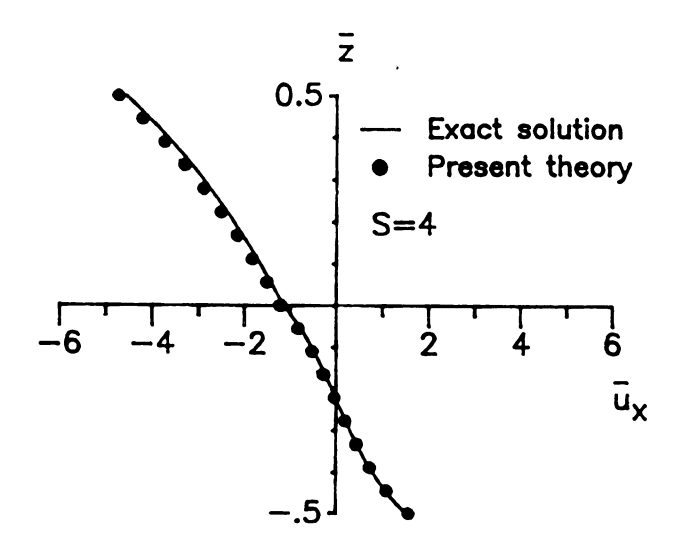


Figure 3.6 - Comparison of $\bar{\tau}_{xz}$ between elasticity analysis and present theory for a [0/90/0] laminate.



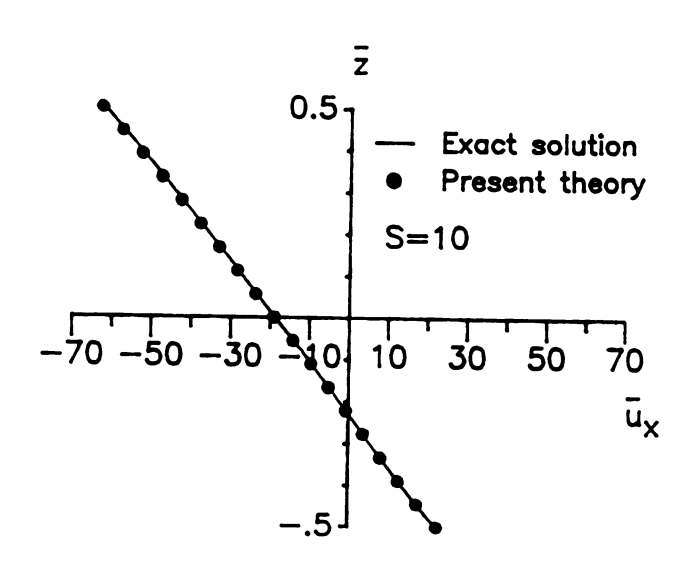
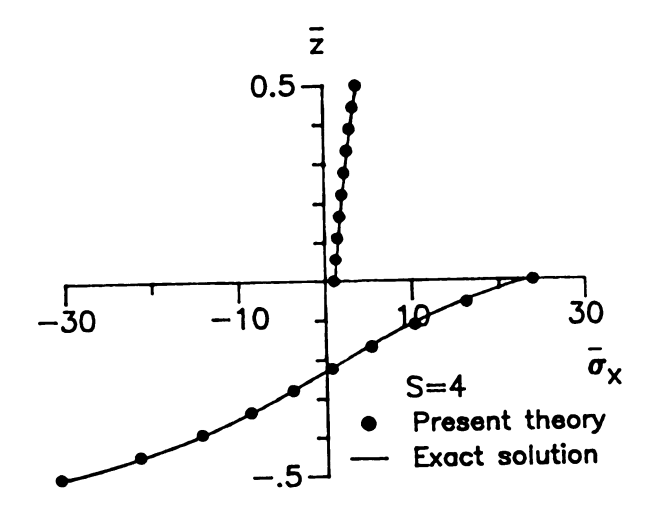


Figure 3.7 - Comparison of \overline{u} between elasticity analysis and present theory for a [90/0] laminate.



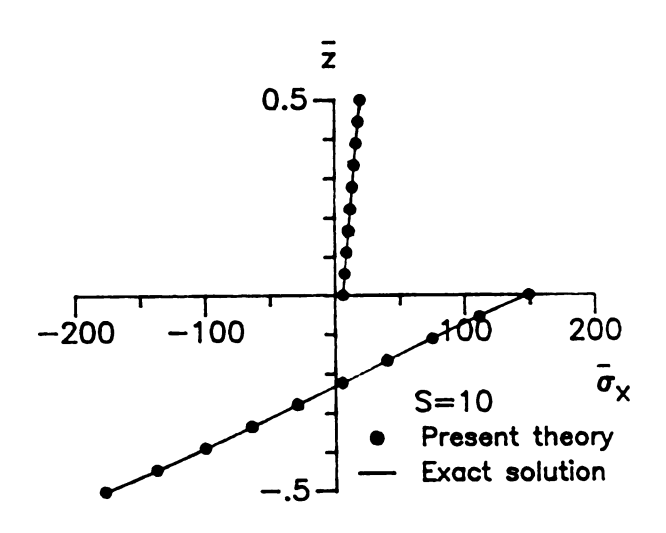
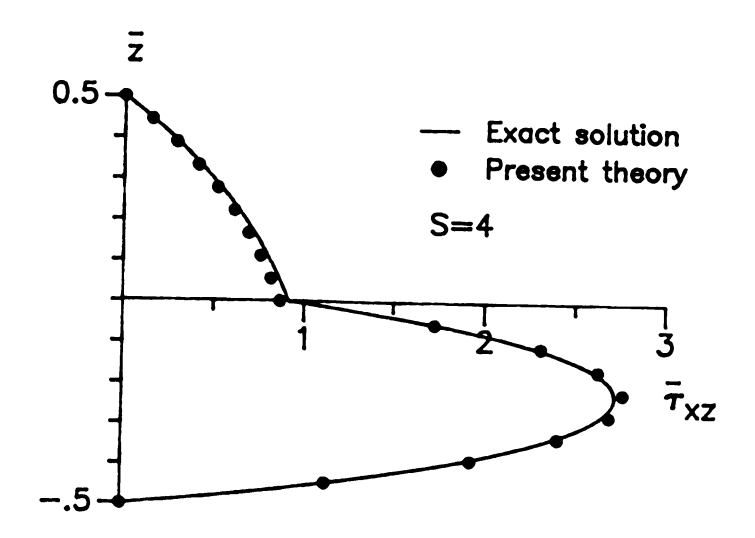


Figure 3.8 - Comparison of $\overline{\sigma}_x$ between elasticity analysis and present theory for a [90/0] laminate.



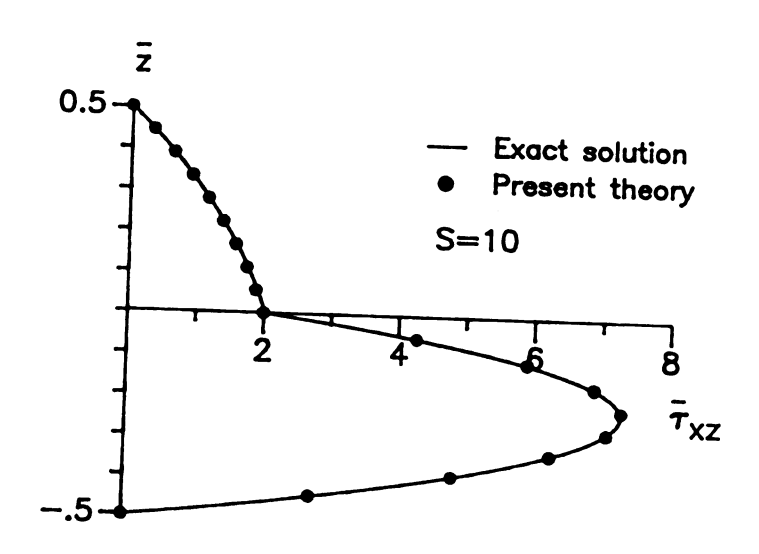


Figure 3.9 - Comparison of $\bar{\tau}_{xx}$ between elasticity analysis and present theory for a [90/0] laminate.

3.3.2 Nonrigidly Bonded Laminates

A. [0/0] Laminates with Nonrigid Interface on Midplane

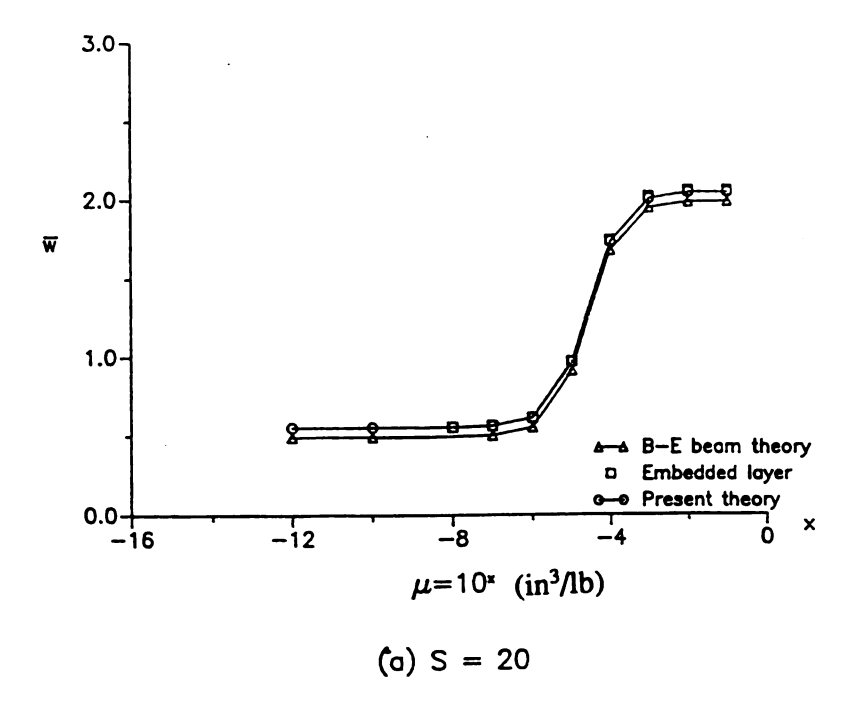
[0/0] composite laminates with a nonrigid interface on the midplane are studied. The numerical results from the closed-form solution, Equation (3.7) are summarized below with the use of nondimensional terms defined in Equation (3.12)

a. transverse shear effect

The maximum deflections calculated from different approaches are presented in Figure 3.10 as a function of interfacial shear bonding coefficient μ for both S=4 and S=20. The approach of Bernoulli-Euler beam theory can be referred to Reference [33]. It is concluded that the results from the interlayer shear slip theory (ISST) are close to those from Bernoulli-Euler beam theory when S=20. However, the difference between them is very significant for S=4. This difference is apparently due to the transverse shear effect. In addition, the results from the embedded-layer technique are very close to those from ISST for both S=4 and 20. It verifies that it is feasible to use ISST to study composite laminates with nonrigid bonding. Furthermore, it may imply that the analysis used to find the relation between ISST and embedded-layer approach is acceptable.

b. bonding coefficient

As shown in Figure 3.10, the maximum deflection reaches an upper limit as μ approaches one while lower limit as μ goes to zero. The former corresponds to a completely debonded interface while the latter a rigidly bonded interface. It is verified that the deflections from ISST are very close to those obtained in the previous section for perfectly bonded laminates. The investigation of complete debonding is performed with μ =10⁻¹ in this study. In addition, it is concluded from Figure 3.10 that the deflection changes dramatically



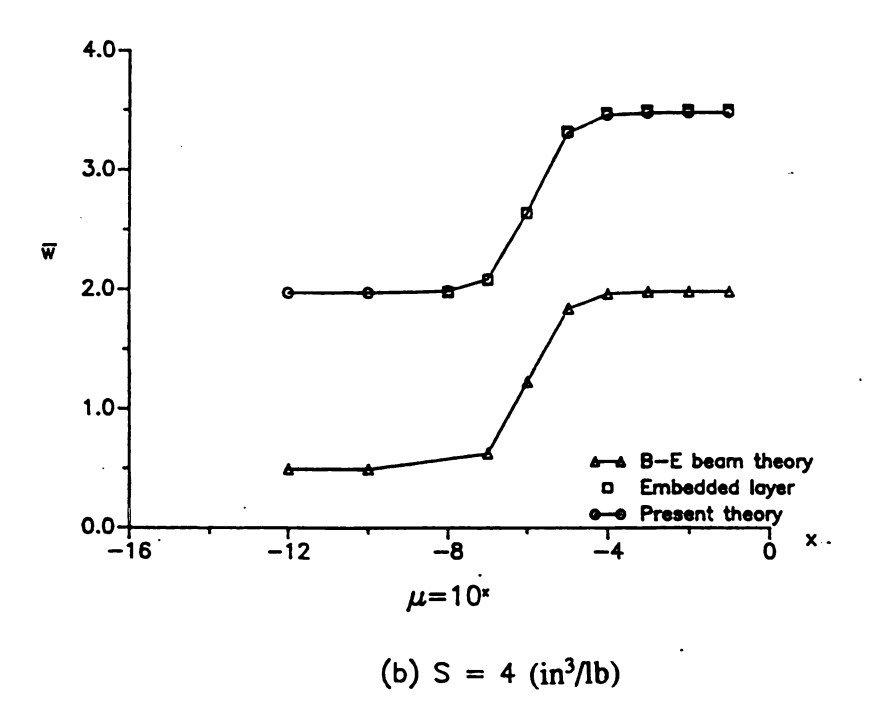


Figure 3.10 - Maximum deflections of [0/0] laminates as functions of bonding coefficients.

within a small range of μ . This implies that nonrigid bonding can have a significant effect on the deflection when the interfacial shear bonding approaches a 'critical' range. However, beyond the 'critical' range, the composite laminate will quickly lose its integrity and behave like two independent layers with a lubricated interface [38]. This phenomenon has also been reported in Reference [38] though the result beyond the 'critical' range are not presented in details. In addition, it needs to point out that the 'critical' range seems to change as the material property or geometry changes.

c. maximum stresses

Figure 3.11, 3.12, and 3.13 represent for the distributions of in-plane stress, transverse shear stress, and in-plane displacement as functions of interfacial shear bonding coefficient μ for S=4 and 20. The solid lines represent for the results from Reference [1] for rigidly bonded laminates while the dash lines from ISST for different shear bonding coefficients. By setting μ =10⁻¹⁰, the results from ISST are very close to those from Reference [1].

From these diagrams, it is also concluded that the in-pane normal stress becomes larger and larger as the bonding gets less and less rigid. For μ =10⁻⁵ and 10⁻¹, the maximum normal stresses increase 27% and 97% in S=20 laminates, respectively, while 25% and 56% in S=4 laminates, respectively. In addition, the maximum transverse shear stress for S=20 is always smaller than that of rigid bonding. However, the maximum value for S=4 with nonrigid bonding can exceed the value of rigid bonding. This is another evidence indicating the important role of the transverse shear effect in thick laminate analysis. Besides, the results seem to further verify the conclusion from Reference [38] that the damage in a composite laminate with nonrigid bonding can take place earlier than the prediction from the analysis based on rigid bonding assumption.

In addition, it is shown in Figure 3.12 that the delaminated interface, i.e., $\mu=10^{-1}$, has no ability to carry any shear stress but the nonrigid interface, e.g. $\mu=10^{-5}$, can transfer

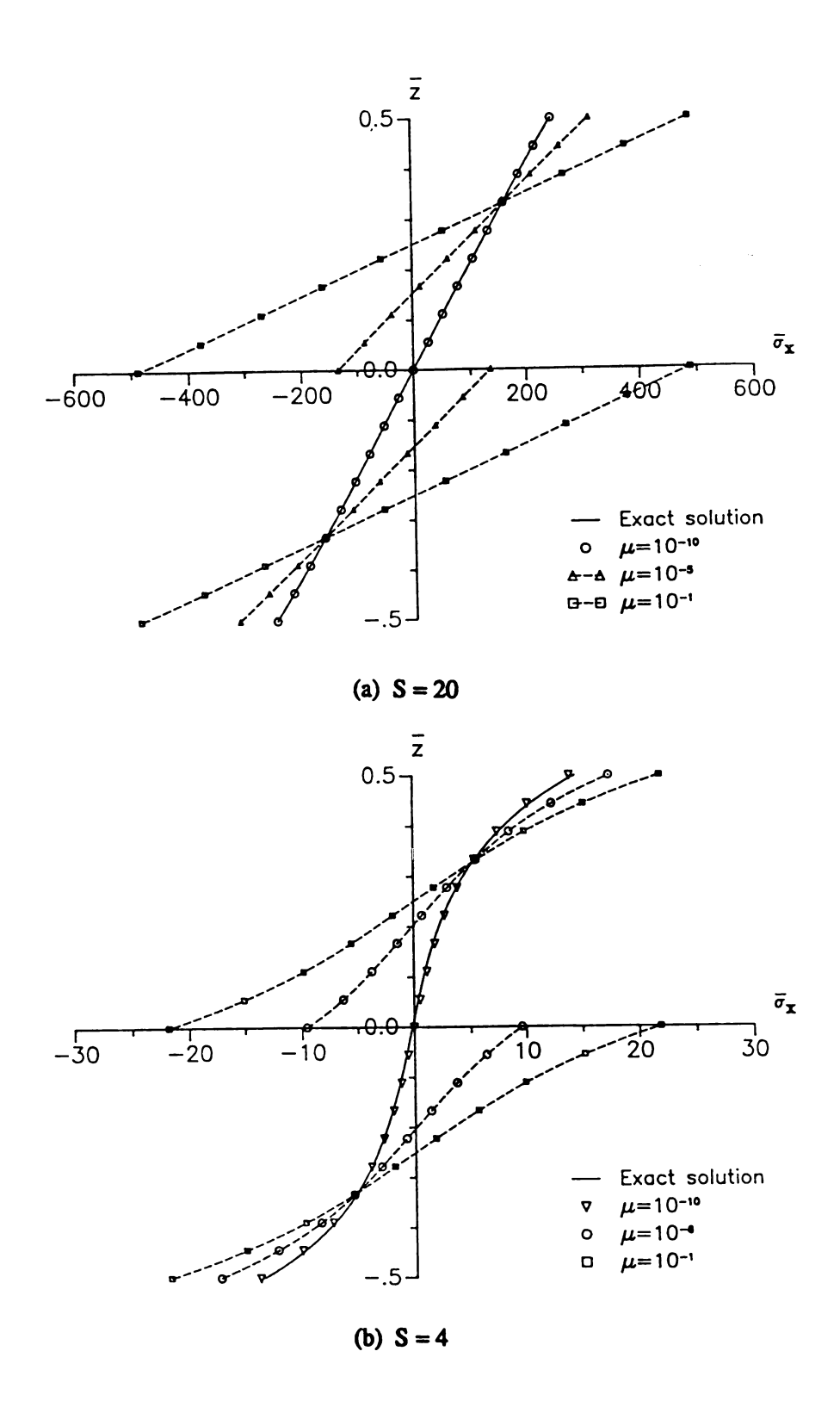


Figure 3.11 - In-plane normal stresses through the thickness in [0/0] laminates.

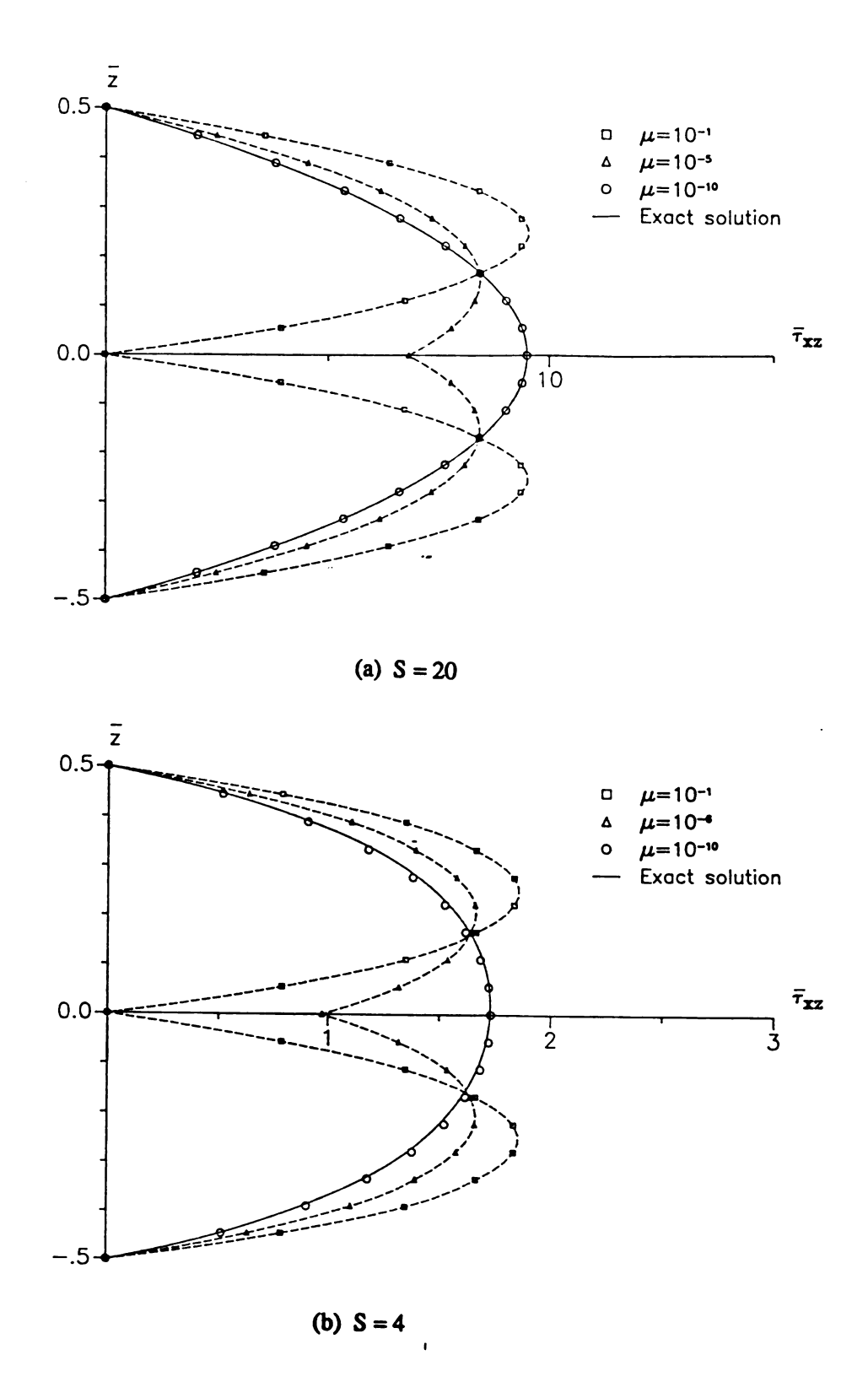


Figure 3.12 - Transverse shear stresses through the thickness in [0/0] laminates.

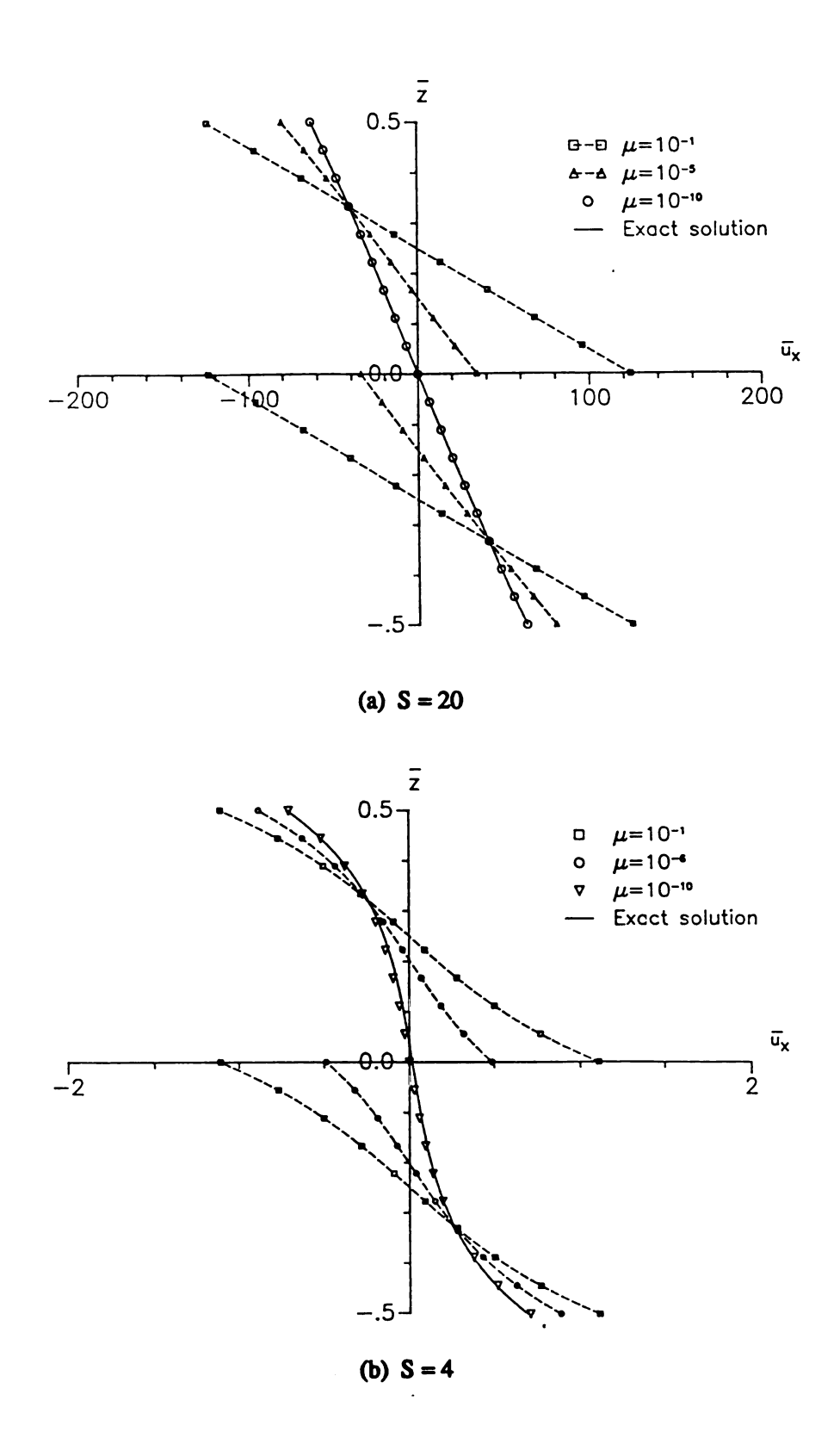


Figure 3.13 - In-plane displacements through the thickness in [0/0] laminates.

shear stress up to some extend.

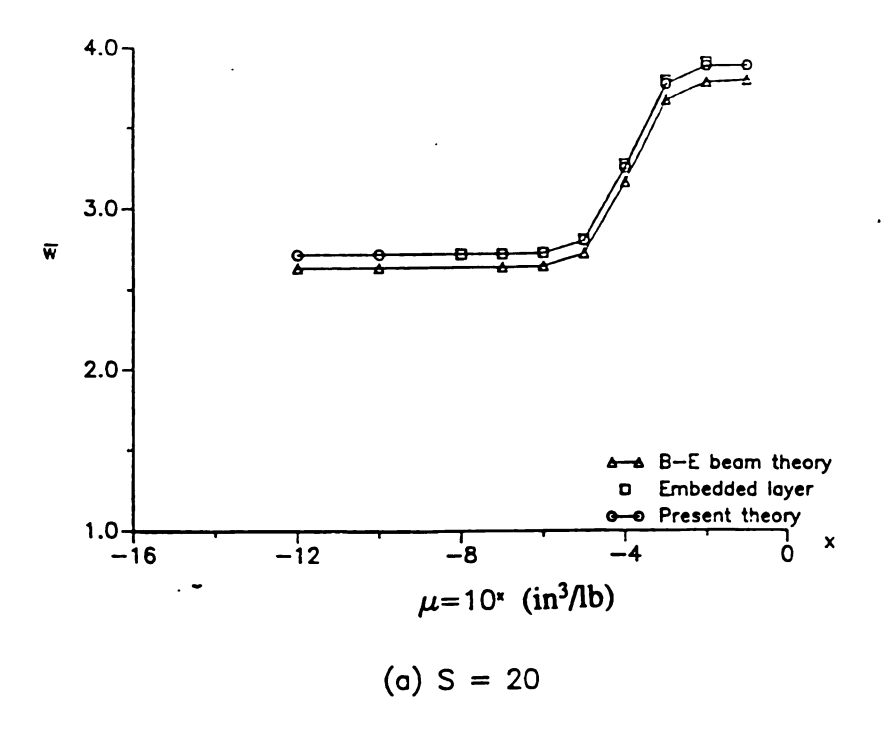
d) singular points

It is interesting to point out that there are four singular (persistent) points in which the normal stress (or in-plane displacement) and the interlaminar shear stress remain to be constants even though the bonding condition changes. The locations of these singular points are near $z=\pm h/3$ for both in-plane normal stress and displacement while around $z=\pm h/6$ for transverse shear stress. A careful discussion about these points is given in Appendix. It is believed that these singular points have special interest for composite laminates with embedded sensors.

B. [90/0] Laminates with Nonrigid Interface on Midplane

The numerical results for [90/0] laminates with nonrigidly bonded interface on the middle plane are shown from Figure 3.14 to Figure 3.17. For maximum deflections, similar conclusions as obtained in [0/0] analysis can be drawn. By comparing the results from the present theory with those from Bernoulli-Euler beam approach, it is concluded again that the shear effect is very important in the study of composite laminates with nonrigidly bonded interface, especially in thick composite laminate analysis. Besides, the results of transverse deflection, in-plane stress and displacement, and transverse shear stress from ISST for both S=4 and S=20 are very close to those given in the rigid bonding analysis when μ =10⁻¹⁰. It concludes that the results from ISST converge to the results from the perfect bonding analysis as μ approaches to 0.

For both S=4 and S=20 laminates, the maximum values of in-plane normal stress and interlaminar shear stress increase as the bonding gets less and less rigid. For μ =10⁻⁴ and μ =10⁻¹, the increases of the maximum normal stress in S=20 laminates are about 15% and 34%, respectively, while the increases of the maximum shear stress are around 11%



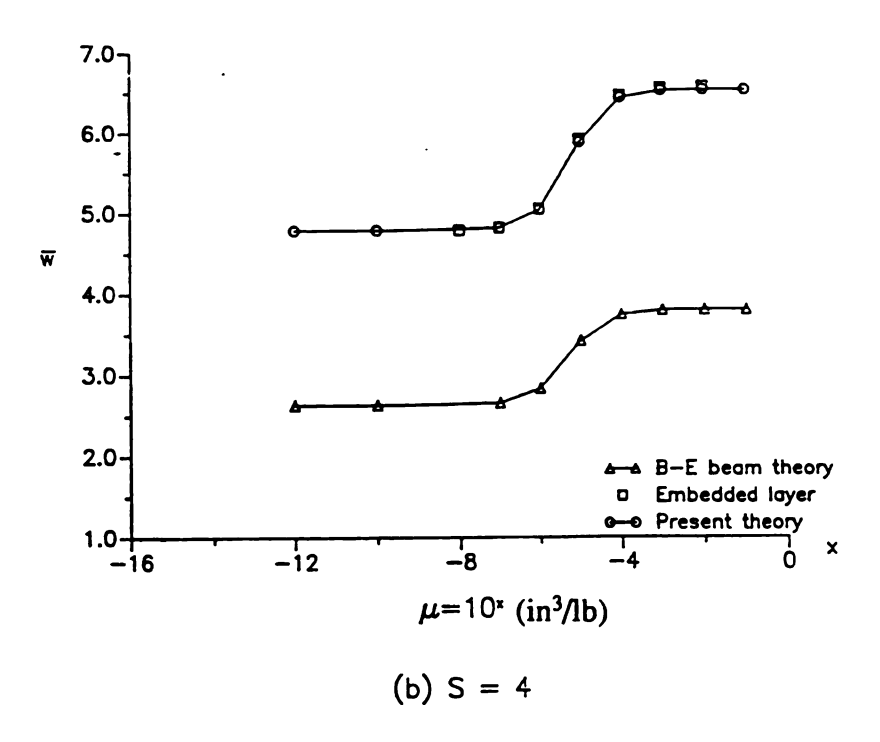


Figure 3.14 - Maximum deflections of [90/0] laminates as functions of bonding coefficient.

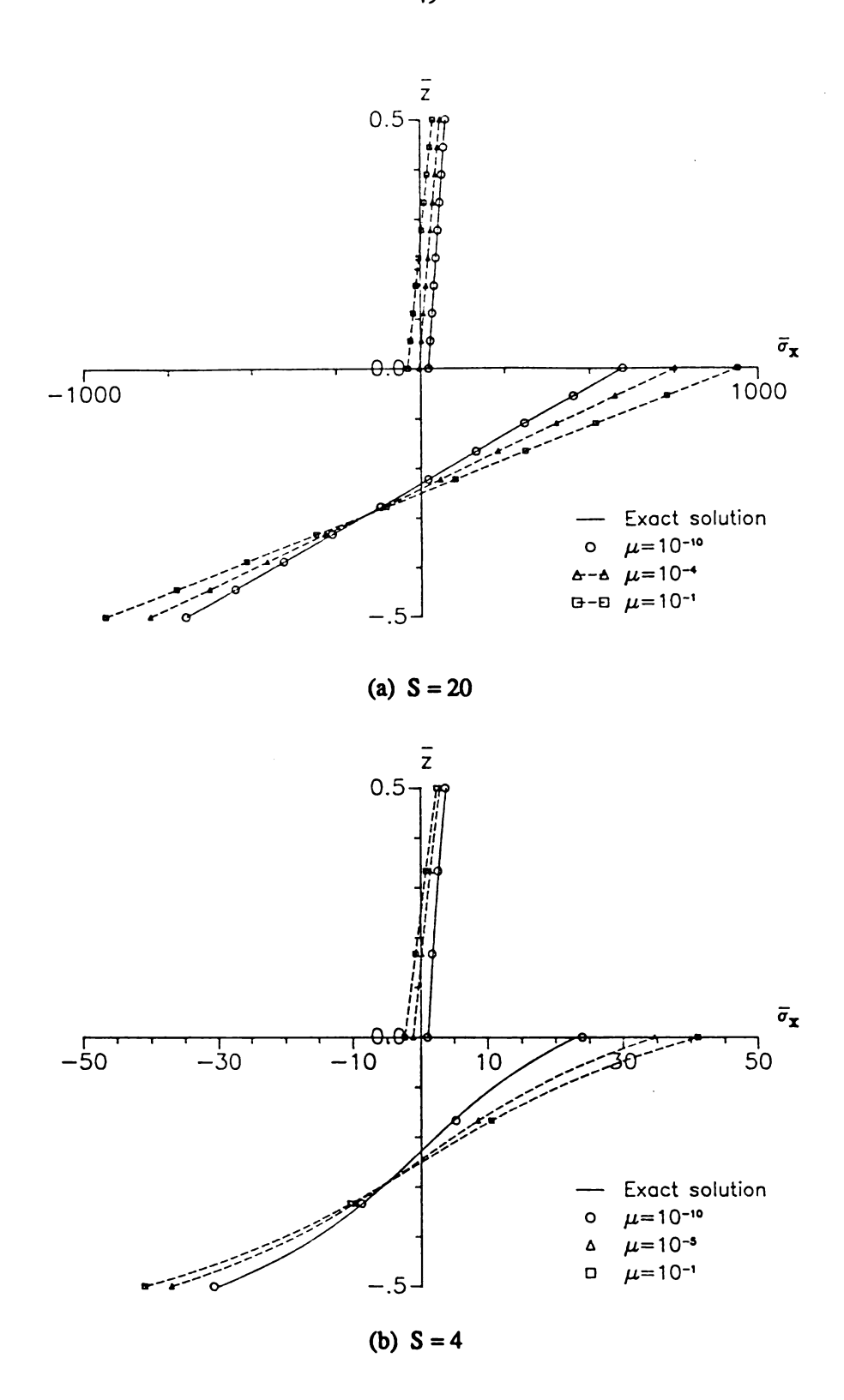


Figure 3.15 - In-plane normal stresses through the thickness in [90/0] laminates.

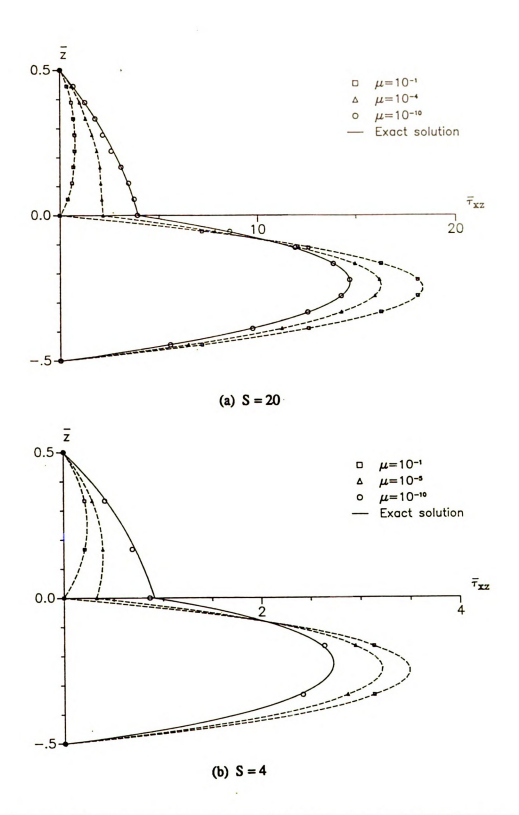


Figure 3.16 - Transverse shear stresses through the thickness in [90/0] laminates.

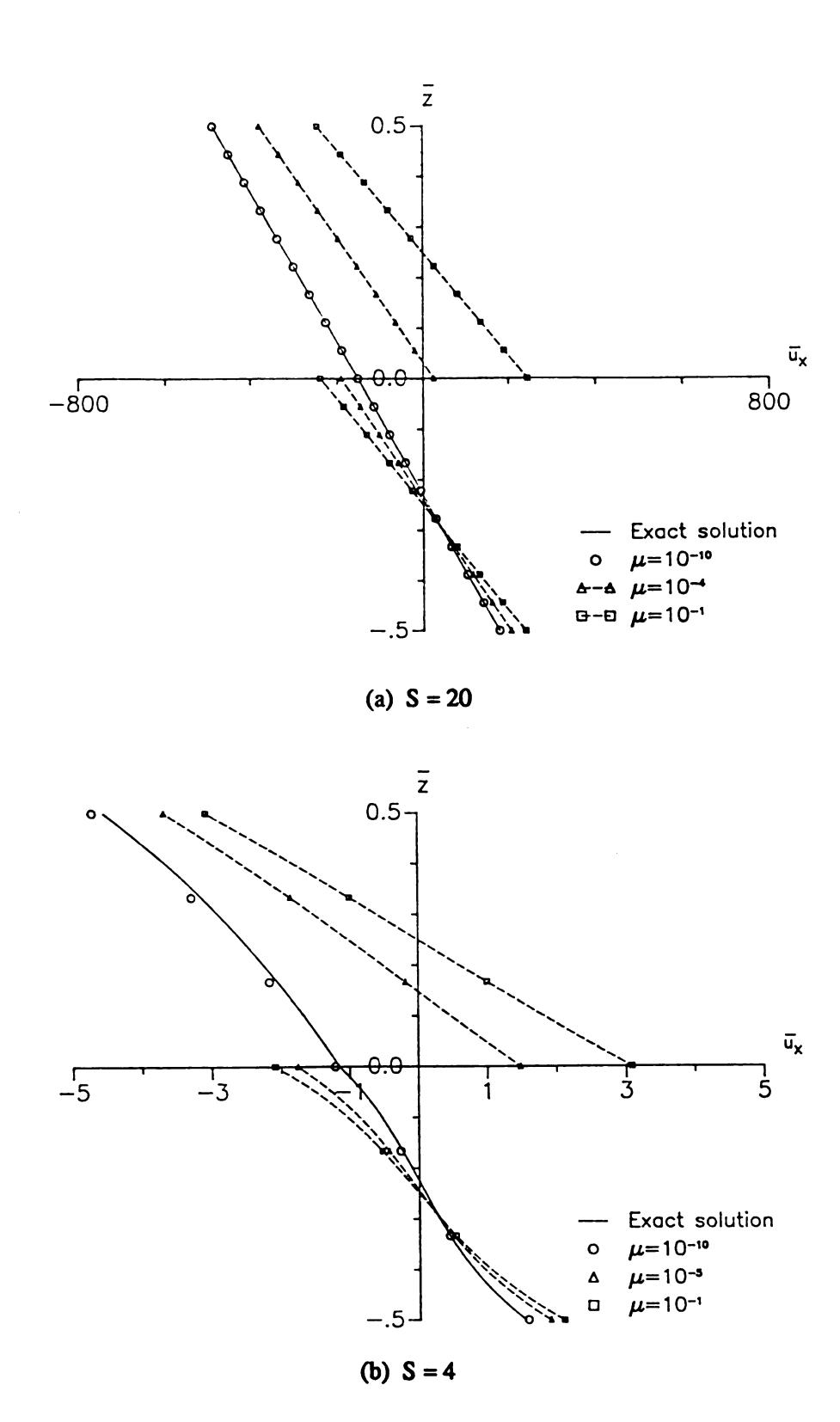
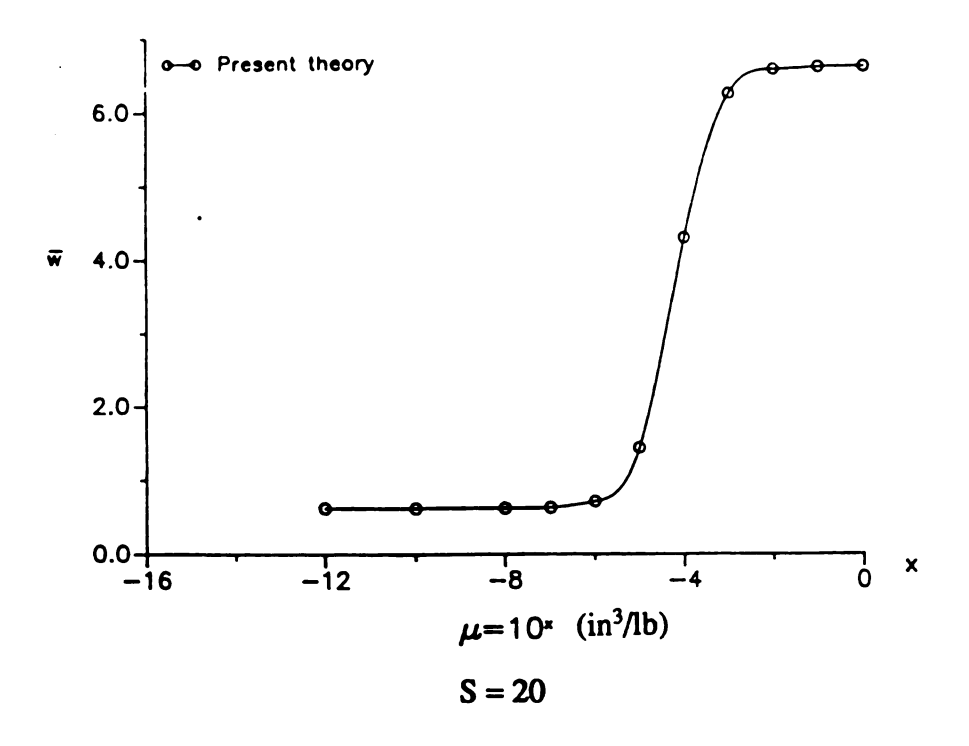


Figure 3.17 - In-plane displacement through the thickness for [90/0] laminates.

and 24%, respectively. In addition, it can be verified from Figure 3.16 that the resultant shear force is independent of bonding coefficient μ . However, there are only two singular points which are both located in 0 layers. For both in-plane normal stress and displacement, it is around z=-0.29 h while near z=-0.09 h for transverse shear stress.

C. [0/90/0] Laminates with Nonrigid Interfaces

[0/90/0] composite laminates with two nonrigid interfaces are also studied. One nonrigid interface is between 0 and 90 layers and the other 90 and 0 layers. In this analysis, it is assumed that both interfaces have the same nonrigidity. The numerical results of the maximum deflection and stress distributions are shown from Figure 3.18 to Figure 3.21. Similar conclusions as obtained for [0/0] and [90/0] laminates about the effects of nonrigid bonding on the maximum deflection and stress distributions can be drawn. It is interesting to find that there are two singular points in each 0 layer for the normal stress and the interlaminar shear stress, respectively. No singular point is found in 90 layer.



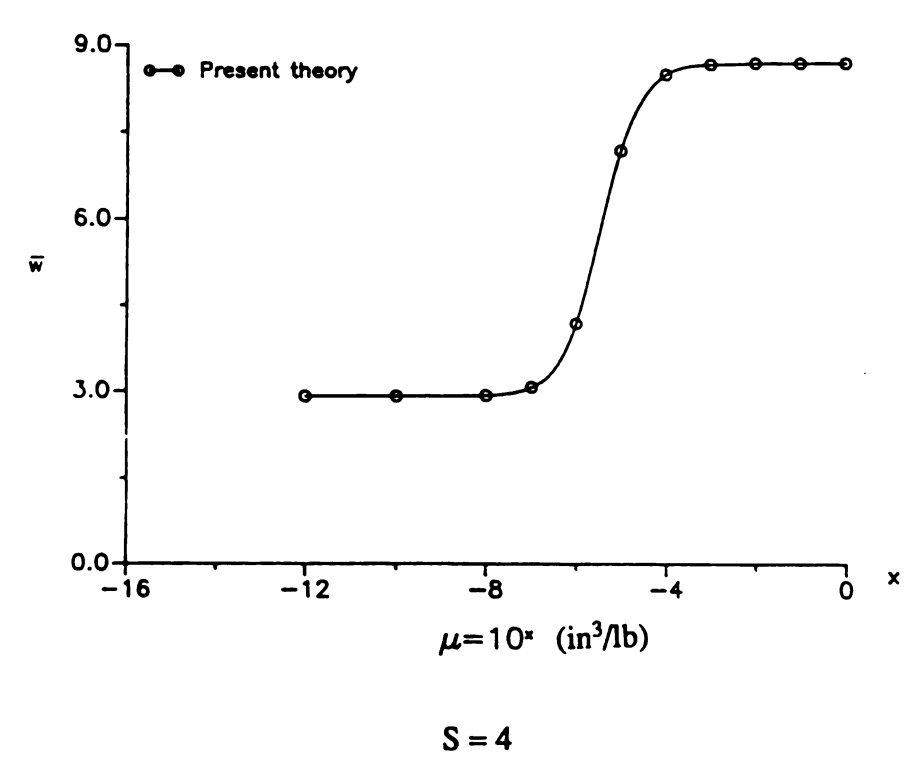
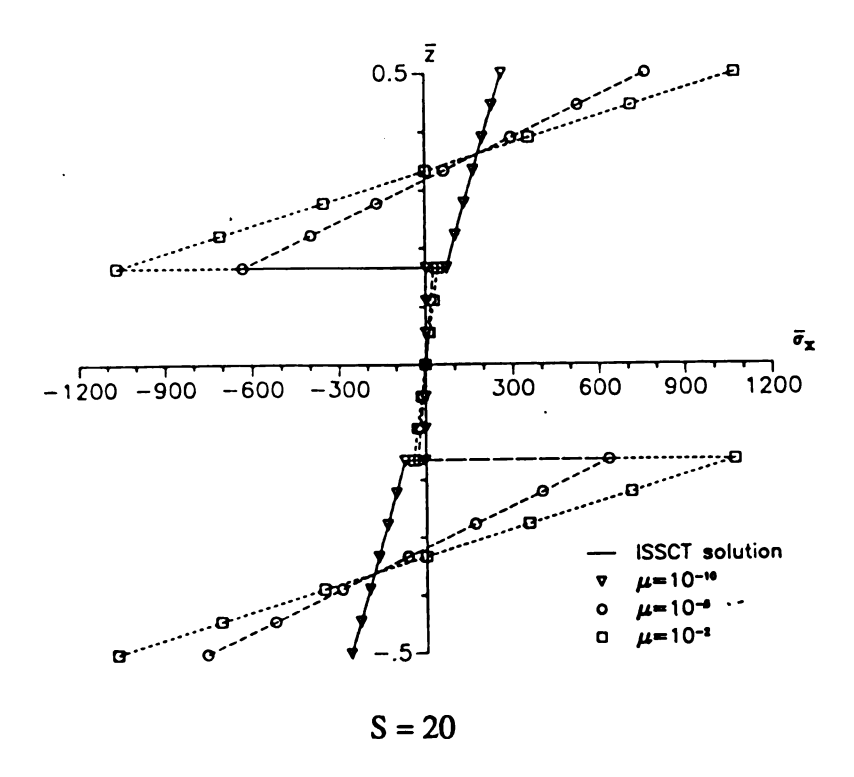


Figure 3.18 - Maximum deflections of [0/90/0] laminates as functions of bonding coefficients.



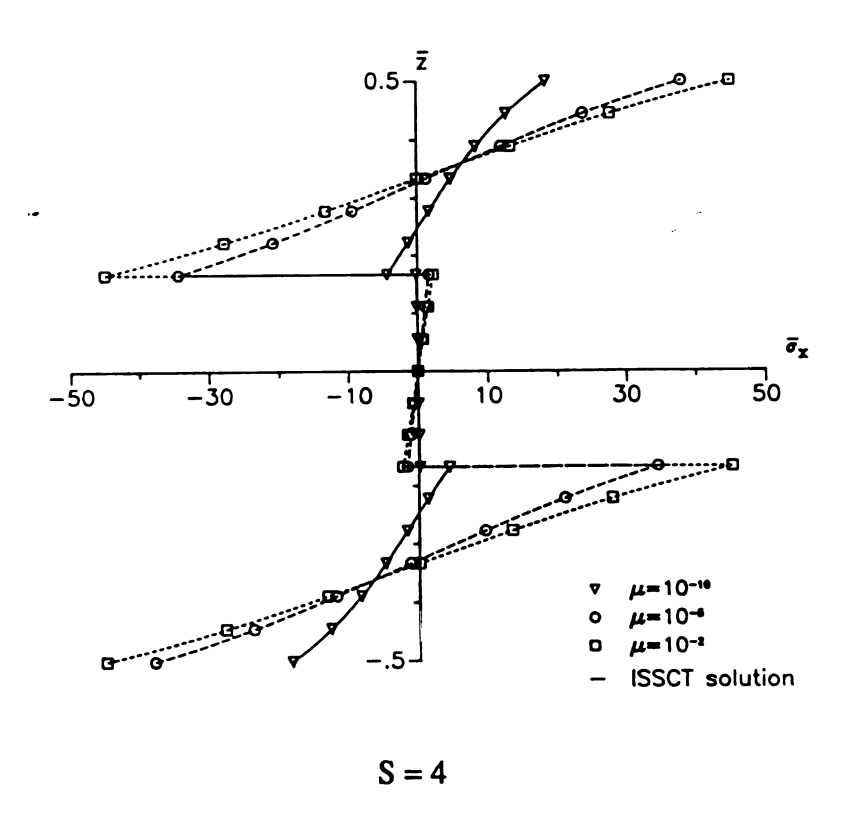
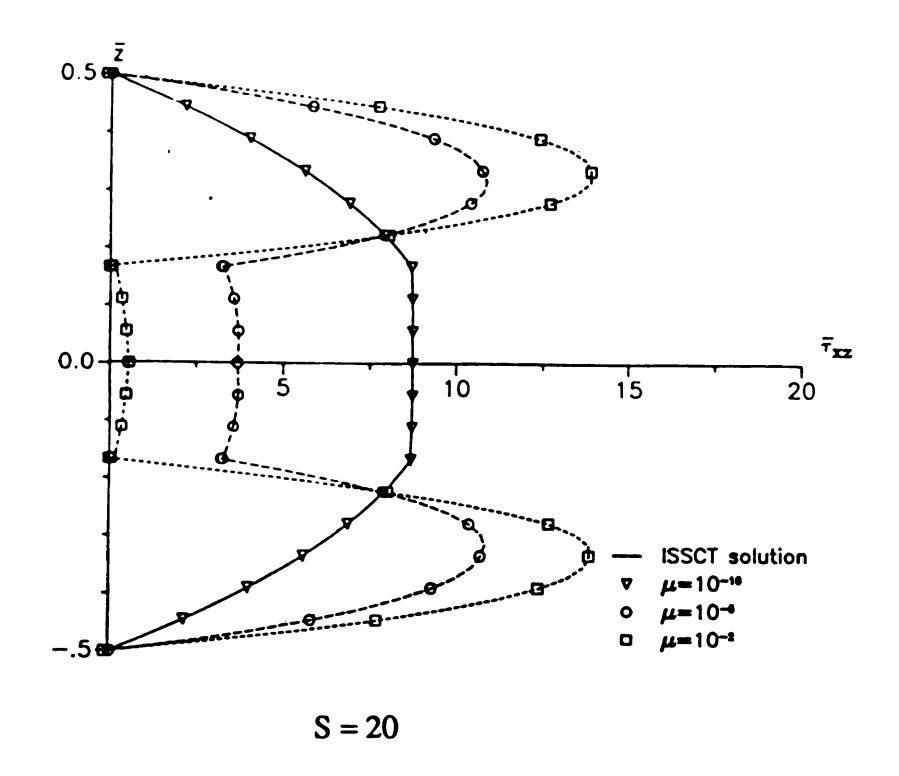


Figure 3.19 - In-plane normal stresses through the thickness in [0/90/0] laminates.



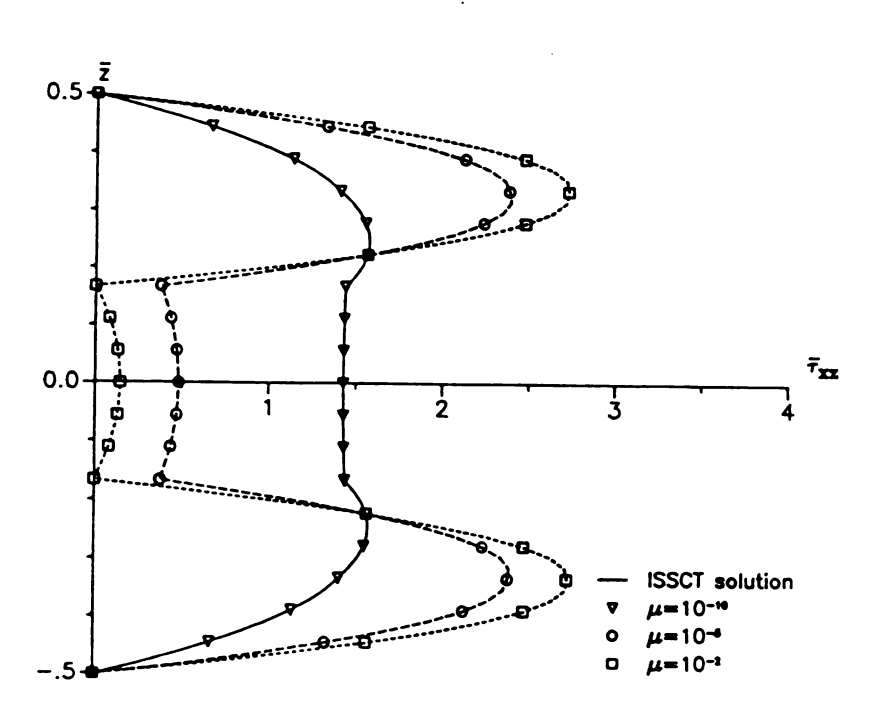
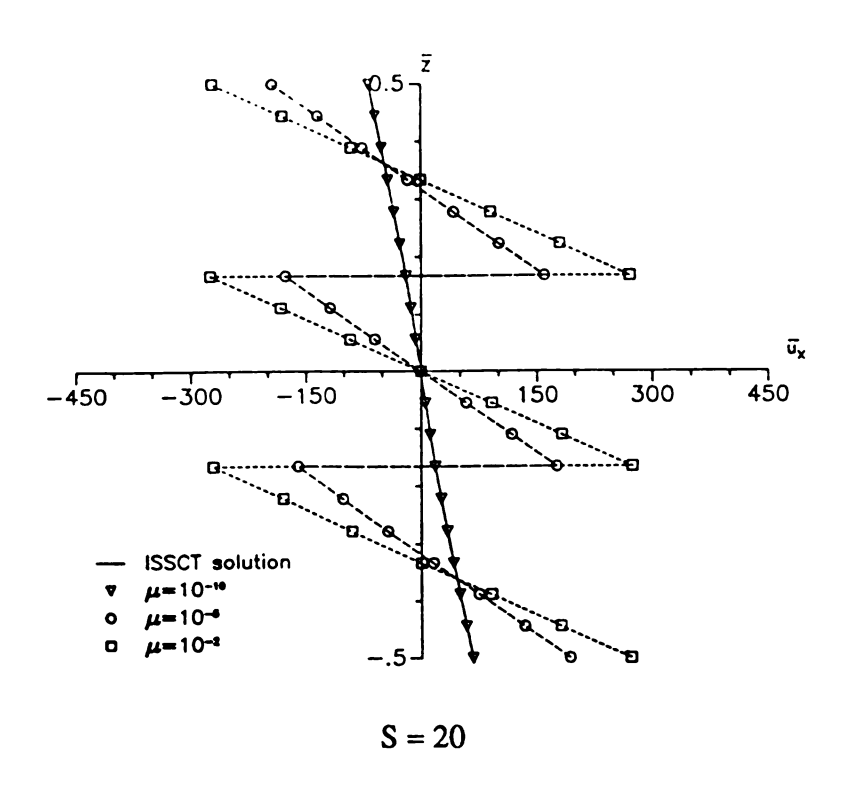


Figure 3.20 - Transverse shear stresses through the thickness in [0/90/0] laminates.

S = 4



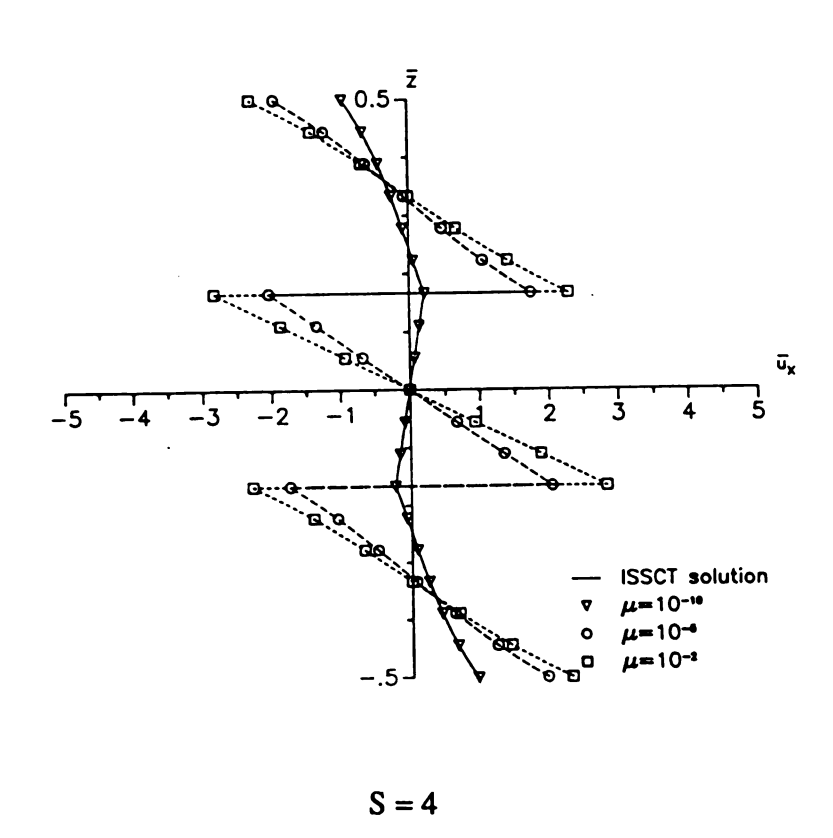


Figure 3.21 - In-plane displacements through the thickness in [0/90/0] laminates.

Chapter 4

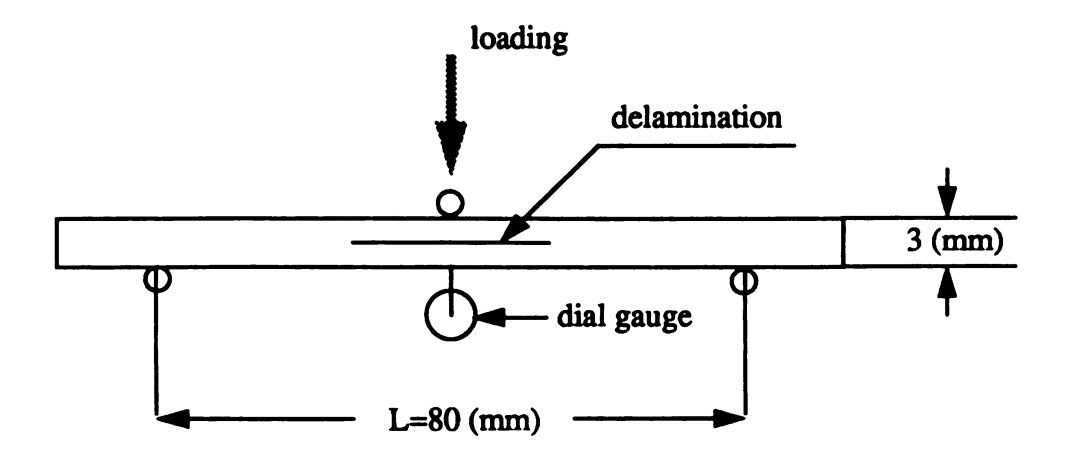
EXPERIMENTAL VERIFICATIONS

4.1 Test Setup and Specimen Preparation

In order to verify the ISST, the following two types of test are performed, one is three-point bend test and the other is free-free vibration test. Both tests are performed for laminated beams with a central delamination on the midplane.

4.1.1 Three-point Bend Test

The test is performed with an Instron materials testing machine. The test setup is shown in Figure 4.1. Specimens of stacking sequence of $[0_6/0_6]$ are fabricated from 3M's glass/epoxy prepreg tapes. The specimens are cured at 160° C (320° F) and 350 KPa (50 psi) for 45 minutes. The effective dimensions of the specimens are 80 mm x 25.4 mm x 3 mm while the artificial central delamination has length either 25.4 mm or 50.8 mm. The delamination is achieved by embedding two layers of teflon film on the midplane. The composite beams are then subjected to three-point bend with the maximum loading of 0.3 kN. The central deflection of the composite beams are measured at the bottom surface of the beams with a dial gauge. It is observed that the maximum deflections are around 1.8 mm which is within the range of small deflection assumption. The material constants are given in Figure 4.1. The experimental results are normalized with the deflection of a composite beam without delamination and are shown in the Table 4.1 and Figure 4.2.



$$E_{11} = 38.6 \text{ Gpa}, \ E_{22} = E_{33} = 8.27 \text{ Gpa}, \ G_{12} = G_{13} = 4.14 \text{ Gpa}$$

$$G_{23} = 3.22 \text{ Gpa}, \ \nu_{12} = \nu_{13} = 0.21, \ \nu_{23} = 0.28$$

Figure 4.1 - Three-point bending test.

Table 4.1 - Central deflections of glass/epoxy beams from three-point bending test.

Specimen No.	Central Deflection (mm)				
	no delamination	25.4 mm delamination	50.8 mm delamination		
No. 1	1.792	1.842	1.854		
No. 2	1.787	1.812	1.858		
No. 3	1.854	1.793	1.908		
No. 4	1.761	1.801	1.971		
No. 5	1.830	1.762	1.923		
Mean	1.8048	1.802	1.9028		
Standard deviation	1 0.0509 1 0.0291		0.0487		

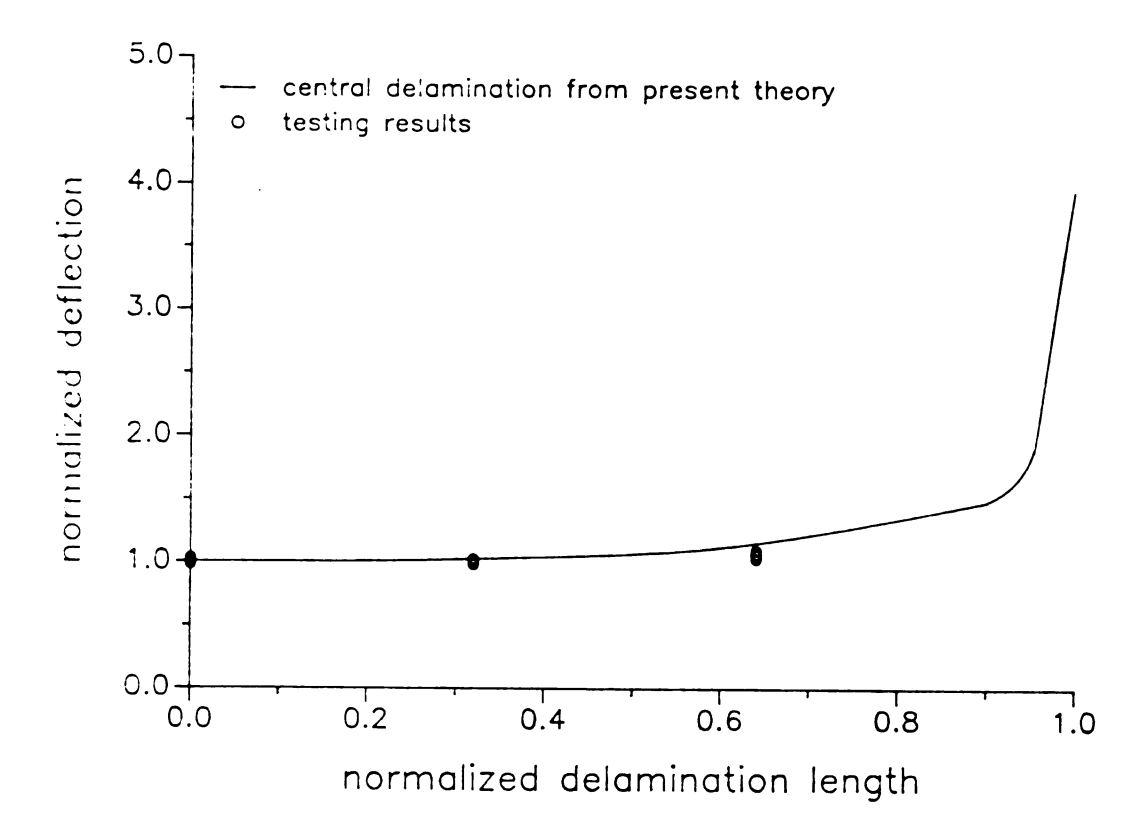


Figure 4.2 - Normalized central deflections of a glass/epoxy beam with a central midplane delamination of different lengths.

4.1.2 Free-free Vibration

Two types of specimen are employed in the vibration test. One is the same glass/epoxy beams as used in three-point bend test. The other is pure glass beams with artificially central delamination. More specifically, the beams are made from two pieces of microglass and bonded together by super glue. By carefully adjusting the bonding area, different lengths of central delamination can be achieved. The dimensions for both types of specimens are given in Figure 4.3. The testing employed to study the effect of delamination on vibration frequency is called resonant frequency measurement method. It is an ASTM standard method designated by C 848-78. Figure 4.4 depicts an overall diagram of the setup. The natural frequencies for the first and second bending modes are measured for both types of specimens. The results are shown in Tables 4.2 and 4.3 and Figures 4.5 and 4.6.

4.2 Analytical Solutions

To verify the testing results, a finite element scheme for ISST is developed for both static and vibration analysis.

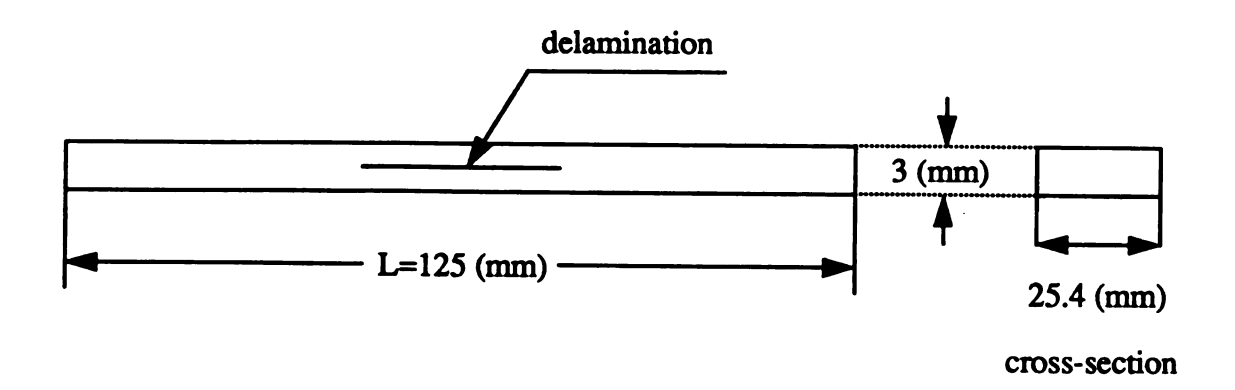
4.2.1 Static Analysis

The total potential energy of a composite beam with nonrigid interfaces can be written as

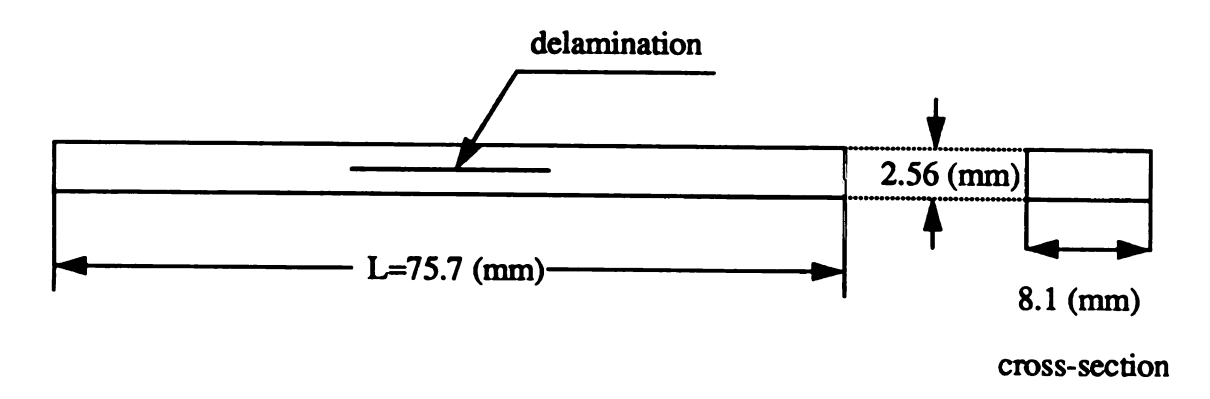
$$\overline{W} = \int_{\Omega} \left\{ \int_{-\frac{h}{2}}^{\frac{h}{2}} \left[\frac{1}{2} \sigma_{x} \varepsilon_{x} + \frac{1}{2} \tau_{xz} \gamma_{xz} - P_{z} w \right] dz + \sum_{i=1}^{n} \frac{1}{2} T_{i} \Delta U_{i} \right\} dA$$

$$(4.1)$$

After considering the continuity requirements on the composite interfaces and assuming μ to be constant in a section of interest along x-direction, the strain components in layer (i) can



a) glass/epoxy beam specimen



E = 70.7 Gpa, G = 43 Gpa, and v = 0.185

b) glass beam specimen

Figure 4.3 - The dimensions of specimens for free-free vibration test.

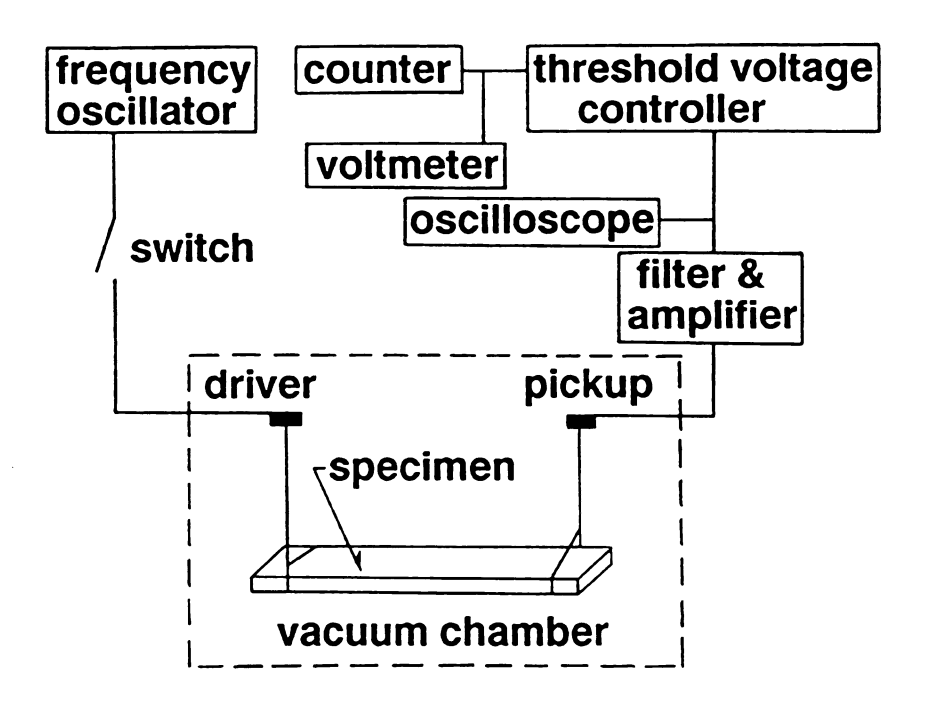


Figure 4.4 - Block diagram of the apparatus for resonance frequency measurement.

Table 4.2 - Natural frequencies of glass/epoxy beams from free-free vibration test

	vibration t				
Natural Frequency (Hz)					
Specimen No.	mode 1	mode 2	mode 1 (torsion)	Comment	
0 - 1	849	2321	1307	No delamination	
0 - 2	847	2309	1253	No delamination	
0 - 3	822	2210	1281	No delamination	
0 - 4	860	2350	1301	No delamination	
0 - 5	847	2286	1290	No delamination	
Mean	845	2296	1286		
Standard deviation	13.95	52.92	21.18		
1 - 1	828	2221	1288	25.4 mm delamination	
1 - 2	848	2293	1328	25.4 mm delamination	
1 - 3	846	2265	1290	25.4 mm delamination	
1 - 4	852	2290	1314	25.4 mm delamination	
1-5	863	2321	1314	25.4 mm delamination	
Mean	847	2278	1307		
Standard deviation	12.68	37.54	17.24		
2 - 1	842	2251	1305	50.8 mm delamination	
2 - 2	864	2281	1329	50.8 mm delamination	
2 - 3	822	2210	1306	50.8 mm delamination	
2 - 4	810	2185	1280	50.8 mm delamination	
2 - 5	820	2210	1276	50.8 mm delamination	
Mean	832	2227	1299		
Standard deviation	21.51	38.19	21.65		

Table 4.3 - Natural frequencies of glass beams from free-free vibration test.

Specimen	Natural Frequency (Hz)				
No.	mode 1 mode 2		Comment		
1	1232 3366		One layer specimen		
2	1234	3370	One layer specimen		
Specimens 1 and 2	2466	6376	No delamination		
bonded together	1241	3338	75.7 mm delamination		
oonada togoana	2375	3918	38 mm delamination		
3	1215	3326	One layer specimen		
4	1217	3324	One layer specimen		
Specimens 3 and 4	2432	6650	No delamination		
bonded together	1272	3294	75.7 mm delamination		
bonded together .	2013	3977	57 mm delamination		
5	1209	3305	One layer speciemn		
6	1210	3303	One layer specimen		
Specimens 5 and 6 bonded together	2420	6608	No delamination		
	1217	3304	75.7 mm delamination		
	2412		7.6 mm delamination		

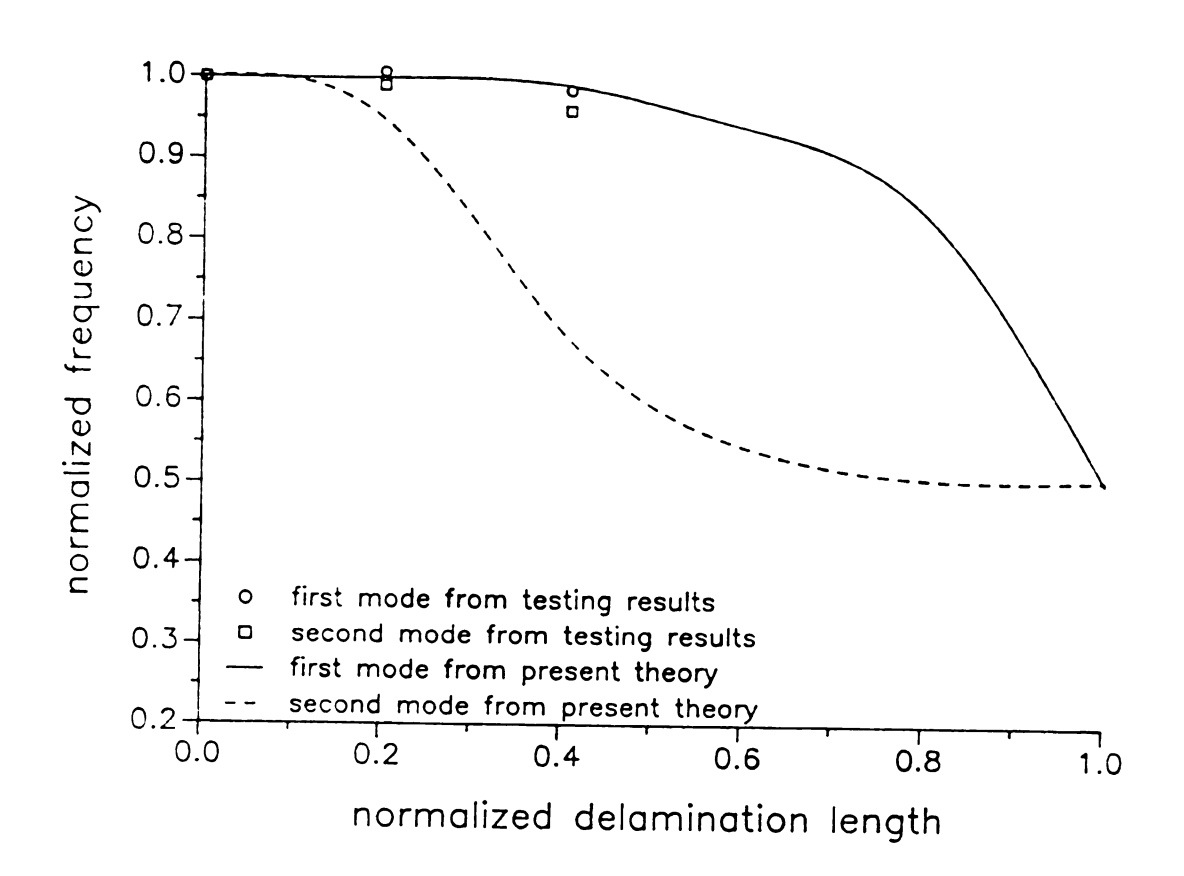


Figure 4.5 - Normalized natural frequencies of a glass/epoxy beam with a central midplane delamination of various lengths.

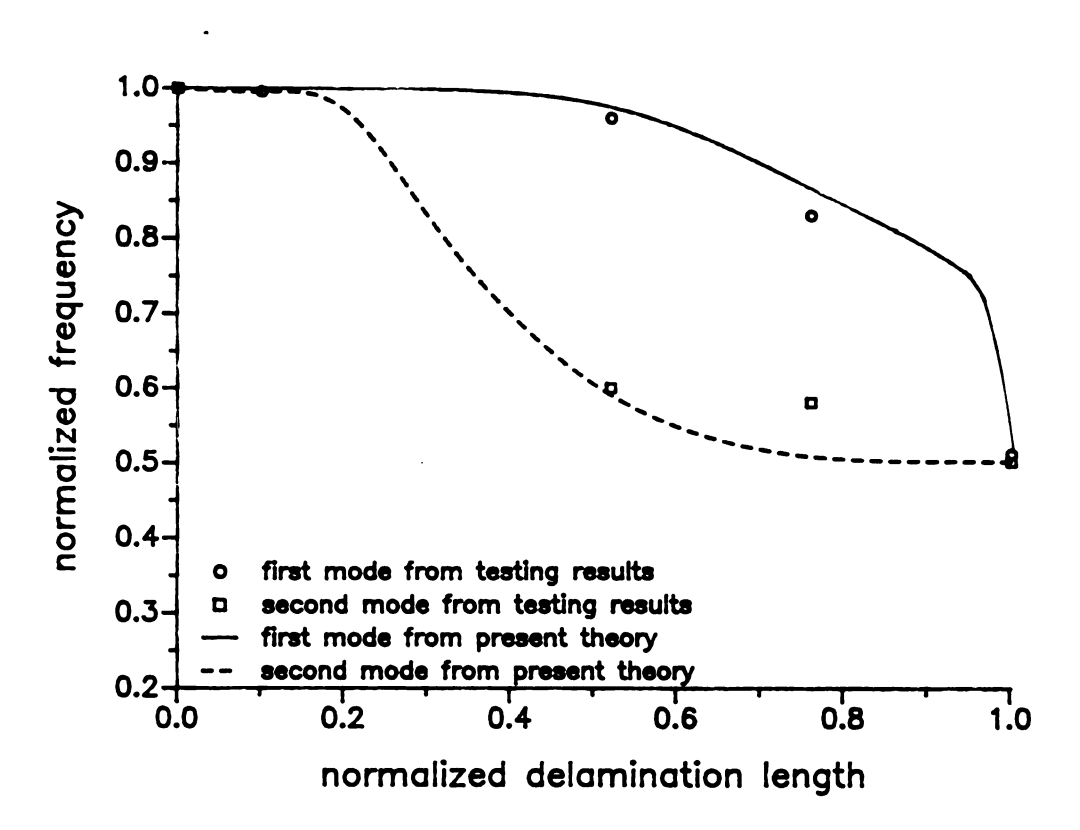


Figure 4.6 - Normalized natural frequencies of a glass beam with a central midplane delamination of various lengths.

be expressed in terms of reduced displacement variables, i.e.,

$$\varepsilon_{x}^{(i)} = \left\{ \frac{dU_{i-1}}{dx} \phi_{1}^{(i)} + \frac{dU_{i}}{dx} \phi_{2}^{(i)} + \frac{d\tilde{S}_{i-1}}{dx} \phi_{3}^{(i)} + (A_{1}^{(i)} \phi_{4}^{(i)} - \mu_{i} \overline{Q}_{55}^{(i+1)} \phi_{2}^{(i)}) \frac{d\tilde{S}_{i}}{dx} \right\} \\
+ (B_{1}^{(i)} \phi_{4}^{(i)} - \mu_{i} Q_{55}^{(i+1)} \phi_{2}^{(i)}) \frac{d^{2}w}{dx^{2}} \\
= [N_{n}^{(i)}] \left\{ X_{1}^{(i)} \right\} \qquad (4.2)$$

$$\gamma_{xx}^{(i)} = \left\{ U_{i-1} \frac{d\phi_{1}^{(i)}}{dx} + U_{i} \frac{d\phi_{2}^{(i)}}{dx} + \tilde{S}_{i-1} \frac{d\phi_{3}^{(i)}}{dx} + \tilde{S}_{i} \left(A_{1}^{(i)} \frac{d\phi_{4}^{(i)}}{dx} - \mu_{i} \overline{Q}_{55}^{(i+1)} \frac{d\phi_{2}^{(i)}}{dx} \right) \right\} \\
+ \left(A_{1}^{(i)} \frac{d\phi_{4}^{(i)}}{dx} - \mu_{i} Q_{55}^{(i+1)} \frac{d\phi_{2}^{(i)}}{dx} + 1 \right) \frac{dw}{dx}$$

$$= [N_{s}^{(i)}] \left\{ X_{2}^{(i)} \right\}$$

where

$$A_{1}^{(i)} = \begin{cases} \frac{Q_{55}^{(i+1)}}{Q_{55}^{(i)}} & i = 1, 2, ..., n-1 \\ i = n \end{cases}$$

$$i = 1, 2, ..., n-1$$

$$B_{1}^{(i)} = \begin{cases} \frac{\overline{Q}_{55}^{(i+1)}}{\overline{Q}_{55}^{(i)}} - 1 & i = 1, 2, ..., n-1 \\ 0 & i = n \end{cases}$$

$$[N_{s}^{(i)}] = \begin{bmatrix} \overline{\phi}_{1, z}^{(i)}, \overline{\phi}_{2, z}^{(i)}, \overline{\phi}_{3, z}^{(i)}, \overline{\phi}_{4, z}^{(i)}, \overline{\phi}_{5, z}^{(i)} \end{bmatrix}; \qquad [N_{n}^{(i)}] = \begin{bmatrix} \overline{\phi}_{1}^{(i)}, \overline{\phi}_{2}^{(i)}, \overline{\phi}_{3}^{(i)}, \overline{\phi}_{4}^{(i)}, \overline{\phi}_{5}^{(i)} \end{bmatrix}$$

$$\{X_{2}^{(i)}\} = \{U_{i-1}, \overline{S}_{i-1}, U_{i}, \overline{S}_{i}, \frac{dw}{dx} \}^{T} = \mathbf{x}^{(i)T}$$

$$\{X_1^{(i)}\} = \{\frac{dU_{i-1}}{dx}, \frac{d\bar{S}_{i-1}}{dx}, \frac{dU_i}{dx}, \frac{d\bar{S}_i}{dx}, \frac{d^2w}{dx}\}^T = \mathbf{x}^{(i)T}$$

In the above equations, the shape functions are defined as follows.

$$\tilde{\phi}_{1}^{(i)} = \phi_{2}^{(i)}; \qquad \tilde{\phi}_{2}^{(i)} = \phi_{3}^{(i)}; \qquad \tilde{\phi}_{3}^{(i)} = \phi_{2}^{(i)};
\tilde{\phi}_{4}^{(i)} = (A_{1}^{(i)} \phi_{4}^{(i)} - \mu_{i} Q_{55}^{(i+1)} \phi_{2}^{(i)}); \qquad \tilde{\phi}_{5}^{(i)} = (B_{1}^{(i)} \phi_{4}^{(i)} - \mu_{i} Q_{55}^{(i+1)} \phi_{2}^{(i)})$$
(4.4)

Substituting strains and stresses into Equation (4.1) and then integrating through the thickness, it yields

$$\overline{W} = \int_{\Omega} \left\{ \frac{1}{2} \sum_{i=1}^{n} \left(\mathbf{x}^{(i)T} A^{(i)} \mathbf{x}^{(i)} + \mathbf{x}^{(i)T} (B^{(i)} + C^{(i)}) \mathbf{x}^{(i)} \right) - P_z w \right\} dA \tag{4.5}$$

in which $A^{(i)}$, $B^{(i)}$, and $C^{(i)}$ are matrices defined as follows.

$$A_{lm}^{(i)} = \int_{z_{i-1}}^{z_i} Q_{11}^{(i)} \tilde{\phi}_l^{(i)} \tilde{\phi}_m^{(i)} dz \qquad B_{lm}^{(i)} = \int_{z_{i-1}}^{z_i} Q_{55}^{(i)} \tilde{\phi}_{l,z}^{(i)} \tilde{\phi}_{m,z}^{(i)} dz$$

$$C_{lm}^{(i)} = \mu_i (Q_{55}^{(i+1)})^2 \{N_p\}_l^T \{N_p\}_m \qquad l, m = 1, 2, ..., 5$$

$$\{N_p\} = \{0, 0, 0, 1, 1\}$$

Once the assembly in the thickness direction is achieved, the assembly of the finite elements in the x-direction can be performed. In this study, Hermite cubic shape functions are also used for in-plane assembly. The details of the finite element formulation can be found in Reference [54]. Accordingly, the potential energy can be expressed as

$$\overline{W} = \frac{1}{2}\hat{\mathbf{x}}^T \mathbf{K}\hat{\mathbf{x}} - \hat{\mathbf{x}}^T \mathbf{F} \tag{4.7}$$

where \hat{x} is the vector of the nodal variables, K is the total stiffness matrix, and F is the associated external loading vector. By using the principle of minimum potential energy, the finite element equations in terms of the nodal variables are

$$\mathbf{K}\hat{\mathbf{x}} - \mathbf{F} = 0 \tag{4.8}$$

4.2.2 Vibration Analysis

In vibration analysis, the kinetic energy associated with the assumed displacement field can be written as

$$KE = \frac{1}{2} \int_{\Omega_{-h}}^{\frac{h}{2}} (\dot{u}^2 + \dot{w}^2) \, dz dA \tag{4.9}$$

Substituting the time derivatives of u and w into the above equation, it yields

$$KE = \frac{1}{2} \int_{\Omega_{i=1}}^{R} (\dot{\mathbf{x}}^{(i)}^{T} K^{(i)} \dot{\mathbf{x}}^{(i)} + \rho_{i} h_{i} w^{2}) dA$$
 (4.10)

where ρ_i is the density of layer (i),

$$\dot{\mathbf{x}}^{(i)} = \frac{\partial \mathbf{x}^{(i)}}{\partial t} \quad \text{and} \quad K_{lm}^{(i)} = \int_{z_{i-1}}^{z_l} \rho_i \tilde{\boldsymbol{\phi}}_l^{(i)} \tilde{\boldsymbol{\phi}}_m^{(i)} dz \tag{4.11}$$

With the same fashion as used in deriving potential energy, the kinetic energy can be expressed in terms of mass matrix M and the vector of nodal variables \hat{x} as

$$KE = \frac{1}{2} (\hat{\mathbf{x}}^T M \hat{\mathbf{x}}) \tag{4.12}$$

With the use of the Hamilton's principle, the finite element equations for free vibration analysis are

$$\mathbf{M}\hat{\mathbf{x}} + \mathbf{K}\hat{\mathbf{x}} = 0 \tag{4.13}$$

4.3 Comparisons and Discussions

4.3.1 Static Test

The normalized transverse deflections obtained from both testing and finite ele-

ment analysis are shown in Figure 4.2 as functions of normalized delamination length, which is defined as the ratio of the length of the delamination, a, to the effective length of the beam, L. In this study, the delamination is located on the midplane of the composite beams and is symmetric with respect to the beam center, namely central delamination. A reasonable agreement between experimental results and finite element analysis can be concluded from this diagram. Figure 4.2 also shows that the central delamination remains to be insensitive to the delamination length if the delamination does not extend to the specimen end. However, as the delamination approaches the beam end, a significant increase in the central deflection can take place.

4.3.2 Vibration Test

A. Glass/Epoxy Beams

For a glass/epoxy composite beam with different lengths of central delamination, the first two natural frequencies of bending type are measured. The measured results are normalized by that without delamination and plotted as functions of normalized delamination length as shown in Figure 4.5. There is a pronounced disagreement between the finite element analysis and the testing results for the second vibration frequency. It is believed that there are three reasons for the disagreement. One is the effect of inhomogeneity of the material properties in the composite beams. It is found that the variation of the material properties is as much as 7% among the different specimens. The inhomogeneity is owing to the fabrication process or due to the defects in the prepreg tapes. Another reason is the poor quality control of the specimen thickness. The variation of the thickness in the specimens can be as large as 0.25 mm which is about 8% of the total thickness of the specimens. Unfortunately, it is very hard to control the thickness of the specimen in the fabrication. The third reason is the effect of the embedded layer. It is reported in Reference [51] that the embedded layer can strongly affect the results. In addition, it is impossible to

remove the embedded material after fabrication. However, it is not easy to fabricate a specimen with natural delamination but without matrix cracking.

B. Glass Beams

In order to eliminate the three undesired causes as stated in the previous section, pure glass beams are used for vibration test. It is verified that the variations of the modulus and the thickness of the specimens are less than 1%. In addition, when two pieces of glass beams are bonded together by super glue, it is confirmed that the composite beam behaves like a solid beam [56]. Hence, this type of specimen are used for a comprehensive analysis. The delamination is created by carefully adjusting the bonding area. By using the resonant frequency measurement method, the effect of delamination length on the natural frequencies of the beam is studied.

The normalized first two natural frequencies obtained from testing and finite element analysis are shown in Figure 4.6 as functions of normalized delamination length. Reasonable agreements between the experiments and the theoretical results for both modes are shown in the diagram. It appears that the frequency of the first mode of a glass beam with a central delamination does not change significantly until the delamination length extends to the beam end. This conclusion is similar to that from the three-point bend test. However, both experiment and analysis reveal that there is a considerable change of frequency for the second mode when the delamination length is moderately large. By comparing the experimental results with analytical solutions, it can be concluded that ISST can be employed to study composite laminates with damaged interfaces.

Chapter 5

APPLICATIONS OF THE INTERLAYER SHEAR SLIP THEORY

5.1 Introduction

In characterizing the interlaminar shear strength of composite laminates, both end notch flexure (ENF) and center notch flexure (CNF) tests [44,45] have been widely used. By measuring the change of compliance of specimens with different delamination lengths, it is possible to determine the interfacial shear fracture toughness G_{IIC}. In section 5.2, the effect of delamination on transverse deflection is examined by using ISST. In section 5.3, the ISST is used to study the free vibration of a graphite/epoxy beam with different kinds of delamination. The effects of delamination size, location, and position on the vibration frequencies and mode shapes are examined.

5.2 Static Analysis

The finite element scheme presented in 4.2.1 is used to analyze a [0/0] composite beam with a midplane delamination. The loading, boundary conditions, and material properties are shown in Figure 4.1. First of all, the effect of delamination location on the transverse deflection is investigated. In this study, the delamination length remains to be 25.4 mm while the center of the delamination is moved along the laminate midplane between the beam center and end. Figure 5.1 indicates that the change of the central deflection is moderate unless the delamination approaches the beam end. Secondly, the effect of delamondary conditions, and material properties are shown in Figure 4.1. First of all, the effect of delamination is moved along the laminate midplane between

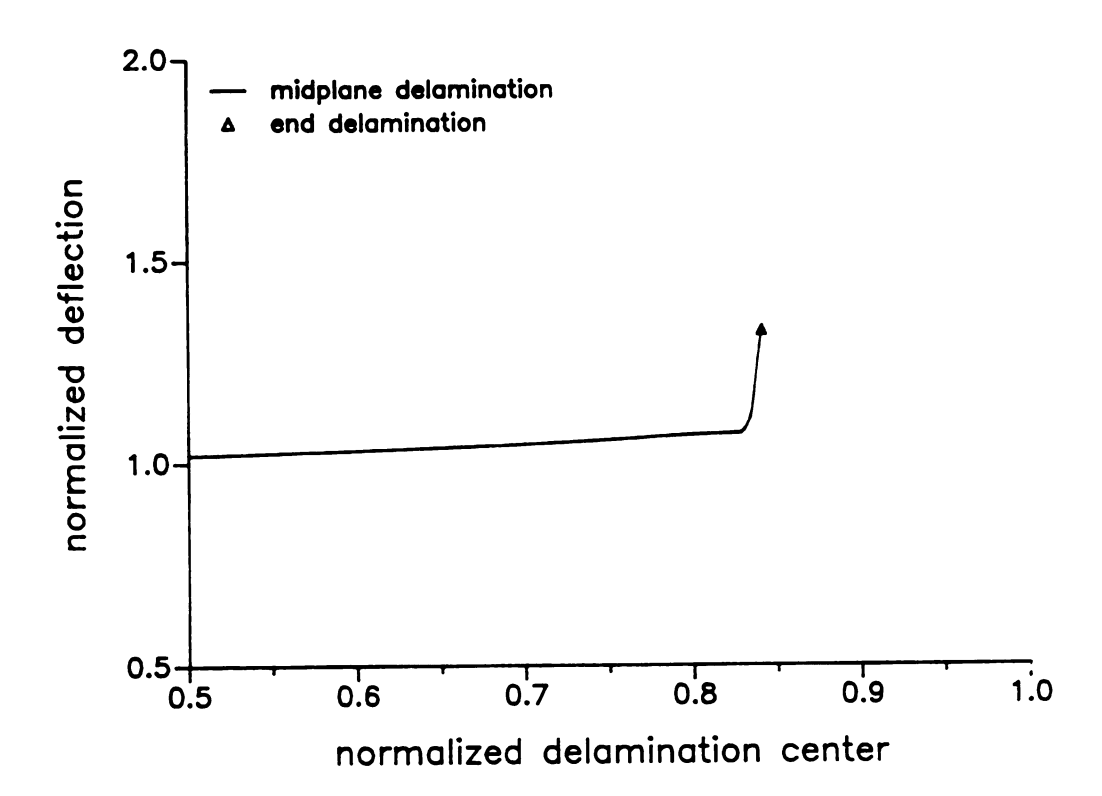


Figure 5.1 - Normalized central deflection of a glass/epoxy beams with a 25.4 mm midplane delamination at various locations.

mination length is studied. The results are shown in Figures 5.2 and 5.3. Based on Figures 5.1, 5.2, and 5.3, it can be concluded that the transverse deflection is very sensitive to the delamination which covers the beam end.

Delamination is not necessary to be restricted to the composite midplane. It can take place in any thickness position. The sensitivity of delamination in the thickness direction is of a major concern in damaged composite analysis. In this study, both 25.4 mm and 50.8 mm delamination are investigated. The delaminations are positioned at the midspan of the composite beams and can be located between midplane and top surface. Figure 5.4 shows the results from the finite element analysis. Apparently, the delamination of 25.4 mm long only causes very little change in central deflection while that of 50.8 mm shows noticeable influence when the delamination is close to the midplane. However, both cases reveal that the effect of delamination on the deflection is getting weaker and weaker as the delamination moves away from the midplane.

5.3 Vibration Analysis

Similar to static analysis, the finite element scheme from the ISST is employed to study the effect of delamination on vibration frequency and mode shape of a composite beam. In this study, a simply supported graphite/epoxy beam with delamination is examined. The material properties of the beam are given in Figure 3.1. In this analysis, the effect of transverse shear on vibration frequencies is evaluated. The natural frequencies for the first four modes calculated from ISST, classical laminate theory, and elasticity analysis [57] are listed in the Table 5.1. It can be seen that the transverse shear effect is more significant to the higher order modes than to the lower order modes.

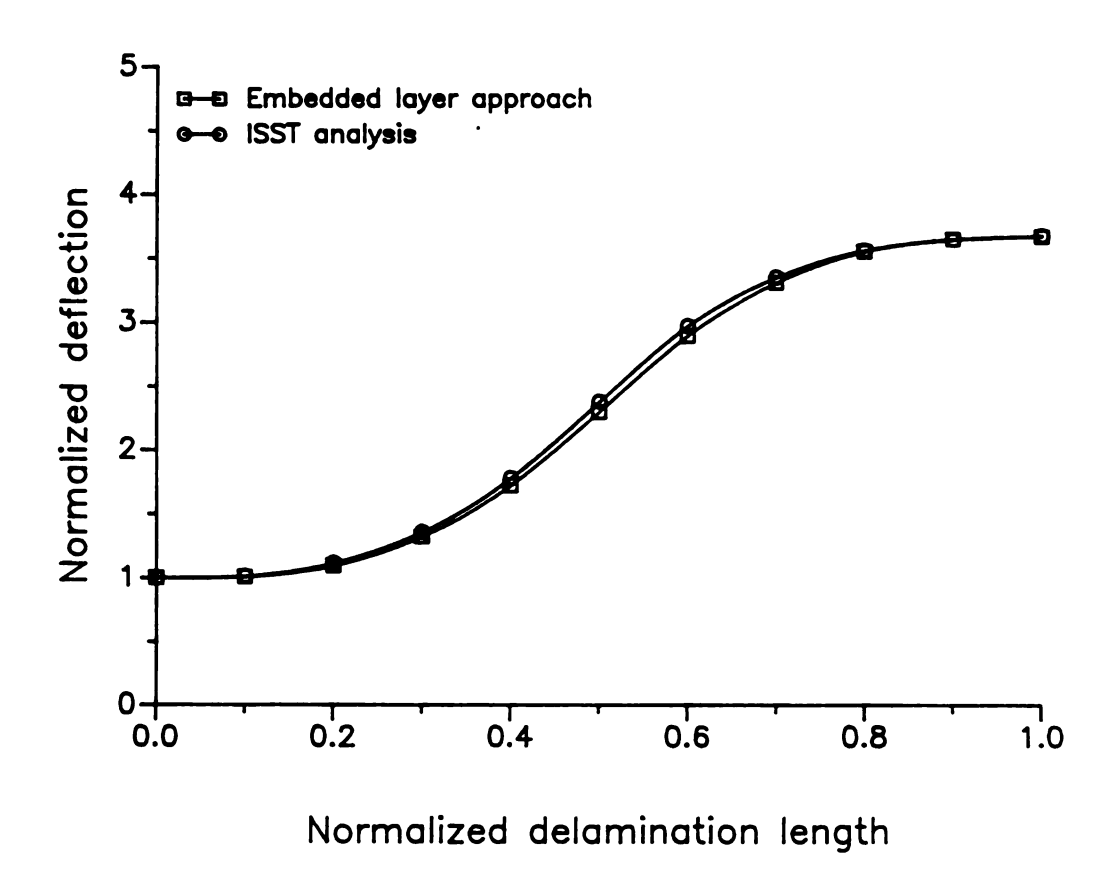


Figure 5.2 - Normalized central deflection of a glass/epoxy beam with an end midplane delaminations of various lengths.

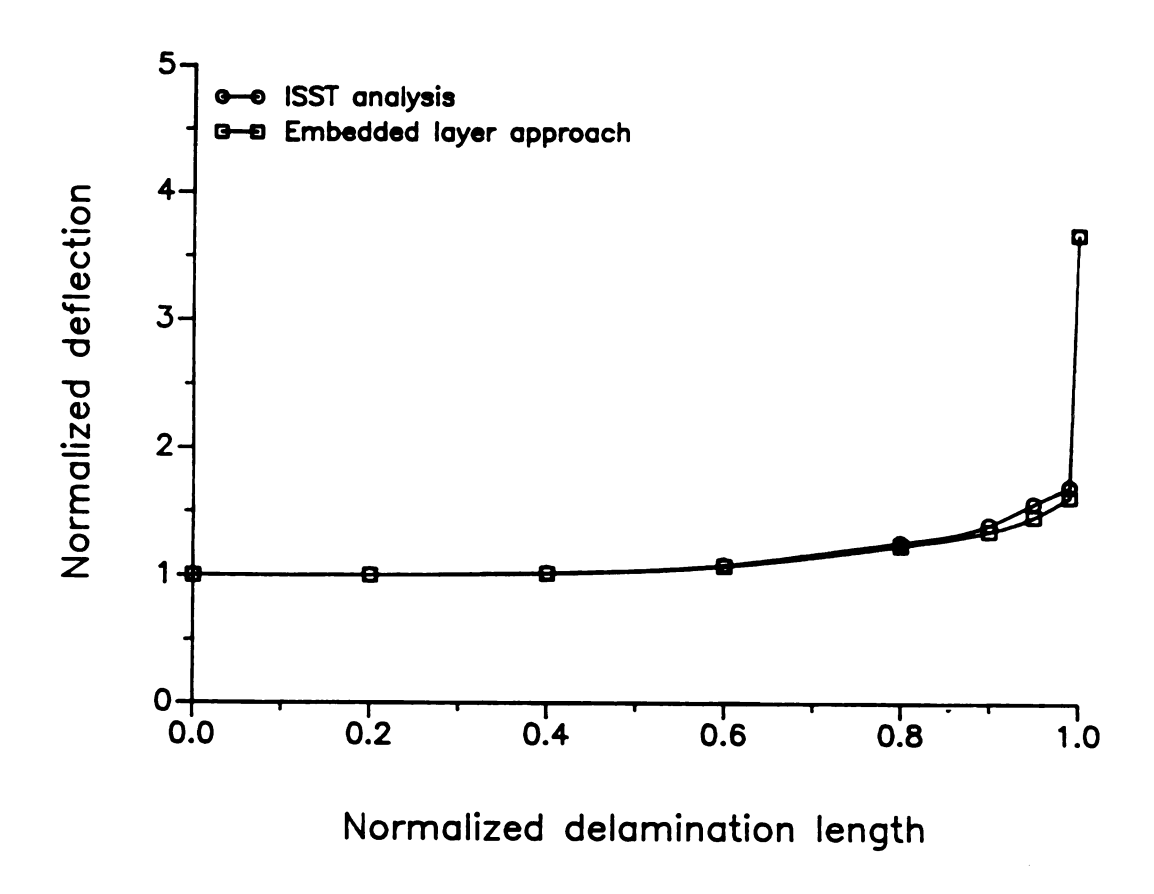


Figure 5.3 - Normalized central deflection of a glass/epoxy beam with a central midplane delamination of various lengths.

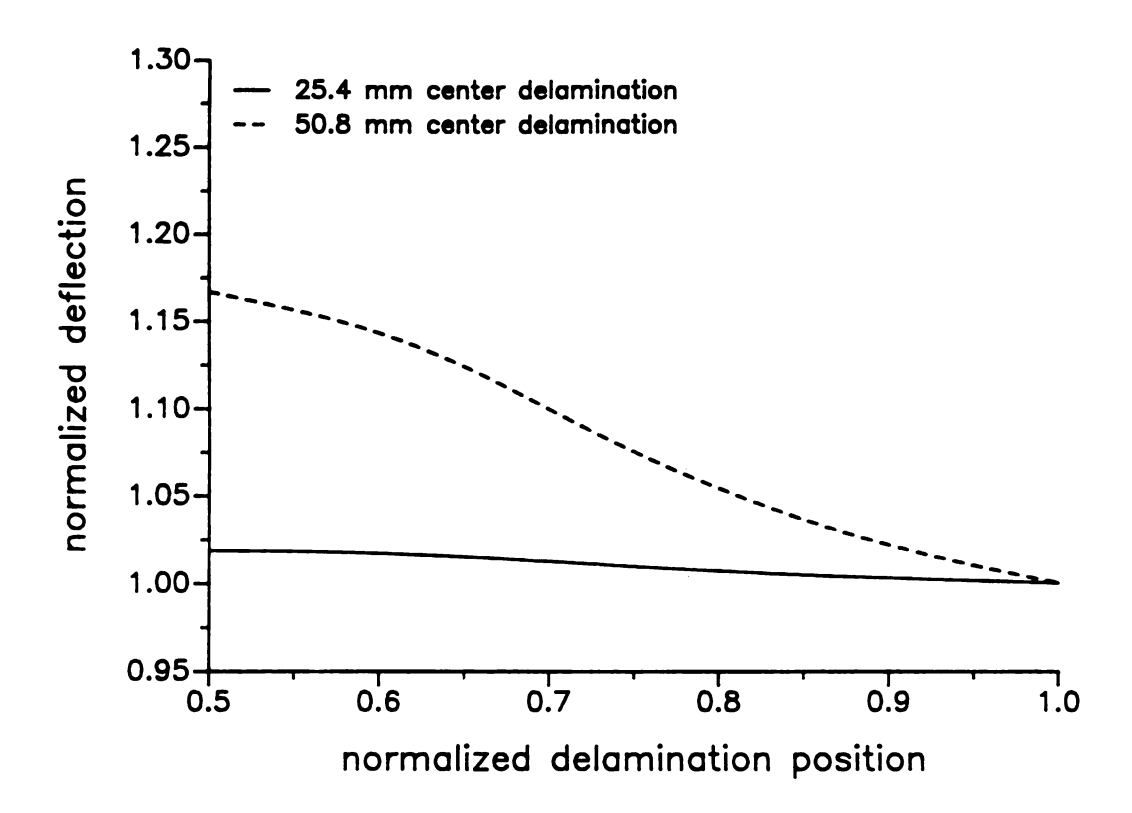


Figure 5.4 - Normalized central deflections of glass/epoxy beams with 25.4 mm and 50.8 mm central delaminations at various positions.

Table 5.1 - Comparisons of natural frequencies calculated from ISST, CLT, and elasticity analysis.

	Natural Frequency (Hz) S = 20			Natural Frequency (Hz) $S = 100$				
	mode 1	mode 2	mode 3	mode 4	mode 1	mode 2	mode 3	mode 4
ISST	5.3498	18.550	35.171	52.850	.2264	.8991	1.9987	3.4962
CLT	5.6681	22.672	51.103	90.690	.2267	.9096	2.0405	3.6276
Elasticity	5.3444	18.5394	35.161	52.838	.2262	.8980	1.9961	3.4907

5.3.1 Delamination Length

Figure 5.5 reveals the effect of delamination length on the natural frequencies for the first four mode. The normalized frequencies and delamination lengths shown in this diagram have the same definitions as those given in Chapter 4. It is noted that the effect of the central delamination on the vibration frequencies is more sensitive to the even modes than to the odd modes.

5.3.2 Delamination Location

Figure 5.6 shows that the normalized frequencies are functions of delamination location. The delamination length in this study remains to be 20% of the beam length while its center is moved along the midplane from the beam center to the end. For all four modes, the frequencies experience significant reductions as the delaminations move from the beam center to the beam end. In addition, the patterns of the change seem to match with the vibration mode shapes. The largest changes in the individual mode seem to coincide with the nodal points. This implies that the vibration modes may have significant change if the delamination is located at the nodal point. In order to further verify this result, the change of the first four vibration mode shapes are studied with the center of a delamination located at x=0.5 or x=0.2. For the case of x=0.5, it covers a nodal point for both the second and the fourth modes while for the case of x=0.2 only the fourth mode. Numerical results are shown from Figure 5.7 to Figure 5.14. When the delamination center is located at x=0.5, the second and the fourth modes experience noticeable changes in vibration mode shapes. However, only the fourth mode shape shows a significant change when the delamination center is located at x=0.5.

5.3.3 Delamination Position

The change of vibration frequency due to the position of a 20% central delamina-

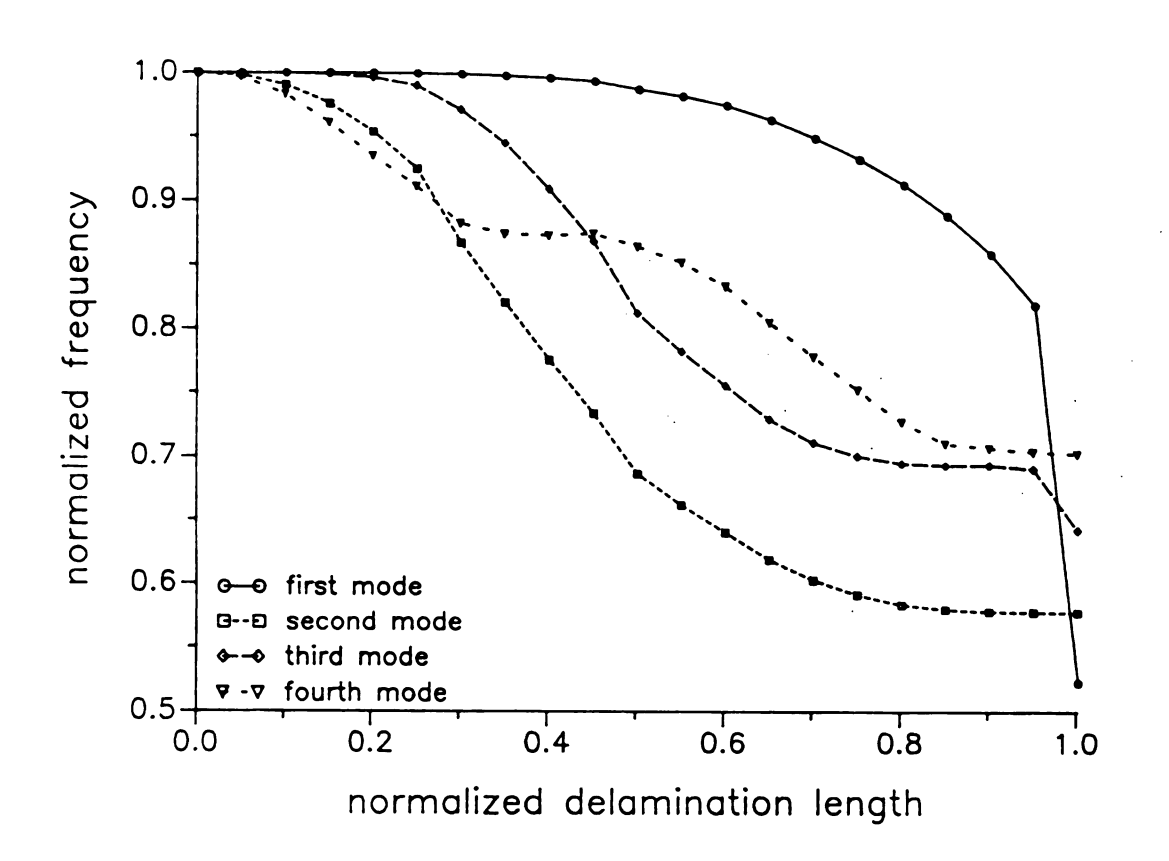


Figure 5.5 - Normalized natural frequencies of graphite/epoxy beams with central midplane delamination of lengths.

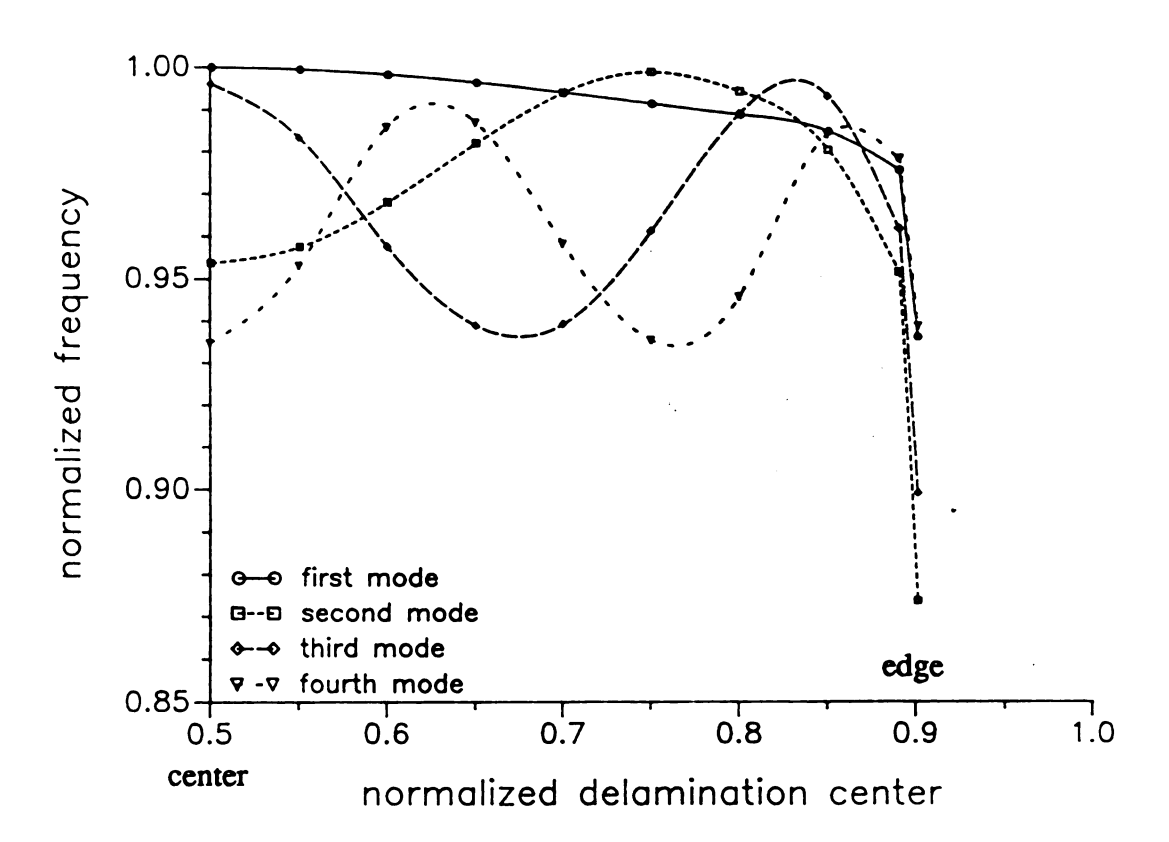


Figure 5.6 - Normalized natural frequencies of graphite/epoxy beams with 20% midplane delamination at different locations.

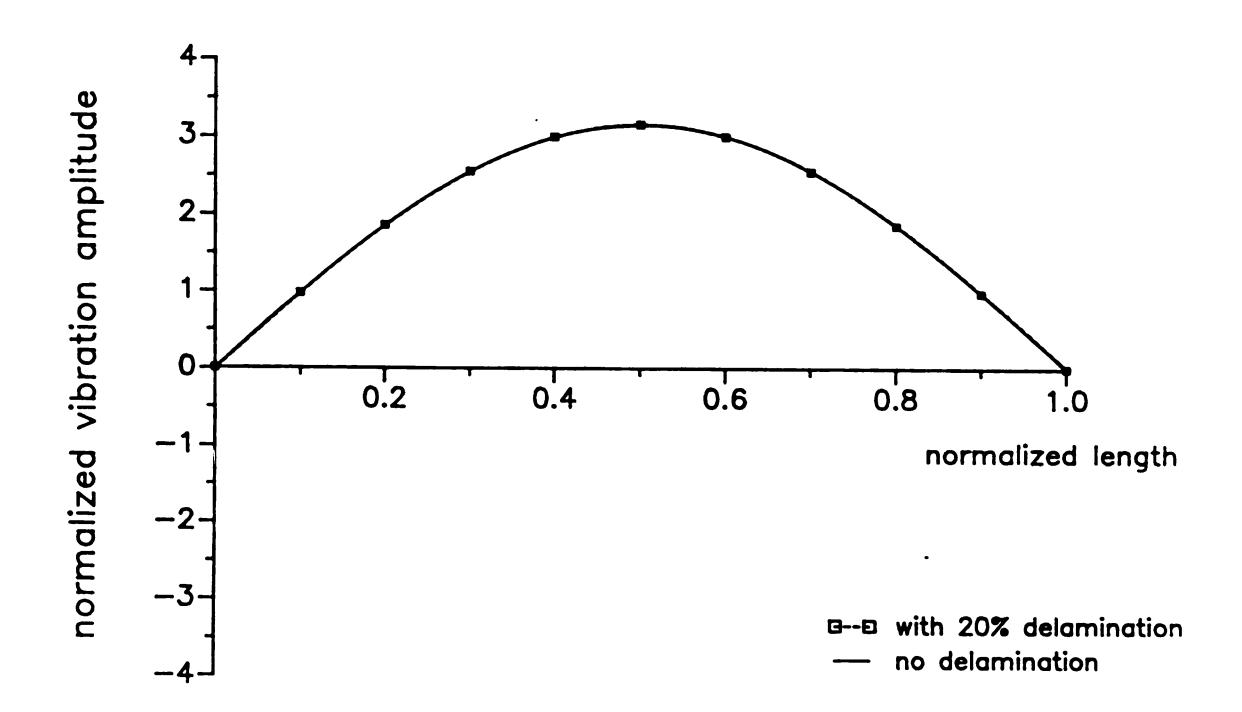


Figure 5.7 - Normalized first mode shape of a graphite/epoxy beam with 20% delamination which has center at x=0.5.

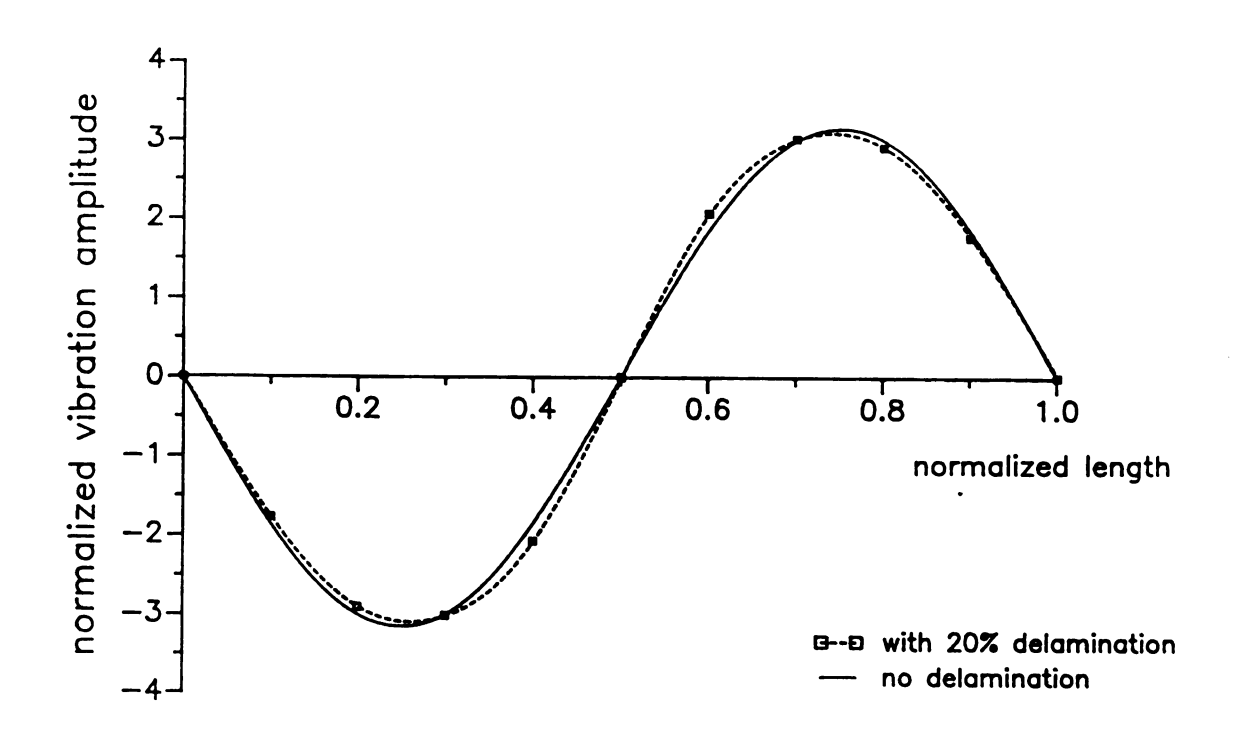


Figure 5.8 - Normalized second mode shape of a graphite/epoxy beam with 20% delamination which has center at x=0.5.

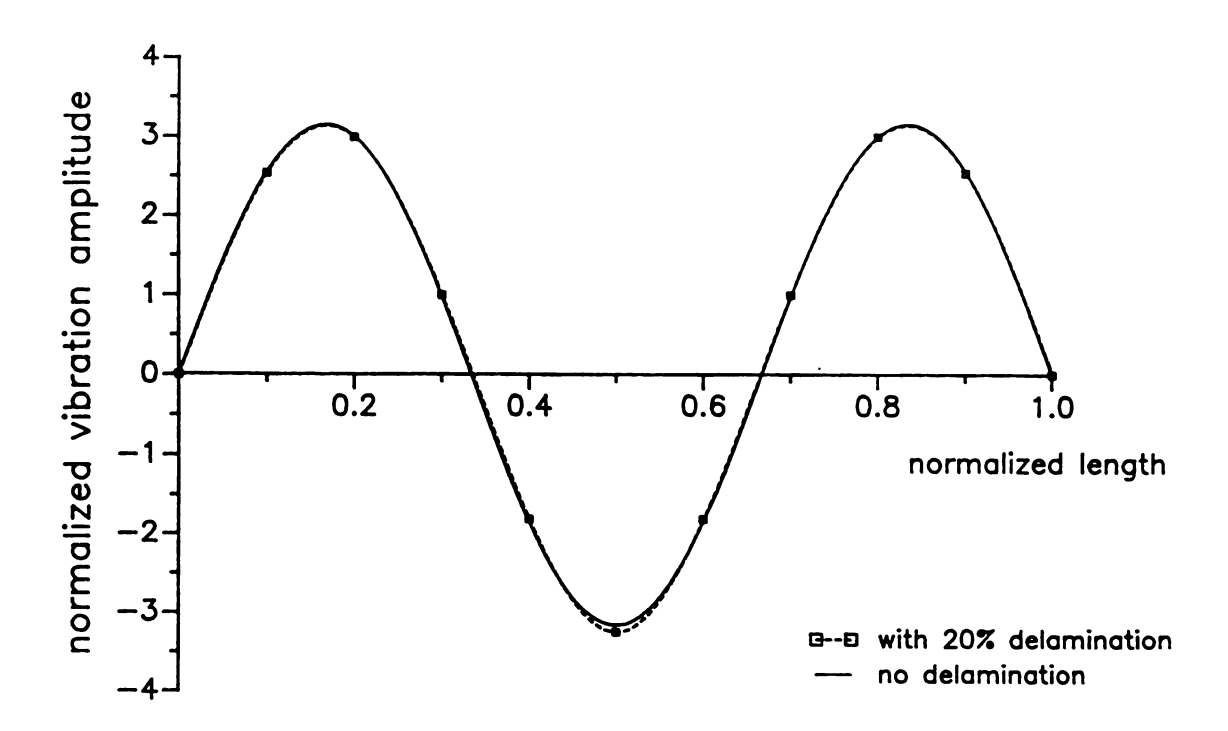


Figure 5.9 - Normalized third mode shape of a graphite/epoxy beam with 20% delamination which has center at x=0.5.

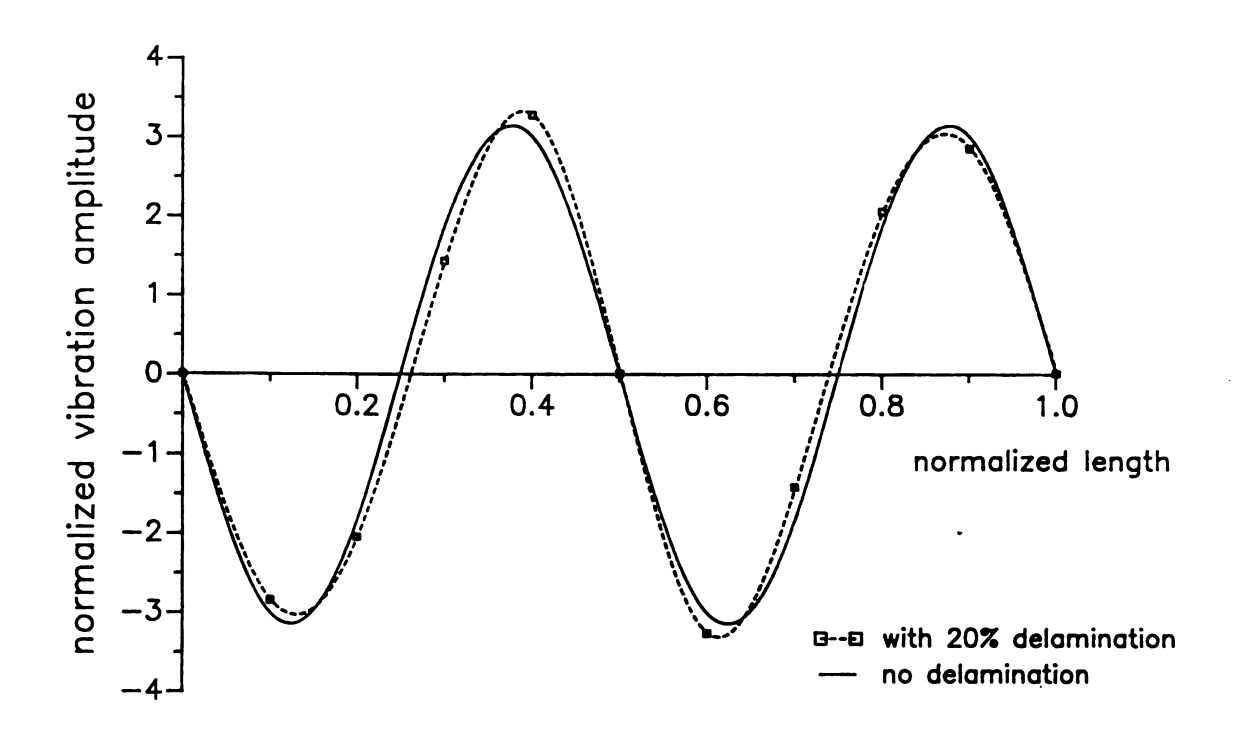


Figure 5.10 - Normalized fourth mode shape of a graphite/epoxy beam with 20% delamination which has center at x=0.5.

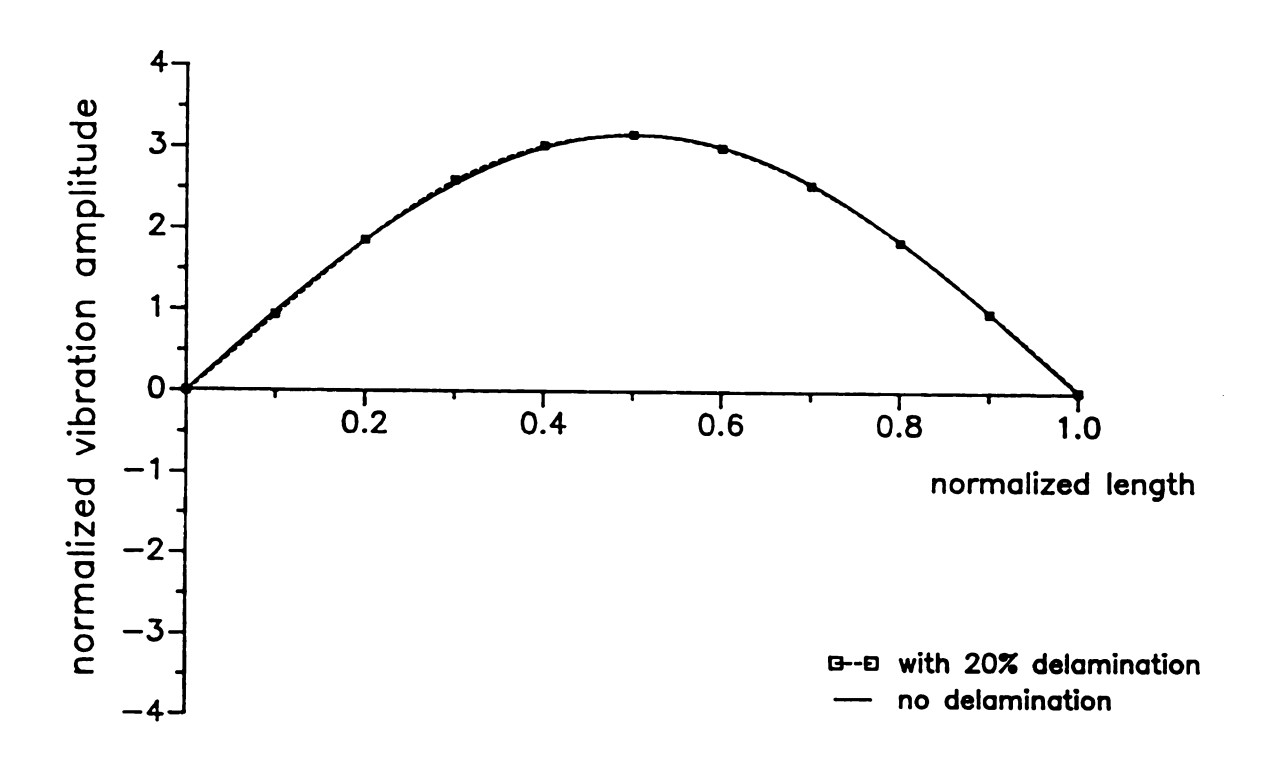


Figure 5.11 - Normalized first mode shape of a graphite/epoxy beam with 20% delamination which has center at x=0.2.

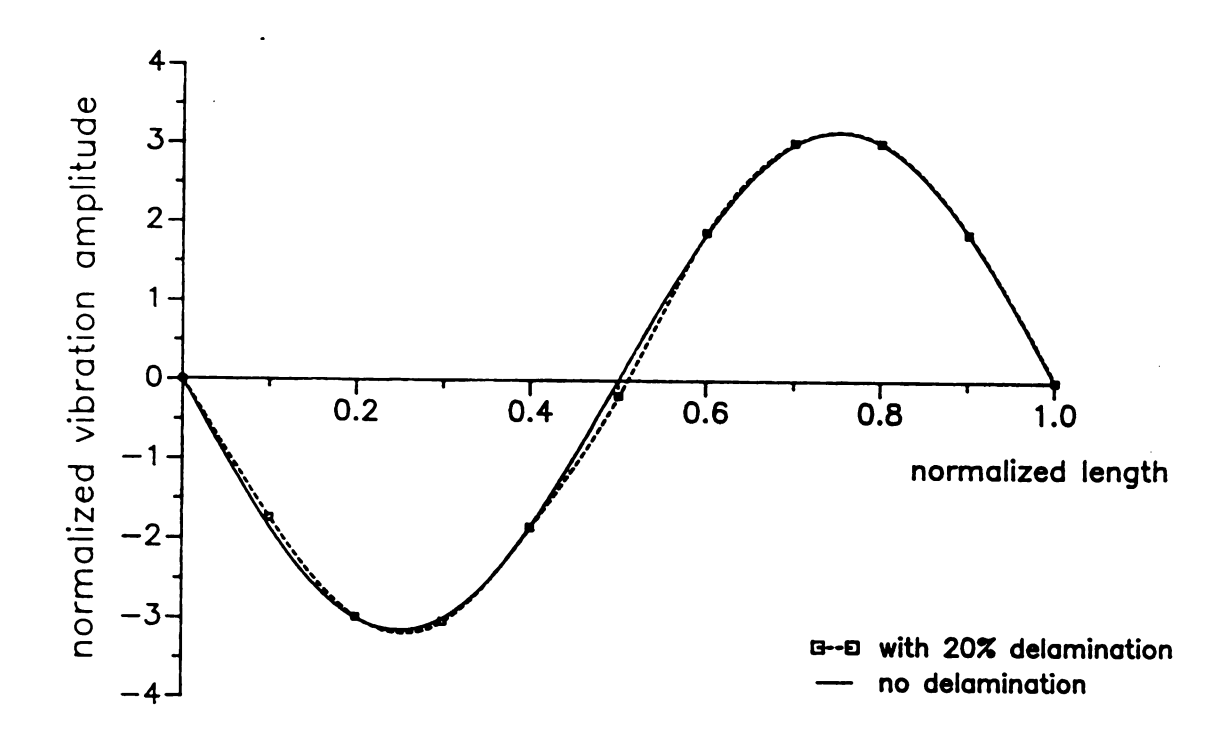


Figure 5.12 - Normalized second mode shape of a graphite/epoxy beam with 20% delamination which has center at x=0.2.

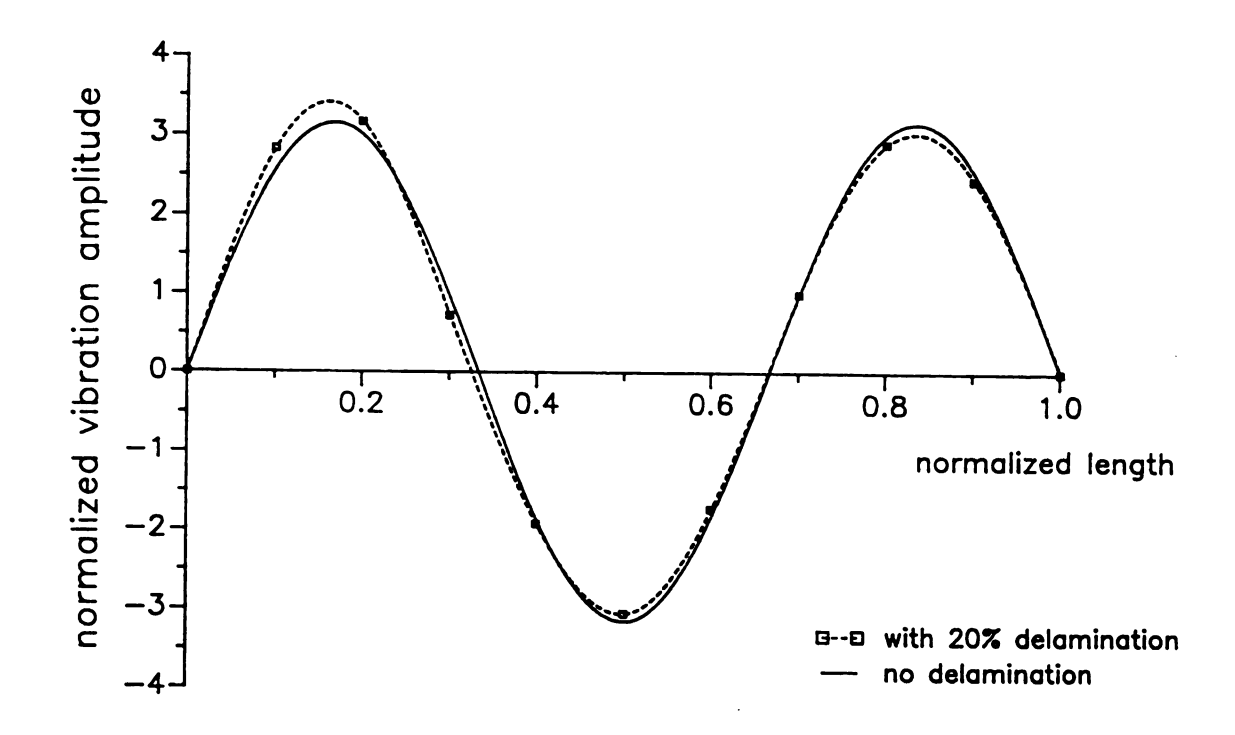


Figure 5.13 - Normalized third mode shape of a graphite/epoxy beam with 20% delamination which has center at x=0.2.

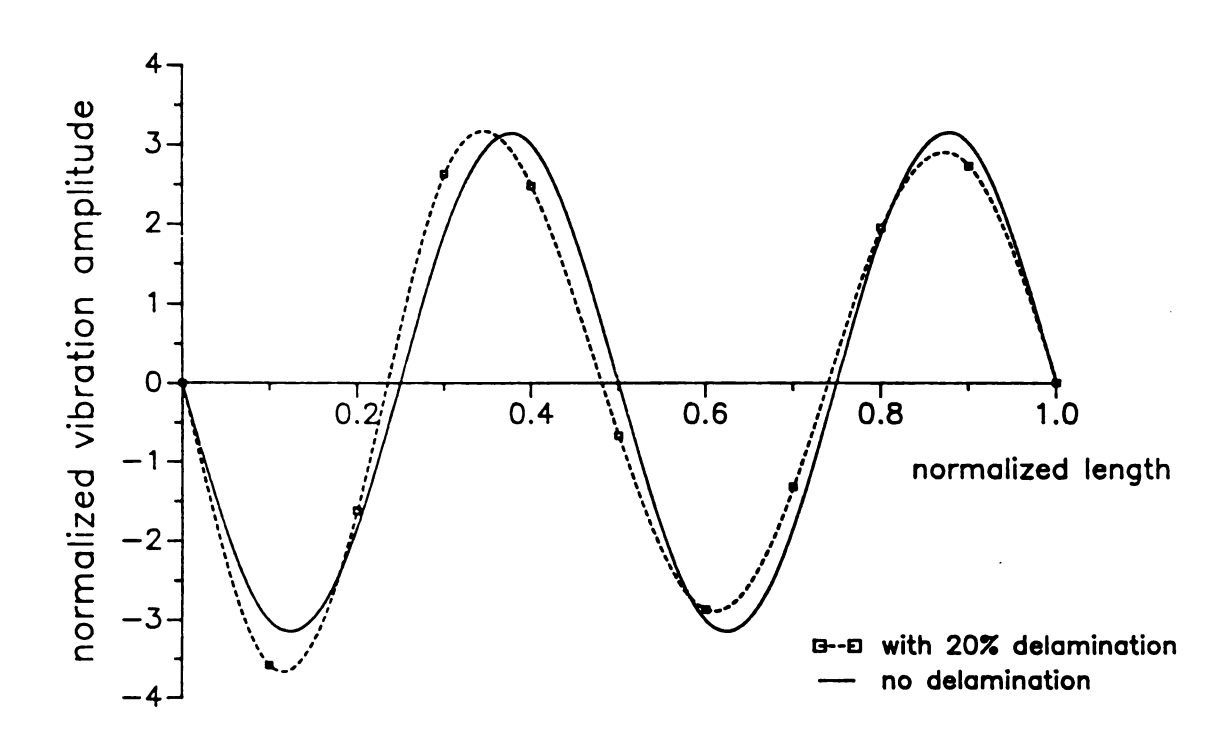


Figure 5.14 - Normalized fourth mode shape of a graphite/epoxy beam with 20% delamination which has center at x=0.2.

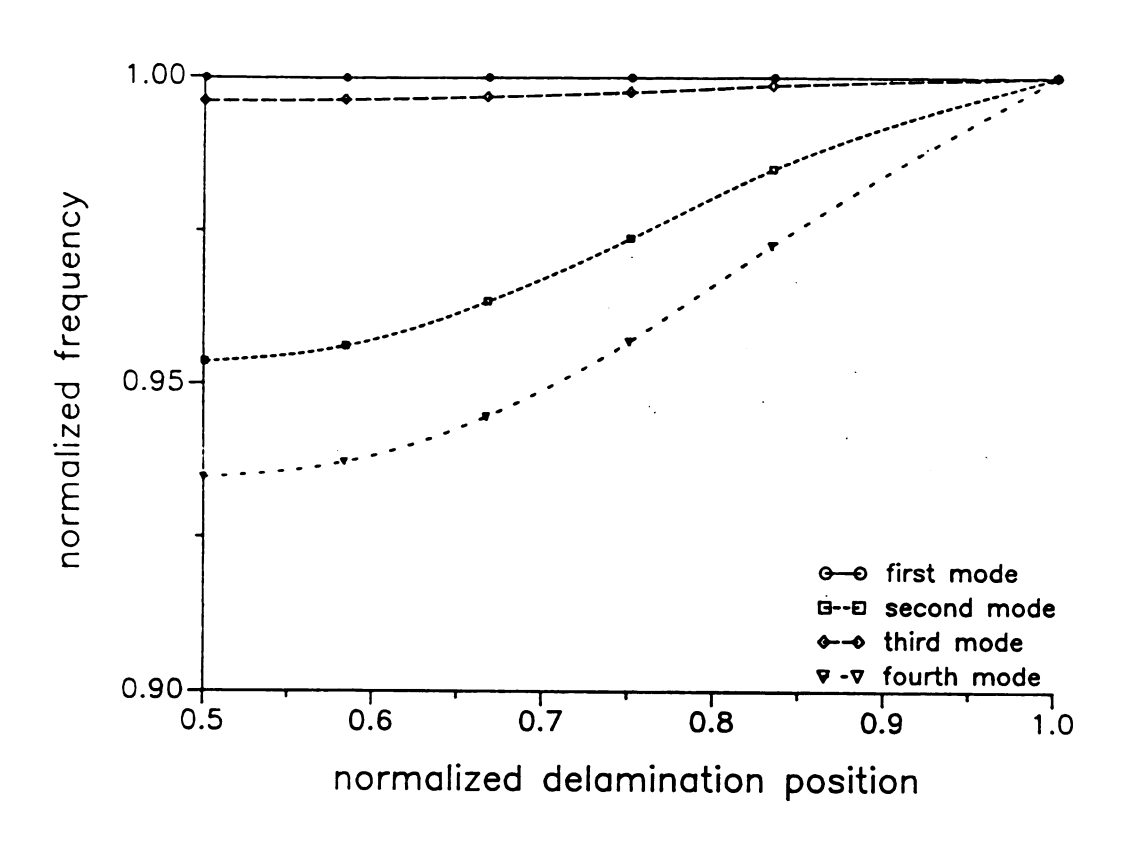


Figure 5.15 - Normalized natural frequencies of graphite/epoxy beams with 20% central delamination at different positions.

tion in the thickness direction, as shown in Figure 5.15, is not significant although the even modes seem to be more sensitive than the odd ones. However, they seem to reveal that the effect of delamination on the natural frequencies becomes smaller and smaller as the delamination moves away from the midplane.

5.4 Conclusions

For a simply supported composite beam, the effects of delamination on the vibration frequencies can be summarized as follows.

- (1) A delamination covering the beam end has more significant effect on the transverse deflection and first vibration mode than those not extending to the beam end.
- (2) The effect of delamination on the central deflection and all vibration modes (first to fourth) becomes weaker and weaker as the delamination moves away from the midplane to the surface of the beam.
- (3) In vibration analysis, if a delamination covers a nodal point of a vibration mode, the effect of the delamination on the mode shape is very significant.

Based on the above conclusions, it has been found that delamination has strong effect on the composite response wherever the transverse shear stress reaches a maximum, e.g., nodal point, midplane, and beam end. This conclusion implies that the transverse shear effect should be considered in the study of composite laminates with delamination.

Chapter 6

CONCLUSIONS AND SUGGESTIONS

6.1 Conclusions

By allowing displacement discontinuity on the composite interface, an interlayer shear slip theory (ISST) is developed to study composite laminates with both rigid (perfect) and nonrigid (imperfect) bonding conditions. This study is based on multiple-layer technique. It is derived from an interlaminar shear stress continuity theory [29] and an assumed linear shear slip law on the nonrigid interface. A comprehensive assessment of using the ISST to study composite laminates with different degrees of interfacial bonding is given while limited cases for experimental verifications and delamination analysis are also presented. As a summary, the following conclusions are drawn:

- 1. ISST can be employed to study composite laminates with both rigid and nonrigid bonding interfaces. It has been verified that ISST can be used to calculate displacements, in-plane stresses, and interlaminar shear stresses in composite laminates accurately. In addition, the interlaminar shear stresses, which play a critical role in interfacial bonding, can be obtained directly from the constitutive equations instead of being recovered from the equilibrium equations because of the consideration of the continuity of interlaminar shear stresses on the composite interfaces.
- 2. By comparing the results from ISST with those from other approaches, e.g., elasticity analysis and embedded-layer technique, excellent agreements are concluded. In addition, a reasonable agreement between the results from ISST and the experiments is also concluded. These comparison provide evidences for the conclusion that it is feasible to use

ISST to study composite laminates with nonrigid bonding.

- 3. It is shown that ISST can be used to study the effects of delamination on both static and vibration performances of laminated beams.
- 4. Some closed-form solutions for cross-ply laminates with different kinds of interfacial bonding are presented. These results are valuable for more studies in this area since very limited elasticity solutions exist.
- 5. Because of the variational consistence in the development of ISST, this theory can be extended to finite element formulation and applied to the study of imperfectly bonded laminated structures with complex configuration and various boundary conditions.
- 6. From the results of stress distributions of composite laminates with nonrigid bonding interfaces, it is concluded that the maximum in-plane normal stress and the maximum transverse shear stress are underestimated by using theories based on perfect bonding assumption.
- 7. It is interesting to find that at some special locations, namely singular points, the transverse shear stress or in-plane normal stress and displacement remain insensitive to the condition of interfacial bonding. These results have important application in composite laminates with embedded sensors.
- 8. Nonrigid bonding can have a significant effect on transverse deflection when the interfacial shear bonding approaches a 'critical' range. However, beyond the 'critical' range, the composite laminate will quickly lose its integrity and behave like two independent layers with a lubricated interface.
- 9. For a composite beam with a delamination, the effect of delamination on the deflection is strongly dependent on the location and position of the delamination. In addition, the effects of delamination on vibration frequencies and mode shapes also depend on the location and position of the delamination. It is found that the effects are very significant if delamination is located in an area where the transverse shear stress is very high. This con-

clusion is helpful in developing nondestructive testing method for delamination investigation.

6.2 Suggestions

Based on the work performed in this thesis, the following studies are suggested for future investigation.

- 1. In this study, the continuity requirements for transverse displacement and transverse normal stress are neglected. The effect of the transverse normal stress is considered in the Reference [31]. It is believed that it will be a very useful work to extend interlayer shear slip theory to include the displacement slip in the thickness direction for studying mode-I interface fracture and delamination buckling.
- 2. In order to study the initiation and propagation of delamination in composite laminates, it is suggested to combine the stresses analysis provided by ISST with numerical schemes to calculate the strain energy release rates [37].
- 3. The present study is mainly for laminated beams. The study for delamination in composite laminates is recommended. This study will have more significant impact in the study of composite structures. In addition, it can be extended to include nonlinear strain-displacement relations and dynamic analysis.
- 4. More experimental studies in the effect of delamination on the static, vibration, and buckling performances of composite laminates are suggested.

Appendix

ANALYSIS OF SINGULAR POINTS BASED ON

CLASSICAL BEAM THEORY

1. Two-layer Laminates

Consider a composite beam made of two layers shown in Figure A1. The interface between the layers is of nonrigid bonding.

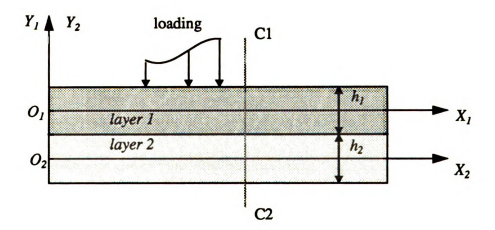


Figure A1 - The geometry and coordinate system of a two-layer beam.

 $X_iO_iY_i$ is the local coordinate system of layer (i) which has the thickness of h_i . For simplicity, it is assumed that h_i is equal to h_2 . In addition, only beams with large length-to-thickness ratio are considered in this analysis. Therefore, the classical beam theory can be used in the following derivation.

Assume that the beam is subjected to a transverse load. The normal stress in each layer at a generic cross-section C1-C2 can be expressed as follows,

$$\sigma_x^{(1)} = \frac{F_1}{A_1} - \frac{M_1}{I_1} \gamma_1; \qquad \qquad \sigma_x^{(2)} = -\frac{F_2}{A_2} - \frac{M_2}{I_2} \gamma_2$$
 (A-1)

where A_i and I_i are the cross-sectional area and moment of inertia of layer (i). F_i and M_i are the corresponding resultant force and moment and are shown in Figure A2.

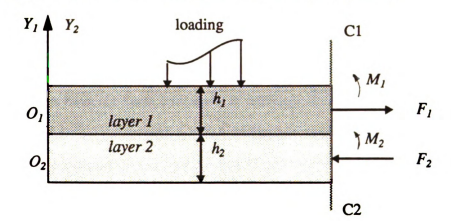


Figure A2 - The resultant forces and moments at the cross-section C1-C2.

Because of the equilibrium requirements, the following relations can be obtained.

$$F_1 = F_2 = F;$$
 $M = M_1 + M_2 - Fh_1$ (A-2)

M is the total moment applied at the cross-section C1-C2. Moreover, it is assumed that both layers have the same curvature. Therefore,

$$\frac{M_1}{I_1E_1} = \frac{M_2}{I_2E_2} = \frac{M + Fh_1}{I_1E_1 + I_2E_2}.$$
 (A-3)

In the above equation, E_1 and E_2 are Young's Modulus of layer (1) and (2), respectively. Combining Equation (A-2) and Equation (A-3) together, and substituting the result into Equation (A-1), it yields

$$\sigma_x^{(1)} = \frac{F}{A_1} - \frac{M + Fh_1}{I_1 E_1 + I_2 E_2} E_1 Y_1, \qquad \sigma_x^{(2)} = -\frac{F}{A_2} - \frac{M + Fh_1}{I_1 E_1 + I_2 E_2} E_2 Y_2. \tag{A-4}$$

Equation (A-4) can be rewritten as

$$\sigma_x^{(1)} = \left(\frac{F}{A_1} - \frac{Fh_1E_1Y_1}{I_1E_1 + I_2E_2}\right) - \frac{M}{I_1E_1 + I_2E_2}E_1Y_1 \tag{A-5a}$$

$$\sigma_x^{(2)} = \left(-\frac{F}{A_2} - \frac{Fh_1 E_2 Y_2}{I_1 E_1 + I_2 E_2} \right) - \frac{M}{I_1 E_1 + I_2 E_2} E_2 Y_2 \tag{A-5b}$$

Equations (A-5a) and (A-5b) are expressions for normal stress distribution in the individual layers. It is important to note that they are true for any kind of interfacial bonding as long as the two layers have the same curvature. In addition, the moment M, the moduli E_1 and E_2 , and the geometrical parameters I_i and A_i in Equations (A-5a) and (A-5b) are independent of bonding condition. In fact, only F is affected by the interfacing status. Define the following two variables.

$$\xi_1 = \left(\frac{F}{A_1} - \frac{Fh_1E_1Y_1}{I_1E_1 + I_2E_2}\right); \qquad \qquad \xi_2 = \left(-\frac{F}{A_2} - \frac{Fh_1E_2Y_2}{I_1E_1 + I_2E_2}\right). \tag{A-6}$$

If the composite beam has no interlaminar shear bonding on its interface, F will vanish. Consequently, ξ_1 and ξ_2 are zeros. In Chapter 3, it was defined that the singular point is a point at which the normal stress, transverse shear stress, or in-plane displacement is independent of bonding condition. Since the second terms in Equations (A-5a) and (A-5b) are not affected by the interfacial bonding, the singular points for the normal stress in each layer can be determined by the following equations.

$$\xi_1 = \left(\frac{F}{A_1} - \frac{Fh_1E_1Y_1}{I_1E_1 + I_2E_2}\right) = 0$$
 for layer (1) (A-7a)

$$\xi_2 = \left(-\frac{F}{A_2} - \frac{Fh_1 E_2 Y_2}{I_1 E_1 + I_2 E_2} \right) = 0$$
 for layer (2)

Furthermore, if it is assumed that layer (1) and layer (2) have the same cross-section, i.e., A_1 equals to A_2 and I_1 equals to I_2 , the associated singular points for normal stress are located at

$$Y_1^{(n)} = \frac{(E_1 + E_2)h_1}{12E_1}$$
 in layer (1), (A-8a)

$$Y_2^{(n)} = -\frac{(E_1 + E_2)h_2}{12E_2}$$
 in layer (2). (A-8b)

By considering the equilibrium of a free body in the beam, the transverse shear stress in each layer can be expressed as

$$\tau_{xz}^{(i)} = \int_{Y_1}^{\frac{h_1}{2}} \left(\frac{1}{A_1} \frac{dF}{dX_1} - \frac{Y}{I_1} \frac{dM_1}{dX_1} \right) dY,$$

$$\tau_{xz}^{(2)} = -\int_{-\frac{h_2}{2}}^{Y_2} \left(\frac{1}{A_2} \frac{dF}{dX_2} - \frac{Y}{I_2} \frac{dM_2}{dX_2} \right) dY.$$
(A-9)

Similar to the normal stress, the singular points for the transverse shear stress are

$$Y_1^{(T)} = 2Y_1^{(n)} - \frac{h_1}{2}$$
 in layer (1), (A-10a)

$$Y_2^{(T)} = \frac{h_2}{2} + 2Y_2^{(n)}$$
 in layer (2). (A-10b)

Since there is no X_i variables explicitly involved in the derivation of the singular points for the normal stress, the singular points for the in-plane displacements are the same as those given in Equations (A-8a) and (A-8b).

2. Three-layer Laminates

For a three-layer beam as shown in Figure A3, only the case in which layer (1) and layer (3) have the same geometry and material constants is presented.

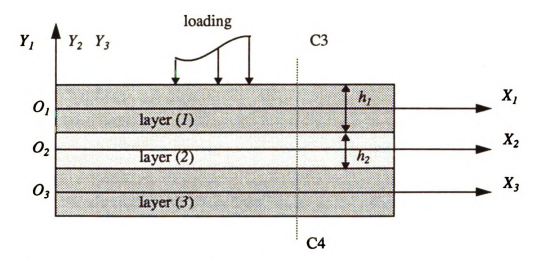


Figure A3 - The geometry and coordinate system of a three-layer beam.

Hence, it results in

$$I_1 = I_3;$$
 $A_1 = A_3$ (A-11)
$$M_1 = M_3;$$
 $E_1 = E_3$

The resultant force F and moments M_1 and M_2 at a generic cross-section C3-C4 are shown in Figure A4.

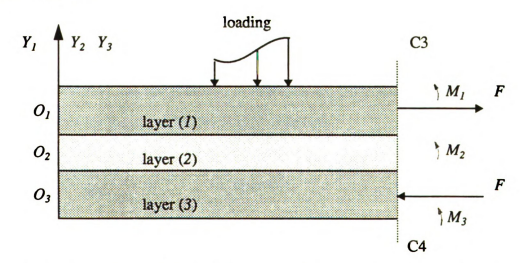


Figure A4 - The resultant forces and moments at the cross-section C3-C4.

The normal stress in each layer can be expressed by the following equations.

$$\sigma_x^{(1)} = \frac{F}{A_1} - \frac{M_1}{I_1} Y_1$$

$$\sigma_x^{(2)} = -\frac{M_2}{I_2} Y_2$$

$$\sigma_x^{(3)} = -\frac{F}{A_1} - \frac{M_1}{I_1} Y_3$$
(A-12)

By considering the assumption that every layer has the same deflection, it yields

$$\frac{M_1}{I_1 E_1} = \frac{M_2}{I_2 E_2} = \frac{M_3}{I_3 E_3} = \frac{M + F(h_1 + h_2)}{2E_1 I_1 + E_2 I_2}$$
(A-13)

where M is the total moment exerted on the cross-section. After combining Equations (A-12) and (A-13) together, Equation (A-12) can be rewritten as

$$\sigma_{x}^{(2)} = -\frac{F(h_{1} + h_{2})E_{2}}{2E_{1}I_{1} + E_{2}I_{2}}Y_{2} - \frac{ME_{2}}{2E_{1}I_{1} + E_{2}I_{2}}Y_{2}$$

$$\sigma_{x}^{(1)} = \left(\frac{F}{A_{1}} - \frac{F(h_{1} + h_{2})E_{1}}{2E_{1}I_{1} + E_{2}I_{2}}Y_{1}\right) - \frac{ME_{1}}{2E_{1}I_{1} + E_{2}I_{2}}Y_{1}$$

$$\sigma_{x}^{(3)} = \left(-\frac{F}{A_{2}} - \frac{F(h_{1} + h_{2})E_{3}}{2E_{1}I_{1} + E_{2}I_{2}}Y_{3}\right) - \frac{ME_{3}}{2E_{1}I_{1} + E_{2}I_{2}}Y_{3}$$
(A-14)

If it is further assumed that the geometry of the layer (2) is the same as that of layer (1), the singular points for the normal stress in each layer are

$$Y_1^{(n)} = \frac{h_1(2E_1 + E_2)}{24E_1}$$
 in layer (1), (A-15a)

$$Y_3^{(n)} = -\frac{h_3(2E_3 + E_2)}{24E_3}$$
 in layer (3), (A-15b)

$$Y_2^{(n)} = 0$$
 in layer (2). (A-15c)

It can be found that the singular point in layer (2) is a trivial solution and will not be considered in the following analysis.

Following a similar fashion as used for two-layer beams, the singular points for the in-plane displacements are the same as those given in Equation (A-15) while the singular points for the transverse shear stress are as follows.

$$Y_1^{(T)} = 2Y_1^{(n)} - \frac{h_1}{2}$$
 in layer (1), (A-16a)

$$Y_3^{(T)} = \frac{h_3}{2} + 2Y_3^{(n)}$$
 in layer (3). (A-16b)

Assume that the material of interest is given in Figure 3.1. The singular points in the [0/0] composite beam are given in Table A1.

The singular points in the [90/0] beam are listed in Table A2. Since the coordinate of the singular point cannot be larger than half of the thickness of the associated layer, there is no singular point in 90 layer.

The singular points in the [0/90/0] beam are shown in Table A3.

Table A1 - Singular points in a [0/0] beam.

layer(I)	normal stress and in-plane displacement	$Y_1^{(n)} = \frac{h_1}{6}$
	transverse shear stress	$Y_1^{(T)} = -\frac{h_1}{6}$
layer(2)	normal stress and in-plane displacement	$Y_2^{(n)} = -\frac{h_2}{6}$
	transverse shear stress	$Y_2^{(T)} = \frac{h_2}{6}$

Table A2 - Singular points in a [90/0] beam.

layer(I)	normal stress and in-plane displacement	none
	transverse shear stress	none
layer(2)	normal stress and in-plane displacement	$Y_2^{(n)} = -\frac{13h_2}{150}$
	transverse shear stress	$Y_2^{(T)} = \frac{49 h_2}{150}$

Table A3 - Singular points in a [0/90/0] beam.

layer(I)	normal stress and in-plane displacement	$Y_2^{(n)} = \frac{51h_2}{600}$
	transverse shear stress	$Y_2^{(T)} = -\frac{33h_2}{150}$
layer(3)	normal stress and in-plane displacement	$Y_2^{(n)} = -\frac{51h_2}{600}$
	transverse shear stress	$Y_2^{(T)} = \frac{33h_2}{150}$

References

- 1. P agano, N. J., "Exact Solutions for Composite Laminates in Cylindrical Bending,"

 Journal of Composite Materials, Vol. 3, July, 1969, pp. 398-411.
- 2. Pagano, N. J., "Exact Solutions for Rectangular Bidirectional Composites and Sandwich Plates," *Journal of Composite Materials*, Vol. 4, Jan., 1970, pp. 20-34.
- 3. Yang, P. C., Norris, C. H., and Stavsky, Y., "Elastic Wave Propagation in Heterrogeneous Plates," *International Journal of Solids and Structures*, Vol. 2, No.4, 1966, pp. 665-684
- 4. Nelson, R. B., and Lorch, D. R., "A Refined Theory of Laminated Orthotropic Plates," ASME Journal of Applied Mechanics, Vol. 41, March, 1974, pp. 177-183.
- 5. Reissner, E., "On Transverse Bending of Plate, Including the Effect of Transverse Shear Deformation," *International Journal of Solids and Structures*, Vol. 11, No.5, 1975, pp. 569-573.
- 6. Lo, K. H., Christensen, R. M., and Wu, E. M., "A High-Order Theory of Plate Deformation Part 2: Laminated Plates," *ASME Journal of Applied Mechanics*, Vol. 44, Dec., 1977, pp. 669-676.
- 7. Reddy, J. N., "A Simple Higher-Order Theory for Laminated Composites Plates," ASME Journal of Applied Mechanics, Vol. 51, Dec., 1984, pp. 745-752.
- 8. Noor, A. K., and Burton, W. S., "Assessment of Shear Deformation Theories for Multilayered Composite Plates," *Applied Mechanics Review*, Vol. 42, Jan., 1989, pp.1-13.
- 9. Kapania, R. K., and Raciti, S., "Recent Advanves in Analysis of Laminated Beams and Plates, Part I: Shear Effects and Bulickling," *AIAA Journal*, Vol. 27, No. 7, 1987, pp. 923-934.
 - 10. Kapania, R. K., and Raciti, S., "Recent Advanves in Analysis of Laminated

- Beams and Plates, Part II: Vibration and Wave Propagation," AIAA Journal, Vol. 27, No. 7, 1987, pp. 935-946.
- 11. Reddy, J. N., "A Review of Refined Theories of Laminated Composite Plates," Shock and Vibration Digest, Vol. 22, No. 1, 1990, pp. 3-17.
- 12. Whitney, J. M., "Stress Analysis of Thick Laminated Composite and Sandwich Plates," *Journal of Composite Materials*, Vol. 6, Oct., 1972, pp. 426-440.
- 13. Whitney, J. M, and Pagano, N. J., "Shear Deformation in Heterogeneous Anisotropic Plates," ASME *Journal of Applied Mechanics*, Vol. 37, Dec., 1970, pp. 1031-1036.
- 14. Reddy, J. N., "A Generalization of Two-Dimensional Theories of Laminated Composite Plates," *Communications in Applied Numerical Methods*, Vol. 3, 1987, pp. 173-180.
- 15. Barbero, E. J., and Reddy, J. N., "An Accurate Determination of Stresses in Thick Laminates Using a Generalized Plate Theory," *International Journal for Numerical Methods in Engineering*, Vol. 29, 1990, pp. 1-14.
- 16. Pagano, N. J., and Pipes, R. B., "Some Observations on the Interlaminar Strength of Composite Laminates," *International Journal of Mechanical Sciences*, Vol. 15, No. 8, 1973, pp. 679-688.
- 17. Liu, D., "Impact-Induced Delamination A View of Bending Stiffness Mismatching," *Journal of Composite Materials*, Vol. 22, July, 1988, pp. 674-692.
- 18. Lo, K. H., Christensen, R. M., and Wu, E. M., "Stress Solution Determination for High Order Plate Theory," *International Journal of Solids and Structures*, Vol. 14, No.8, 1978, pp. 655-662.
- 19. Ambartsumyan, S. A., *Theory of Anisotropic Plates*, edited by J. E. Ashton, Technomic Publication Company, Stamford, CT, 1970.
- 20. Whitney, J. M., "The Effect of Transverse Shear Deformation on Bending of Laminated Plates," *Journal of Composite Materials*, Vol. 3, 1969, pp. 534-547.
 - 21. Librescu, L., and Reddy, J. N., "A critical Evaluation on Generalization of the

- Theory of Anisotropic Laminated Composite Panels," <u>Proceedings of the American Society for Composites</u> (First Technical Conference), 1986, Dayton, Ohio, pp. 471-489.
- 22. Mau, S. T., Tong, P., and Pian, T. H. H., "Finite Element Solutions for Laminated Thick Plates," *Journal of Composite Materials*, Vol. 6, April, 1972, pp. 304-311.
- 23. Spilker, R. L., "A Hybrid-Stress Finite-Element Formulation for Thick Multilayer Laminates," *Computers and Structures*, Vol. 26, No. 6, 1980, pp. 507-514.
- 24. Pagano, N. J., "Stress Fields in Composite Laminates," *International Journal of Solids and Structures*, Vol. 14, No.5, 1978, pp. 385-400.
- 25. Di Sciuva, M., "Development of An Anisotropic Multilayered Shear-Deformable Rectangular Plate Element," *Computers and Structures*, Vol. 21, No.4, 1985, pp. 789-796.
- 26. Toledano, A., and Murakami, H., "A Composite Plate Theory for Arbitrary Laminate Configurations," ASME Journal of Applied Mechanics, Vol. 54, March, 1987, pp. 181-189.
- 27. Reissner, E., "On a Certain Mixed Variational Principle and a Proposed Application," *International Journal for Numerical Methods in Engineering*, Vol. 20, July, 1984, pp. 1366-1368.
- 28. Hinrichsen, R. L. and Palazotto, A. N., "Nonlinear Finite Element Analysis of Thick Composite Plates Using Spline Functions," *AIAA Journal*, Vol. 24, Nov., 1986, pp. 1836-1842.
- 29. Lu, X. and Liu, D., "An Interlaminar Shear Stress Continuity Theory for both Thin and Thick Composite Laminates," (to appear in ASME Journal of Applied Mechanics)
- 30. Pagano, N. J., and Soni, S. R., <u>Interlaminar Response of Composite Materials</u>, edited by N. J. Pagano, Elsevier Science Publishing Company Inc., 1989, pp. 1-68.
- 31. Lee, C. Y., and Liu, D., "An Interlaminar Stresses Continuous Theory for Laminated Composite Beams Analysis," (to appear in AIAA Journal).
 - 32. Newmark, N. M., Seiss, C. P., and Viest, I. M., "Tests and Analysis of Composite

- Beams with INcomplete Interaction," *Proc., Society for Experimental Stress Analysis*, Vol. 9, No. 1, 1951, pp. 73-79.
- 33. Goodman, J. R., and Popkov, E. P., "Layered Beam Systems with Interlayer Slip," *Journal of Structural Division*, ASCE, Vol. 24, Nov., 1968, pp. 2535-2547.
- 34. Goodman, J. R., "Layered wood Systems with Interlayer Slip," Wood Science, Vol 1, No. 3, 1969, pp. 148-158.
- 35. Thompson, E. G., Goodman, J. R., and Vanderbilt, M. D., "Finite Element Analysis of Layered wood Systems," *Journal of Structural Division*, ASCE, Vol 101, Dec., 1975, pp. 2659-2672.
- 36. Vanderbilt, M. D., Goodman, J. R. and Criswell, W. E., "Service and Overload Behavior of Wood Joist Floor Systems," *Journal of Structural Division*, ASCE, Vol. 100, Jan., 1974, pp. 11-29.
- 37. Barbero, E. J., and Reddy, J. N., "An Application of the Generalized Laminate Plate Theory to Delamination Buckling," *Proceeding of the American Society for Composites*, Forth Technique Conference, Oct. 3-5, 1989, pp. 244-251.
- 38. Toledano, A., and Murakami, H., "Shear-deformable Two-Layer Plate theory with Interlayer Slip," *Journal of Engineering Mechanics Div.*, ASCE, Vol 114, April, 1988, pp. 605-623.
- 39. Rao, K. M., and Ghosh, B. G., "Imperfectly Bonded Unsymmetric Laminated Beam," Journal of Engineering Mechanics Div., ASCE, Vol. 106, Aug., 1980, pp. 685-697.
- 40. Fazio, P., Hussein, R., and Ha, K. H., "Beam-Columns with Interlayer Slips," *Journal of Engineering Mechanics Div.*, ASCE, Vol 108, April, 1982, pp. 354-366.
- 41. Lu, X., and Liu, D., "Finite Element Analysis of Strain Energy Release Rate at Delamination Front," *Journal of Reinforced Plastics and Composites*, Vol. 10, 1991, pp. 279-292.
- 42. Whitcomb, J. D., "Three-Dimensional Analysis of a Postbuckling Embedded Delamination," *Journal of Composite Materials*, Vol. 23, Sept., 1989, pp.862-889.
- 43. Carlsson, L. A., and Pipes, R. B., <u>Experimental Characterization of Advanced Composite</u>

 Materials, Prentice-Hall, Inc., Englewood Cliffs, New Jersey 07632, 1987.

- 44. Carlesson, L. A., Gillespie, J. W., Jr., and Pipes, R. B., "On the Design and Analysis of the End Notched Flexure (ENF) Specimen for Mode II Testing," *Journal of Composite materials*, Vol. 20, 1986, pp. 594-604.
- 45. Maikuma, H., Gillespie, J. W., Jr., and Whitney, J. M., "Analysis and Experimental Characterization of the Center Notch Flexural Test Specimen for Mode II Interlaminar fracture," *Journal of Composite Materials*, Vol. 23, 1989, pp. 756-786.
- 46. Whitney J. M., "Analysis of Interlaminar Mode II Bending Specimenss Using a Higher Order Beam Theory," *Journal of reinforced Plastics and Composites*, Vol. 9, 1990, pp. 522-536.
- 47. Gillespie, J. W., Jr., Carlesson, L. A., and Pipes, R. B., "Finite element Analysis of the End Notched Flexure (ENF) Specimen," *Composite Science and Technology*, Vol. 27, 1986, pp. 177-197.
- 48. Abrate, S., "Impact on Laminated composite Materials," Applied Mechanics Review, Vol. 44, No.4, 1991, pp. 151-190.
- 49. Liu, D., Lillycrop, L. S., Malvern, L. E., and Sun, C. T., "The Evaluation of Delamination-An Edge Replication Study," *Experimental Technique*, Vol. 11, 1987, pp. 20-25.
- 50. Malvern, L. E., Sun, C. T, and Liu, D., "Damage in Composite Laminates from Central Impacts at Subperformation Speeds, in Recent Trends in Aeroelasticity Structures and Structural Dynamics," <u>Pro. symp. Mem for Prof. Bisplinghoff</u>, P. Hajela edit, Univ. Florida Press, Gainesville, FL, pp. 298-312.
- 51. Tracy J. J., and Padoen G. C., "Effect of Delamination on the Natural Frequencies of Composite Laminates," *Journal of Compossite Materials*, Vol. 23, 1989, pp. 1200-1215.
- 52. Tracy, J. J., "The Effect of Delamination on the response of advanced composite Laminates," Ph.D. Dissertation, University of California, Irvine (1987).
 - 53. Vinson, J. R., and Sierakowski, R. L., The behavior of Structures Composed of

Composite Materials, Martinus Nijhoff Publishers, Dordrecht, 1986.

- 54. Lee, C. Y., Liu, D. and Lu, X., "Static and Vibration Analysis of Laminated Beams by Using an Interlaminar Shear Stress Continuity Theory," (to appear in *International Journal for Numerical Methods in Engineering*)
 - 55. ASTM standards, Designation: C 848-78, Vol. 15.02, Section 15, 1988.
- 56. Chiu, C. C. and Eldon, D. C., "Elastic modulus determination of coating layers as applied to layered ceramic composites," *Material Science and Engineering*, 1991, pp. 39-47.
- 57. Jones, A. T., "Exact Natural Frequencies for Cross-ply laminates," *Journal of Composite materials*, Vol. 4, 1970, pp. 476-491.

